Promotor

> **prof. dr. ir. Joris Van Acker**
> Department of Forest and Water Management
> Laboratory of Wood Technology, Ghent University

> **dr. ir. Jan Van den Bulcke**
> Department of Forest and Water Management
> Laboratory of Wood Technology, Ghent University

Chair of examination committee

> **Prof. dr. Bernard De Baets**
> Department of Applied Mathematics, Biometrics and Process Control
> Ghent University

Members of examination committee

> **prof. dr. Mark Irle**
> École Supérieure du Bois (ESB)

> **prof. dr. ir Kathy Steppe**
> Department of Applied Biology and Environmental Biology
> Laboratory of Plant Ecology, Ghent University

> **prof. dr. ir. Arnold Janssens**
> Department of Architecture & Urban Planning
> Ghent University

> **dr. ir. Manuel Dierick**
> Department of Physics and Astronomy
> Institute of Nuclear Sciences, Ghent University

> **dr. Christian Brischke**
> Faculty of Architecture and Landscape Sciences
> Leibniz University Hannover

> **prof. dr. ir. Staf Roels**
> Department of Civil Engineering
> Building Physics Section, Katholieke Universiteit Leuven

Dean

> **Prof. dr. ir. Marc Van Meirvenne**

Rector

> **prof. dr. Anne De Paepe**

Experimental investigation of the relation between structure and moisture behavior of wood-based panels

Wanzhao Li

Thesis submitted in fulfillment of the requirements for the degree of Doctor (PhD) in Applied Biological Sciences

Dutch translation of the title: Experimenteel onderzoek naar de relatie tussen structuur en vochtgedrag van houten plaatmaterialen

(Cover: The internal structure before water uptake and water distribution after water uptake of cross sections of the OSB specimens obtained with X-ray CT scanning)

Preface

It is already hard to recall every detail of my first experience in Belgium. Beautiful church, strange noodles (spaghetti) and quite street on Sunday… Four years later, these details cannot surprise me anymore because they have become part of my life.

I like the happiness acquired from the life and also appreciate the people who accompanied me in the past years.

I deeply appreciate my two promotors: Prof.dr.ir. Joris Van Acker and Dr.ir. Jan Van den Bulcke.

Prof.dr.ir. Joris Van Acker, thanks for offering me the opportunity to obtain my PhD at Ghent University. You are always supportive ever since I started my PhD. Your agreeable and positive attitude is always a great encouragement for me to move on and a big release of my pressure. Your jokes (in Dutch?) and laughter (I do can feel) in the corridor let me realize PhD work is just a fun part of life.

Dr.ir. Jan Van den Bulcke, I would like to call you 'problem solver' instead of promotor or supervisor. You always can give me an answer whenever I go to you. You spend your time to discuss with me no matter how busy you are or how 'unclear' my questions are. Your enthusiastic and motivated attitude on science will influence me in my future academic career and life.

I would like to thank my examination committee: Prof.dr. Bernard De Baets, Prof.dr. Mark Irle, Prof.dr.ir. Kathy Steppe, Prof.dr.ir. Arnold Janssens, Dr.ir. Manuel Dierick, Dr. Christian Brischke, Prof.dr.ir Staf Roels. Thank you for your time on reading and correcting my thesis. Your valuable advice helped me a lot to improve my study.

Dear colleagues from Woodlab: Nele Defoirdt, Imke De Windt, Sam Colpaert, Erik Botter, Tom De Mil, Hanna Kuisch, Victor Deklerck, Patrick Kondjo, Piet Dekeyser, Rik De Rycke, Stijn Willen, Marijke De Wilde, Wannes Hubau. Although we do not have too many opportunities to talk with each other due to my poor Dutch, you always give me the kind help whenever I need. I would like to give my special thanks to Rik and hope he can come back to the lab in the near future.

I appreciate the help from the colleagues from UGCT. You are a group of people who are extremely smart and very kind. Without the excellent X-ray CT scanners you built, my PhD work would be much more difficult to be accomplished. Without your help, I could not obtain the images with the perfect resolution allowing to reveal the internal information of my panels.

My Chinese friends. We are a big family and you are my sisters and brothers. Thanks for all the happiness you brought to me and unconditional help you offered me whenever needed.

Finally, the people I love the most: my wife Shengrun and my son Ziji.

Shengrun, I have to say that you are the most important motivation for me to start my life and study abroad. My life becomes bright because of you although I have to cook every day for you. I will miss the moment when we studied together in the library of Ghent University after dinner. You learned the complicated economic models, while I just sat nearby you and watched NBA matches.

Ziji, you are the best gift I ever acquired in my life. The moment of playing with you at 2 o'clock in the morning is the precious memory in my mind although it makes it very difficult for me to focus on working during the day.

谢谢你们，爸爸，妈妈，岳父，岳母。感谢你们的无私奉献与支持。

Wanzhao

31 December 2015

Samenvatting

Houten plaatmaterialen (HPM) worden reeds decennia lang gebruikt als basis voor decoratieve producten en als bouwmateriaal. Ze spelen een steeds belangrijker rol gezien hun vele voordelen, o.a. omwille van hun grondstof-compatibiliteit, het feit dat ze in te passen zijn in een continu productieproces en omwille van mogelijke standaardisatie van de producten. Enkele nadelen van deze HPM kunnen echter niet worden genegeerd, namelijk blootstelling aan wateropname leidt tot vermindering van fysische en mechanische eigenschappen. Momenteel zijn de meest gebruikte technieken om het hygroscopisch gedrag van HPM te verbeteren, het aanbrengen van een waterafstotende coating, het toevoegen van waterafstotende additieven of het gebruik van specifieke behandelingsmethoden. Het verbeteren van het hygroscopisch gedrag kan ook worden bereikt door het optimaliseren van de structurele eigenschappen van HPM, wat aldus milieuvriendelijk en economisch haalbaar kan zijn. De eerste stap in het optimaliseren is het begrijpen van de relatie tussen de structurele opbouw en het hygro-mechanisch gedrag van HPM.

In dit proefschrift ligt de nadruk op het onderzoeken van de hygro-mechanische eigenschappen van multiplex, MDF en OSB met behulp van standaard en nieuwe niet-destructieve methoden. Om de invloed van de structurele karakteristieken op de hygro-mechanische eigenschappen van HPM te ontrafelen, werden volgende stappen ondernomen:

i. X-stralen tomografie en neutronen radiografie werden gebruikt om de interne structuur te visualiseren en vochtverdeling te kwantificeren in multiplex stalen. Vochtverdeling in MDF en OSB werd dynamisch in kaart gebracht met een uniek X-stralen computer tomografie systeem.

ii. Een aangepaste elektrische vochtmeetmethode werd getest om vochtverdeling in verschillende lagen van multiplex continu op te volgen. Door combinatie van deze methode met periodieke X-stralen CT scans, kon het hygroscopisch gedrag van multiplex in een buitenopstelling bestudeerd worden.

iii. Het gedrag van multiplex en MDF onder invloed van biologische aantasting werd onderzocht door het bepalen van de mechanische eigenschappen, het massaverlies en de structurele veranderingen.

Er kan gesteld worden dat de niet-destructieve methoden erg waardevol zijn om de hygro-mechanische eigenschappen van HPM te doorgronden. De factoren die van invloed zijn op de hygro-mechanische eigenschappen van HPM kunnen als volgt gerangschikt worden:

Multiplex: *houtsoort; lijmtype; vezelrichting fineer; dikte topfineer.*

MDF: *vezelbehandeling; vezelgrootte; dichtheid; lijmtype; additieven.*

Samenvatting

OSB: *richting van de schilfers; grootte van de schilfers; dichtheid; lijmverdeling.*

De bovengenoemde factoren beïnvloeden de hygro-mechanische eigenschappen van HPM niet onafhankelijk van elkaar. Het is niet vanzelfsprekend om de onderliggende verbanden te vinden, wat dit onderzoek moeilijk en interessant maakt. Meer dan alleen de hierboven genoemde kunnen ook andere factoren de hygro-mechanische eigenschappen van HPM beïnvloeden. Deze werden echter niet in beschouwing genomen gezien ze niet aanwezig waren in het beperkte aantal soorten plaatmaterialen die in dit onderzoek werden gebruikt. De methoden en ideeën onderzocht in dit proefschrift, kunnen echter ook worden gebruikt in toekomstig onderzoek rond dit onderwerp. Dit werk bevat uiteindelijk een aantal richtlijnen om HPM te creëren met een goed hygroscopisch gedrag door het optimaliseren van hun structurele opbouw.

De methoden, namelijk X-stralen tomografie en neutronen radiografie, maken het mogelijk om de inwendige structuur van de HPM te visualiseren en te bestuderen. De Resonalyser techniek kan gebruikt worden om op een niet-destructieve manier de mechanische eigenschappen te achterhalen van stalen verzaagd uit multiplex en MDF. De elektrische weerstandsmethode, mits correcte installatie van de elektroden, is in staat om continu vochtverdeling in multiplex te volgen. Met behulp van deze niet-destructieve methoden, kan zowel kwaliteitscontrole als de levensduurvoorspelling van HPM worden verbeterd. Tot nu toe zijn deze methoden hoofdzakelijk in laboratoriumomstandigheden beschikbaar en getest vanwege de omvang en het concept van sommige van de apparatuur en de strenge eisen voor de conditionering van de stalen.

Deze nieuwe werkwijzen laten toe de eigenschappen, die snel over het hoofd gezien worden in klassieke standaardtesten, te onthullen. Zo worden bijvoorbeeld de interne structurele veranderingen en vochtverdeling meestal niet beschouwd bij de beoordeling van de prestaties van HPM. Er wordt, bij de beoordeling van de biologische duurzaamheid van HPM, eveneens niet altijd rekening gehouden met een reeds aanzienlijke afname in sterkte in de beginfase van schimmelaantasting. Deze parameters kunnen echter een significante invloed hebben op de prestaties van HPM producten. De nieuwe methoden, zoals deze in dit werk worden gebruikt, laten nu toe dit soort parameters op te nemen in de kwaliteitscontrole van HPM.

In het algemeen zijn de werkwijzen en ideeën die in dit doctoraatswerk uitgewerkt worden een manier om HPM te bestuderen op microschaal en op niet-destructieve wijze. Dit is nuttig voor het verbeteren van het hygroscopisch gedrag van HPM door middel van het optimaliseren van bepaalde structurele karakteristieken. De algemeen gebruikte theorie ter evaluatie van de eigenschappen en het uitvoeren van kwaliteitscontrole van HPM dient vermoedelijk ook opnieuw te worden bekeken in dit opzicht.

Summary

Wood-based panels (WBP) have been used as base decorative products and construction material for decades. They play an increasingly important role due to the multiple advantages, *e.g.* raw material compatibility, ease of implementation, adaptability to continuous processing and standardization of the products. Some disadvantages of WBP, however, cannot be ignored. Generally speaking, WBP subjected to water uptake induces decrease of their physical and mechanical properties. Currently, the most popular approaches to improve the moisture behavior of WBP are to use a waterproof coating or either to add water repellent additives or to use specific treatment methods. Improving the moisture behavior can also be achieved by optimizing the structural characteristics of the panels, which is environmental friendly and economically viable. The primary step for optimizing the structural characteristics is to understand the relationship between structural characteristics and hygro-mechanical performance of WBP.

In this thesis, the focus is on investigating the hygro-mechanical performance of plywood, MDF and OSB using standard and new non-destructive methods. Therefore, three main steps were considered to unravel the influence of structural characteristics on the hygro-mechanical performance of WBP.

   i. X-ray tomography and neutron radiography were used to reveal the internal structure and quantify the moisture distribution in plywood specimens. Moisture distribution in MDF and OSB was dynamically mapped with a gantry-based X-ray CT scanning system.

   ii. An adapted electrical MC measurement method was introduced to continuously monitor moisture distribution in different layers of plywood. Combining this method with periodic X-ray CT scanning, the moisture behavior of plywood during outdoor exposure was studied.

   iii. The performance of plywood and MDF under biological degradation conditions was investigated by assessing the mechanical properties, the mass loss and structural variations of the specimens.

It can be stated that the state-of-the-art non-destructive methods are valuable to understand the hygro-mechanical performance of WBP. The factors having major impact on hygro-mechanical properties of WBP are the following:

Plywood: *wood species; glue type; veneer grain direction; top veneer thickness.*

MDF: *fiber treatment; fiber size; panels' density; glue type; additives.*

OSB: *strand grain direction; strand size; panels' density; glue distribution.*

The aforementioned factors do not influence the hygro-mechanical properties of WBP independently. It is non-trivial to understand the interrelationship between them, which makes this research difficult and interesting. Apparently, there are more than just the above mentioned factors that can impact the hygro-mechanical performance of WBP. They were not considered as they were not apparent in the limited number of panel types. The methods and ideas explored in this thesis, however, can be used in future research to continue this topic. Finally, the aim of producing WBP products with good moisture behavior by optimizing the structural characteristics is at hand.

The methods, *i.e.* X-ray tomography and neutron radiography, make it possible to visualize and study the internal properties of WBP. Resonalyser can be used to non-destructively monitor the mechanical properties of the specimens from plywood and MDF. Electrical resistance MC measurement method with proper installation of the electrodes allows us to continuously record moisture distribution in plywood. With the assistance of these non-destructive methods, both quality control and service life prediction of WBP can be improved. Up to now, these methods are mainly used in laboratory tests due to the size and concept of the equipment and the strict requirements for the condition of the specimens.

These new methods allow us to reveal the properties that are easily overlooked in classic standard tests. For instance, the internal structural changes and moisture distribution are not usually considered in assessing the performance of WBP. The strength decrease at the incipient stage of fungal decay is not always taken into account when evaluating the biological durability of WBP. These parameters, however, do have significant influence on the performance of WBP products. The new technologies developed allow now to use such approaches for quality control of WBP.

In general, the methods and ideas explored in this PhD work provide an approach to study WBP in a micro, integral and non-destructive view. This is helpful for improving the moisture behavior of WBP through optimizing their structural characteristics. The commonly used theory of evaluating the properties and performing quality control of WBP could also be re-considered.

Table of contents

List of abbreviations

CMM	continuous moisture measurement
CsCl	cesium chloride
EMCT	environmental micro-CT scanner
FSP	fiber saturation point
HECTOR	high energy CT scanner optimized for research
MC	moisture content
MDF	medium density fiberboard
MDI	methylene diphenyl diisocyanate
MOE	modulus of elasticity
NEUTRA	neutron transmission radiography
OSB	oriented strand board
PF	phenol-formaldehyde
PSI	Paul Scherrer Institute
QNI	quantitative neutron imaging
RH	relative humidity
ROI	region of interest
TOW	time of wetness
UF	urea-formaldehyde
UGCT	Ghent University centre for X-ray tomography
UMF	melamine urea formaldehyde
WBP	wood-based panels

1 General introduction

1.1 Objective and research questions of this dissertation

Wood has played an important role for thousands of years due to its availability, flexibility and sustainable character. Due to these advantages and a continuously growing demand, solid wood products with large dimensions from (semi-) natural forests have been intensively harvested. In order to apply wood in a more efficient way, wood-based panels (WBP), made from different wood pieces glued with synthetic adhesives through pressing, are widely used. The raw materials used to produce WBP are low quality and fast-grown logs as well as processing residues and even recovered wood, which makes WBP an environmental friendly material group.

As a wood based material, WBP is prone to water uptake, which can decrease strength and increase decay risk. Many approaches, such as edge sealing, wood modification and preservation, have been used to improve water repellency and decay resistance of WBP. Although the dimensional stability and water resistance of WBP are improved by modifying wood components or entire panels, the mechanical strength can still decrease (Sekino et al., 1999; Youngquist et al., 1986). Wood preservation means that wood is treated (superficially or in depth) with an active ingredient (biocide) to prevent degradation organisms like stain, mould and wood rotting fungi. This method, however, will increase the cost and induce some environmental burden. Sealing or coating WBP with waterproof paint or paper can increase the water resistance, but also here the cost will rise. Another option to improve the water resistance and moisture behavior of WBP is to optimize the structural characteristics, for instance the wood species, the size of wood pieces, the mattress, the glue line parameters and so on. This method is, naturally, environmentally friendly and cost saving. However, there has been few studies focusing on this option. In order to reach this target, investigating the relationship between moisture transport behavior and structural characteristics of WBP is essential. In this dissertation, the idea is explored to improve the moisture behavior of WBP by optimizing the structural characteristics. To reach this objective, the following five research questions were proposed:

i. How do structural characteristics influence water transport behavior of plywood?

ii. What is the impact of structural characteristics on water transport behavior of medium density fiberboard (MDF) and oriented strand board (OSB)?

iii. How can we measure the moisture distribution in WBP in a continuous setup?

iv. What is the moisture behavior of plywood in service according to the moisture distribution and structural variations?

v. How does moisture entrapment impact the mechanical strength and biological durability of WBP?

1.2 Wood-based panels (WBP)

The way of wood usage relates to the degree of social and economic development. Currently, the challenges for the wood industry are the increasing cost of raw materials and labors. In addition, the competition with other materials, such as concrete, plastic and steel, also impacts the market share of wood materials. The WBP produced with wood veneers, particles or fibers are raw material compatible and most adaptable to continuous flow, to automation, to product standardization and to large scale operations. To assure the properties of WBP products, wood particles are preferred to be close to the original state of solid wood. With the support of new technology, this is becoming of less importance and hence there is a trend shifting from plywood to particleboard and fiberboard.

In 2013, the global WBP production reached 358 million m³, which was a 7.8% increase over the previous year and 35% increase over the period from 2009 to 2013 (FAO, 2013). The Asia-Pacific region accounted for 60% of global production, followed by Europe (21%), Northern America (13%), Latin America, the Caribbean (5%) and Africa (1%). Veneer and plywood were the most dominant types of WBP in 2013 with the production of 146 million m³. The 57% increase of veneer and plywood production over the period of 2009 to 2013 was mainly caused by an increased production in China, accounting for 69% of the global production. Fiberboard production increased with 45% in the period of 2009-2013 and reached 113 million m³. The largest growth occurred in MDF that accounts for 78% of all fiberboard production. In contrast to plywood and fiberboard, the production of particleboard was merely 99 million m³ in 2013 and only increased 5% since 2009.

1.2.1 Adhesives for WBP production

The difference between WBP and solid wood is the presence of adhesives to bind wood veneers, particles and fibers. Adhesives play a crucial role in the performance of WBP. In the WBP industry, the adhesive selection is mainly based on the quality requirements and cost. Although the type of WBP is different, similar types of adhesive are widely used in practice, namely urea-formaldehyde (UF), phenol-formaldehyde (PF), methylene diphenyl diisocyanate (MDI) and different so-called natural non-synthetic adhesives.

Urea-formaldehyde

UF is a synthetic adhesive made from urea and formaldehyde and is commonly used in the WBP industry due to its low price and good bonding strength. UF adhesive has a white color and is available in the form of liquid or powder. The curing temperature of UF adhesive ranges from 95 to 130℃. Because of its poor resistance to moisture, UF adhesive is commonly used to produce WBP applied in low humidity conditions (Dunky, 1998). Another disadvantage of the UF adhesive is formaldehyde emission, which is believed to be hazardous for human health. The performance of UF adhesive can be improved by adding additives, such as tannin from larch (*Larix gmelini*) bark and

glyoxalated soda bagasse lignin (Younesi-Kordkheili et al., 2015; Zhang et al., 2014). Currently, mortifying UF adhesive with melamine is the industrialized approach to increase water resistance combined with options to decrease formaldehyde emission (Gao et al., 2011; Pizzi, 2001). Melamine urea formaldehyde (MUF), however, is more expensive than UF and the price difference depends on the amount of melamine added.

Phenol-formaldehyde

PF is available as liquid, powder or as impregnated paper film. The PF adhesive is a synthetic polymer acquired from the reaction of phenol with formaldehyde. The curing temperature of PF adhesive is generally from 115-150℃. WBP glued with the PF adhesive have high strength and high durability under moist conditions. They are commonly used in outdoor situations. The performance of the PF adhesive can even be improved by adding functional additives using nanotechnology (Fang et al., 2014; Gao and Du, 2013). PF emits less formaldehyde than UF due to strong bonding between phenol and formaldehyde. The dark red color of PF could discolor wood with light color, which might influence aesthetics of wood texture. The price of PF adhesive is approximately twice as high as the UF adhesive.

Methylene Diphenyl Diisocyanate

MDI is produced by the reaction of aniline and formaldehyde, and then treated with phosgene. MDI adhesive has been commercially used to produce particleboard and fiberboard. The particleboard glued with MDI adhesive has superior mechanical properties, water resistance and dimensional stability (Abdolzadeh et al., 2011; Kojima et al., 2009; Mo et al., 2003). The disadvantages of MDI adhesive are its high price and the fact that it bonds to metal, resulting in sticking press plates together. Therefore, release agents must be used, which causes added cost and environmental impact. In practice, mixing MDI with other cheap adhesives is regarded as a feasible way to decrease cost and obtain particleboard with high quality (Pan et al., 2006).

Natural adhesive

Compared to synthetic adhesives, natural adhesives are renewable and have few effect on human health. Natural adhesives are mainly produced from plant components. Adhesives made from soya, from a protein contained in the seeds of soya, were widely used as wood adhesive between the 1930s and 1960s. Afterwards, they were replaced by synthetic formaldehyde based adhesives due to poor durability and low strength. Nowadays, with the progress of adhesive technologies, intensive research has been done resulting in a re-booming of the soya adhesives industry (Liu and Li, 2002, 2007; Sun and Bian, 1999; Zhu and Damodaran, 2014). Starch is one of the most abundant natural polymers and the possibility of using starch adhesive to produce plywood has been investigated (Imam et al., 1999). The major disadvantages of starch adhesive are low water resistance, poor

mechanical properties and vulnerability to fungal decay, which could be improved by optimizing the procedures of adhesive preparation and panel processing (Moubarik et al., 2010; Wang et al., 2011). In addition to the aforementioned two important types of bio-adhesive, many other types of adhesives based on the natural materials have also been studied, for instance, Jatropha oil, algal protein and bagasse lignin based adhesives (Aung et al., 2014; Khan et al., 2004; Roy et al., 2014).

Researchers have also attempted to search for other synthetic polymers to replace formaldehyde polymers (Fang et al., 2013; Imam et al., 2001; Jeong et al., 2014). Although many achievements have been attained, formaldehyde polymers still play a dominant role in the present adhesive market in the WBP industry due to their reasonable price, good strength and the widely used production system.

1.2.2 Plywood

Plywood panels are veneer based products, usually with odd number of veneers, glued together by adhesives. The grain of alternate veneers is arranged to cross at right angles, minimizing strength anisotropy in the panel (Fig. 1.1). As plywood became a major industry in the 1930s, its manufacturing procedure has been largely developed as shown in Fig. 1.2. Nowadays, plywood is widely used as decorative and mainly as construction material. Compared to other WBP, the mechanical and physical properties of plywood is closer to solid wood. Plywood has good dimensional stability except in panel thickness direction. Plywood products are, therefore, broadly used as engineered material, even in outdoor conditions that require both superior mechanical and biological durability.
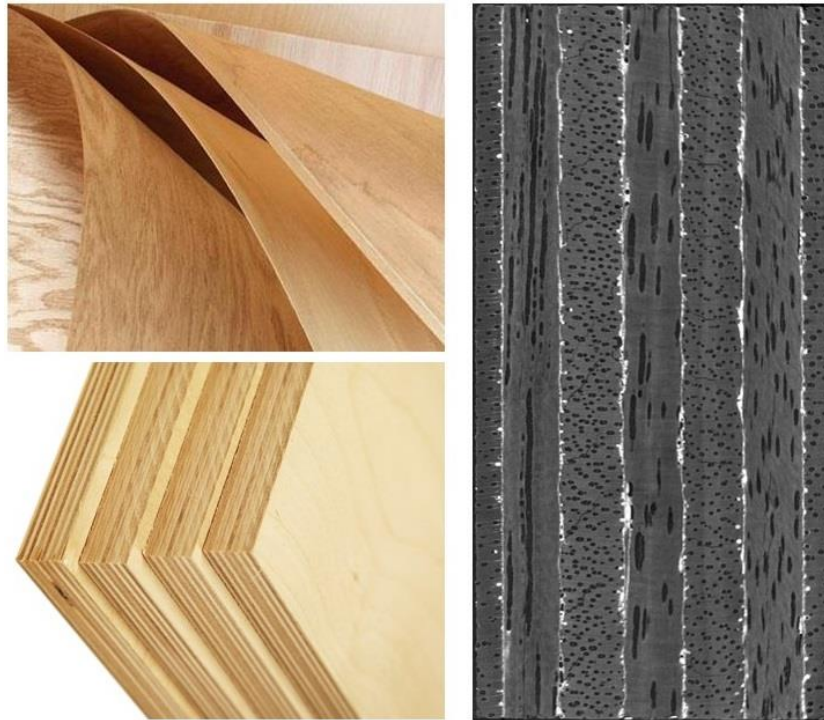
Fig 1.1. The image of veneers (plywood panel edges), plywood and internal microstructure (obtained with X-ray CT scanning).
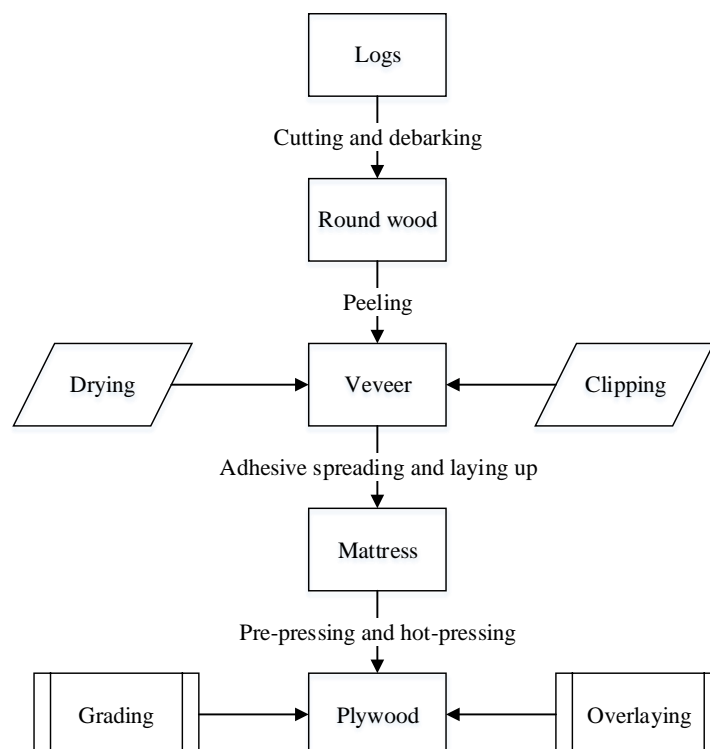

Fig 1.2. The main process steps to produce plywood.

Naturally, the quality of plywood closely relates to the quality of veneers and wood species used. However, increasing cost of logs and lumber has caused the plywood manufacturers to use trees more

efficiently. The efficiency of timber usage has been tremendously improved as the timber can be peeled to as small as 50 mm diameter using innovative spindles peeler machines (Thoemen et al., 2010). Meanwhile, fast-grown plantation trees have been widely used to replace wood from (semi-) natural forest to produce plywood (Knudson et al., 2006; Qin et al., 2013). Wood from fast-grown trees, however, generally has inferior mechanical and physical properties. In order to produce plywood using fast-grown trees, it is necessary to optimize the manufacturing procedures, *e.g.* veneer preparation and hot pressing process (Aydin et al., 2006; Demirkir et al., 2013; Hoong and Paridah, 2013; Ozsahin and Aydin, 2014). A veneer with smooth surface and adequate moisture content (MC) allows sufficient adhesive to be evenly distributed, which is vital to obtain an integral and strong glue line during hot pressing. According to the type of adhesive and veneer thickness, specified hot pressing protocols can strengthen the glue line and reduce energy consumption. In addition to the aforementioned methods, modifying the entire panels or separate veneers using chemical or physical methods has also been used to improve the mechanical and physical performance of plywood as well as its durability (Mendes et al., 2014; Mendes et al., 2013; Trinh et al., 2012a). In special targeted applications, plywood panels need to be surfaced with other materials, such as metal, and plastics (Trinh et al., 2012b; Wang et al., 2014; Zdravkovic et al., 2013). Nowadays, efforts have also been devoted to explore plywood made from other ligno-cellulose materials. For example, plywood panels made from bamboo is already popular in East Asia (Han and Zou, 2012).

1.2.3 Particleboard

Particleboard includes chipboard and OSB produced from gluing wood chips and flakes respectively (Fig. 1.3). The particleboard industry was first started in the 1940s in Germany and later on, particleboard manufacturing was greatly developed. After the Second World War there was an urgent need for wood based products for major construction projects. Particleboard offered a means to do so. Although the process steps are similar with the classical way as shown in Fig. 1.4, the efficiency has been largely improved. For instance, continuous press techniques can increase production efficiency, decrease energy utilization and improve the property consistency of products.

1

Fig 1.3. The image of flakes, OSB and internal microstructure of OSB (obtained by X-ray CT scanning).
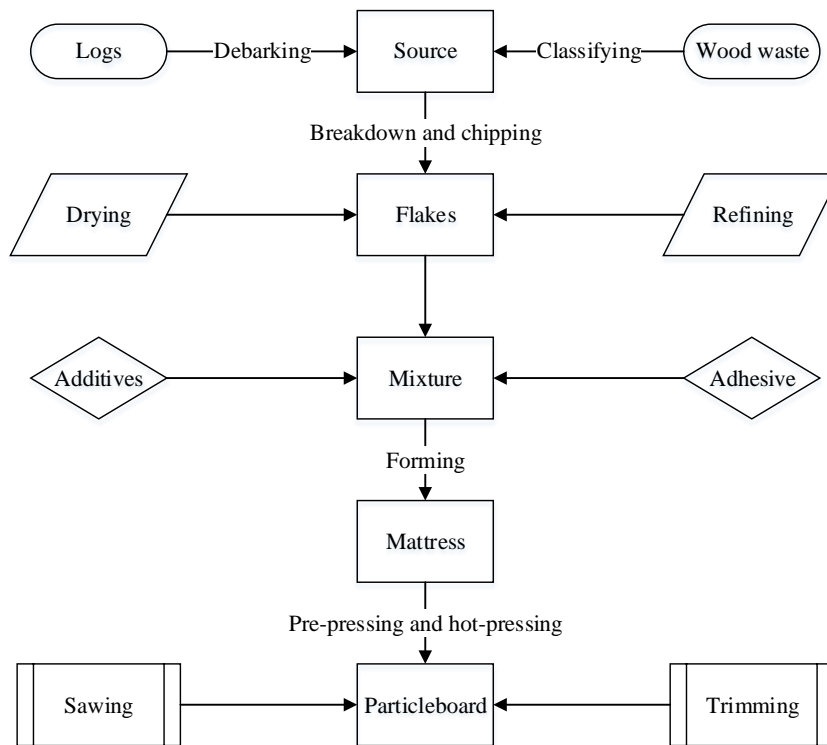

Fig 1.4. The main process steps to produce particleboard.

In industry, softwood and hardwood species with medium density are preferred to produce particleboard. Wood residues and recovered wood can also be used to produce chipboard, which is environmental and economic friendly. However, problems still exist (Hoglmeier et al., 2014). For example, a large number of bark and contaminants (such as minerals, stones and soil) in forest residues as well as in recovered wood will increase the cost of material pre-processing. Thanks to the emerging new material classification technology, the number of wood residues and recovered wood usage in the chipboard industry are increasing (Himmel et al., 2014; Nasser et al., 2014; Santos et al., 2014). In addition to wood materials, particleboard can also be produced using alternative fibrous materials (Azizi et al., 2011; Nazerian and Sadeghiipanah, 2013).

Currently, particleboard is widely used as an engineered product in both interior and exterior applications due to the improved quality. Researchers have found that particle size impacts the final properties of the particleboard panels (Arta-Obeng et al., 2012). Apart from controlling particle size, particle treatment also influences the performance of particleboard in terms of water resistance, mechanical strength and physical stability (Jumhuri et al., 2014; Pelaez-Samaniego et al., 2014; Sari et al., 2013). Adding silver and copper nanoparticles in particle mattress has been proven to be a feasible approach to restrain fungal growth in particleboard (Taghiyari et al., 2014b). Hot pressing process impacts the properties of particleboard as well. Elaborate studies on optimizing hot pressing protocol or searching for new hot press techniques have been performed (Boon et al., 2013; Korai et al., 2014a, b). Good hot pressing processes enhance the bonding strength between wood particles and increase the mechanical property and physical stability of particleboard. After hot pressing, the quality of particleboard is further improved by physical or chemical modification to obtain a good dimensional stability and biological durability (Bonigut et al., 2014). Researchers have also tried to enlarge the application range of particleboard by coating with functional films and treatment with resin (Korai and Hattori, 2013). As particleboard is produced by binding wood particles with adhesives, it is a feasible approach to mix wood particles with other functional particles during mattress forming to acquire a functional particleboard, for example a cement particleboard.

Progress in particleboard production was made in the 1980s because of the emerging oriented strand board (OSB). Specifically, OSB is manufactured from cross-oriented layers of thin and rectangular wooden flakes or strands compressed and bonded together with wax and synthetic resin adhesives. In general, OSB has a layered structure similar with plywood contributing to the high mechanical strength in the length direction. OSB is suitable for load bearing applications in construction, such as roof decking, flooring and sheathing in walls. However, it is still less functional than plywood as designed for class 3 situations. Suzuki and Takeda (2000) found that strands length and layer structure have remarkable influence on the bending strength of OSB. The thickness swell caused by water sorption is reduced by heat pre-treating strands (Paul et al., 2006). The layered structure is one

1

of the main advantages to manufacture functional OSB. For instance, fire retardant OSB is produced by adding particles of expandable graphite in the surface layers (Ford et al., 1995).

1.2.4 Fiberboard

Fiberboard includes three types: hardboard, insulation boards and medium density fiberboard (MDF) (Suchsland and Woodson, 1987). MDF is an engineered product made of ligno-cellulosic fibers, combined with synthetic resin and bonded together in a heat press to form a panel (Fig. 1.5). The manufacturing process of MDF is similar to that of particleboard but MDF panels consist of fibers instead of particles. Fiberboard is mainly classified according to the density and MDF is the most widely used with a density ranging from 500 to 1000 kg/m^3. MDF was first developed in the USA in hardboard manufacturing. The first dry-process MDF factory was built in the USA in 1965, and at the same period, MDF was successfully commercialized. Since then the production capacity of MDF has been rapidly growing across the world.

Fig 1.5. Fibers, MDF and internal microstructure of MDF (obtained with X-ray CT scanning).

Raw material quality requirements for MDF are not as critical as for plywood but more restricted than for chipboard. Fibers from round wood, wood residues, recovered wood, waste paper, bamboo or even agro-fibers are feasible to produce MDF. In general, the performance of MDF is impacted by fibers from non-virgin wood fibers, like fibers from recovered wood and agro-fibers. The bending

1

strength, internal bond strength and dimensional stability of MDF decrease with increasing mixing ratio of these fibers due to low mechanical strength and low superficial adhesion of fibers. Fibers from chromated copper arsenate (CCA) preservative treated wood waste, however, can improve both dimensional stability and internal bond strength of MDF. Therefore, the mixing ratio of these fibers needs to be carefully controlled in order to guarantee the quality requirements (Akgul et al., 2013a; Akgul et al., 2013b; El-Kassas and Mourad, 2013; Marinho et al., 2013; Sabo et al., 2013).

Currently, MDF is largely used in the furniture industry given several advantages, *e.g.* tight edges, smooth surface and homogeneous texture. The shortcomings such as being prone to water uptake and swelling, however, restrict using MDF in humid conditions. Hence, researchers have devoted efforts to improving the quality of MDF and found that the adhesive, hot pressing process and MC of fibers influence the quality of MDF (Ali et al., 2014; Nayeri et al., 2014). A recently developed particle analysis system was used to produce three different types of fibers. These fibers were used to manufacture test MDF panels. Researchers have found that increasing fiber length of MDF could enhance its mechanical properties, i.e. modulus of elasticity, internal bond, modulus of rupture and surface soundness, while decrease its water resistance and panel's dimensional stability (Benthien et al., 2014). By pre-treating fibers or adding functional fibers in the mattress, re-enforced MDF is produced. For example, the biological resistance and the fire-retarding properties of MDF are improved by adding nanowollastonite (Taghiyari et al., 2014a; Taghiyari et al., 2013). The water resistance of MDF can be increased by mixing fibers with nano-zycosil during mattress forming (Taghiyari, 2013). Researchers have also found that adding chestnut shell into MDF made of hardwood fibers decreases the formaldehyde emission, although the dimensional stability and internal bond strength will also decline (Ayrilmis and Kaymakci, 2012). The inherent drawbacks of MDF, such as formaldehyde emission, lower shape stability and dust release, makes coating a necessary procedure for practical applications. A painted surface improves the water resistance and presents an attractive visual surface. MDF is also usually covered with a decorative, laminated plastic film to decrease volatile organic compounds (VOC) emission and to form hard wearing, and easily cleaned surfaces (Barry and Corneau, 2006; George, 1991; Zhang et al., 2013). Hence, the development of coating technology significantly influences the application of MDF and as such many new coating technologies have been invented or introduced. For instance, powder coating is a prevalent method to film metal materials, which has been introduced to surface MDF (Jocham et al., 2011).

1.3 Quality control of WBP

The physical and mechanical properties of WBP have been greatly improved over the last fifty years due to the application of synthetic adhesives. The production capacity, consistency of products and

1

profit of WBP industry were also improved by applying automated sawing, machining and hot pressing techniques (Thoemen et al., 2010). WBP products are widely applied not only indoors as decorative materials but also outdoors as construction materials. Another key field of the WBP development is that products should be selected according to the product property and practical application requirements. Using suitable WBP products in the appropriate application situation increases durability and reduces wood consumption. Meanwhile, it increases the security level of WBP in service.

1.3.1 European standards in evaluating WBP

Table 1.1 summarizes the European standards for measuring the quality parameters of WBP. The most common properties used to evaluate the quality of WBP are density, water resistance, mechanical properties, dimensional stability, biological resistance and formaldehyde emission. Until now, standards are regarded as an accurate, consistent and reliable way to determine the properties of WBP. In addition, it can also be a reference to evaluate the accuracy of other non-standard methods. A number of standards listed in Table 1.1 will be referenced in the following chapters.

Table 1.1 European standards related to WBP properties determination.

Field	Standard	Year	Title
Formaldehyde emission	EN 120	1993	Wood-based panels. Determination of formaldehyde content. Extraction methods called perforator method.
	EN 717	2004	Wood-based panels. Determination of formaldehyde release. Part 1: Formaldehyde emission by the chamber method.
Dimensional stability	EN 325	2012	Wood-based panels – Determination of dimensions of test pieces
	EN 317	1994	Particleboard and fiberboards. Determination of swelling in thickness after immersion in water.
	EN 318	2002	Wood-based panels. Determination of dimensional changes associated with changes in relative humidity.
Mechanical properties	EN 314-1	2004	Plywood – Bond Quality – Test methods
	EN 319	1993	Particleboards and fiberboards. Determination of tensile strength perpendicular to the plane of the board. (Internal Bond)
	EN 320	1993	Fiberboards. Determination of resistance to axial withdrawal of screws.
	ENV 1156	2013	Wood-based panels. Determination of duration of load and creep factors
	EN 789	2004	Timber structures – Test methods – Determination of mechanical properties of wood-based panels
	EN 310	1993	Wood-based panels. Determination of modulus of elasticity in bending and of bending strength
Density	EN 323	1993	Wood-based panels – Determination of density
Moisture content	EN 322	1993	Wood-based panels – Determination of moisture content
Moisture resistance	EN 1087-1	1995	Particleboards and fiberboards. Moisture resistance. Part 1: Boil test.
	EN 321	2002	Wood-based panels. Determination of moisture resistance under cyclic test conditions
Biological durability	EN 636	2012	Plywood. Biological durability. Guidance for the assessment of plywood for use in different hazard classes.
	ENV 12038	2002	Durability of wood and wood-based products. Wood-based panels. Method of test for determining the resistance against wood-destroying basidiomycetes.

1.3.2 Service life prediction of wood based materials

In the building sector, service life planning is a key issue to satisfy the safety requirement and control costs. Effective service life prediction is thus crucial in the application of wood based materials. Wood based material can be degraded by wood-destroying insects (*e.g.* beetles and termites), bacteria, fungi, and marine borers. The risk of wood degradation mainly depends on the application conditions. For example, marine borers can only survive in the sea and destroy wood products used in water with sufficient salinity. Decay fungi are ubiquitous and exist everywhere as long as the environmental conditions are suitable for growth. The growth of fungi requires wood substances as nutrient source, so they will decrease the strength of wood materials. The durability of wood based material is significantly impacted by fungal decay and the growth of fungi is an essential factor for service life prediction. Generally, fungi need optimum temperature (25-30 ℃) and MC higher than FSP to transport enzymes. Hence, temperature and MC of wood are the two fundamental parameters to establish service life prediction models. Dose-response functions like the one established by Brischke et al. (2008) are based on wood temperature and wood MC measured using the electrical resistance method to predict the decay rating of wood samples.

Considering the fact that wood MC and temperature is closely related to the rainfall and air temperature during outdoor exposure, the Scheffer Climate Index was established according to the air temperature and the distribution of rainfall (Brischke and Rapp, 2008; Scheffer, 1971).

The decay hazard increases with the value of the climate index. Researchers have mapped the climate index of Canada, China, Europe, Australia and United States according to the history weather data (Brischke et al., 2011; Carll, 2009; Setliff, 1986; Van den Bulcke et al., 2014; Wang et al., 2007). In addition to the aforementioned two models, other adapted models combining with the specified application conditions have also been established (de Freitas et al., 2010; Viitanen et al., 2010).

Up to now, service life prediction studies of wood based products mainly focus on solid wood. Compared to solid wood, the service life of WBP is influenced by more factors such as, adhesive, internal structure and additives. Hence, it is necessary to understand the relation between moisture behavior and structural characteristics of WBP. With aforementioned knowledge at hand, improving the service life prediction of WBP is an objective.

1.4 Techniques applied to investigate the hygro-mechanical performance of WBP

In this research, different techniques were applied to investigate the properties of specimens.

Flexure vibration method

The flexure vibration method has been used to non-destructively measure the mechanical properties of wood based products since several decades (Haines et al., 1996; Moslemi, 1967). The mechanical strength is indirectly calculated based on the vibrational resonance frequency created by impacting specimens when free hanging. Modulus of elasticity can then be calculated with Eq. (1.1) (Yang et al., 2003).

$$E = 4\rho f^2 L^2 \qquad (1.1)$$

With E: the modulus of elasticity (Gpa); ρ: the density of sample (kg/m^3); f: the resonance frequency of vibration; L: the length of the beam sample (m).

The researchers used the vibration method to measure MOE of samples used in diverse conditions. Depending on the results, the possibility of using this vibration method to measure MOE of WBP and grade mechanical strength of solid wood was discussed (Pommier et al., 2013; Wang et al., 2012). A so-called 'Resonalyser' technique was also used to measure the elastic properties based on resonance frequencies and the shape of the specimens (Eq. (1.2)) (Lauwagie et al., 2003).

$$E = 0.946 \times (mf^2/b) \times (l/h)^3 \times A \qquad (1.2)$$

with E: Modulus of elasticity (Gpa); f: resonance frequency for fundamental mode flexural vibration; b: width of the specimens (m); l: length of the specimen (m); h: thickness of the specimen (m); m: mass of the specimen (kg); A: a shape factor.

Electrical resistance moisture content measurement method

Based on the relationship between the MC and electrical resistance, this can be used to measure MC of wood. The changes of electrical resistance with changing MC is large in the region between zero and fiber saturation point (FSP). Above FSP, the changes are relatively small. Specifically, the electrical resistance of oven-dry wood varies between 3×10^{17} and 3×10^{18} Ω cm; it is reduced to 10^8 Ω cm in air dry wood, and to about 10^6-10^5 Ω cm at FSP. In the region between zero and FSP the electrical resistance is reduced more than 10^{11} times, whereas between FSP and maximum MC the reduction is only 50 times (George, 1991). Hence, the electrical resistance method is widely used to measure the MC of wood based materials typically when MC is below the FSP (Brischke and Lampen, 2014; Shupe et al., 2002). Brischke et al. (2008) found that the general MC of wood still can be monitored using electrical resistance method when MC is higher than FSP although the accuracy is decreased. In addition to moisture, electrical resistance of wood is impacted by other factors, such as species, structure, density and temperature (George, 1991). Specifically, the electrical resistance increases with decreasing temperature and decreases as temperature rises. Although wood structure and density varies between species, the species effect on electrical resistance is also related to

differences in chemical (extractive) composition of the wood. In this research, electrical data loggers (Materialfox mini) were used to record MC of the specimens. The formula of converting electrical resistance to MC at 25 ºC is similar with Eq. (1.3) and the real formula is not provided due to the confidentiality.

$$MC = 24376000 \times (10\lg R)^{-3.2451} - 1410.3 \times (10\lg R)^{-0.8121} + 34.5425 \quad (1.3)$$

with MC: moisture content; R: the electrical resistance (Ω cm).

X-ray CT scanning

X-ray CT scanners were first developed for medical applications and now widely used for material science research. X-ray CT scanning is a technology that uses X-ray projections to produce tomographic images (slices) of specific areas of a scanned object, allowing the user to inspect the inside of the object without cutting (Fig. 1.6). The grey scale value of slices corresponds to the X-ray attenuation. The X-ray absorption coefficient is dependent on chemical composition and density of the specimens. After scanning, the computer calculates the X-ray absorption coefficient in each voxel within a slice (Lindgren, 1991). Due to the different attenuation coefficient between wood and air, X-ray CT scanning can reveal the internal structure and density distribution of wood materials (Bergsten et al., 2001; Chen et al., 2010; Freyburger et al., 2009). Moisture distribution can also be calculated (Fromm et al., 2001; Johansson and Kifetew, 2010; Watanabe et al., 2012).
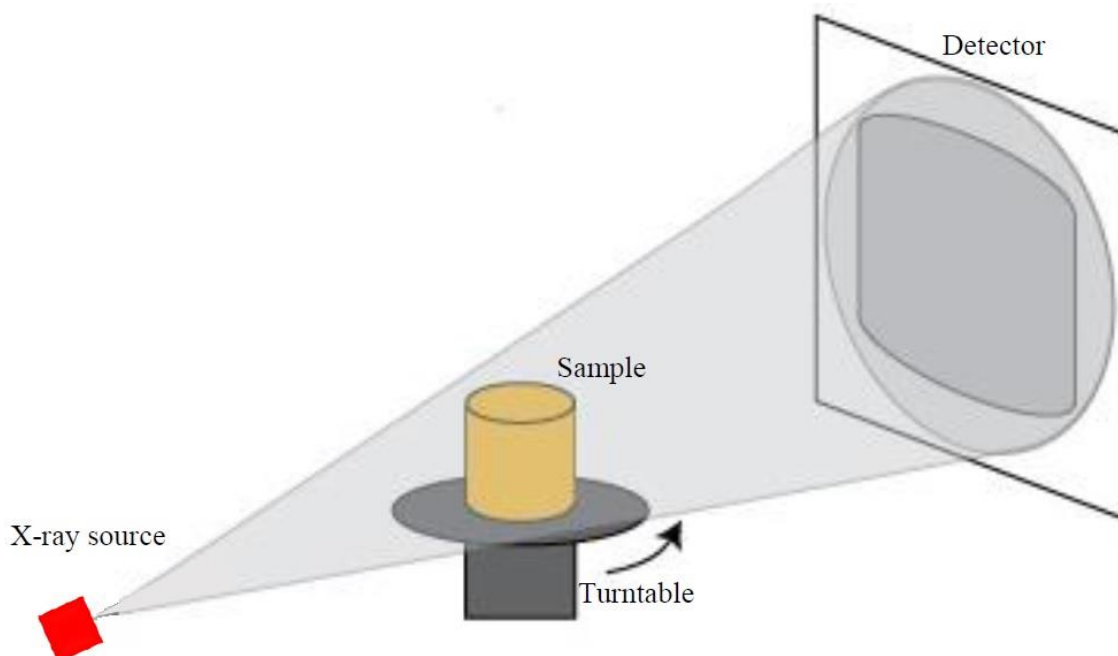

Fig 1.6. Schematic overview of the X-ray CT scanner.

1

X-rays can interact with matter in mainly two ways, i.e. photo-electric absorption and Compton scattering. For a monochromatic X-ray beam, the change in intensity of the beam after passing through an object is expressed by the law of Lambert-Beer (Eq. (1.4)).

$$I = I_0 \times \exp\left(-\int_L \mu_s d_s\right) \qquad (1.4)$$

with I: the measured X-ray intensity at the detector position with an object; I_0: the measured X-ray intensity at the detector position without an object; L: the distance from the source to the detector position; μ_s: the attenuation coefficient at position s.

X-rays are a form of electromagnetic waves with different amplitude, phase and frequency. Mainly two phenomena should be taken into account when scanning objects such as the ones in this PhD: beam hardening and cone beam artefacts.

As only a small piece of the object suffices to stop the low energy photons, the outer layers of the object are attributed an attenuation coefficient which is too high. This induces a high density in the outer layers of the object after reconstruction, which is known as beam hardening (Brabant, 2013). Beam hardening artefacts can be efficiently reduced by, amongst others, filtration and by usage of software tools during the reconstruction.

In laboratory based high resolution tomography, cone beam scanning is commonly used. Cone beam artefacts are induced because less X-rays penetrate the edges in the z direction of the object resulting in unclear images after reconstruction. Cone beam artefacts can be reduced by using helical cone beam scanning or changing source-object and source-detector distance.

Neutron imaging

Neutron imaging is a non-destructive testing method also used in wood science. It is similar to X-ray imaging but with differing sensitivities for different elements. A neutron beam is highly attenuated by hydrogen nuclei (Mannes et al., 2009). It is, therefore, a high-valued method to monitor the moisture behavior of wood materials (Gilani et al., 2014; Nakanishi and Matsubayashi, 1997; Rosner et al., 2012). Due to the high hydrogen content in adhesives used in wood protection and wood based materials production, adhesive distribution in wood can also be visualized with neutron imaging (Lehmann et al., 2005).

1.5 Outline of this dissertation

This dissertation consists of seven chapters. The first chapter is this general introduction. From the second chapter to the sixth chapter, each chapter relates to one research question as described in the first section of the introduction. These five chapters are presented as academic papers published or

at least prepared for publication in peer-reviewed international scientific journals. Chapter 7 is the general conclusion. The outline of this thesis is presented below.

Introduction

Chapter 1 starts with the description of the objectives of this thesis, followed by a literature review of WBP focusing on production and testing. Consequently, the overview of the outline of this thesis is given.

The structural characteristics and moisture transport behavior of WBP

Water sorption can lead to swelling and softening of the wood cell wall when MC is below fiber saturation point (FSP), consequently decreasing the dimensional stability and strength of wood based materials. The presence of free water is a key factor for fungal growth leading to destruction of the structure of the wood cell wall. Investigating moisture behavior is therefore fundamental to improve the physical and biological durability of WBP.

Chapter 2 studies the relationship between moisture transport behavior and structural characteristics of plywood. Neutron radiography and X-ray tomography was applied to monitor the moisture distribution and internal micro-structure of specimens from plywood and related solid wood. According to the findings, suggestions on improving water resistance of plywood by optimizing structural characteristics are given.

Chapter 3 investigates the influence of structural characteristics on the water transport behavior of OSB and MDF. Environmental Micro-CT scanner (EMCT) is used to obtain the micro-structure of specimens and dynamically record moisture distribution. The possibility of improving water resistance of OSB and MDF by optimizing structural characteristics is also discussed.

The moisture behavior of plywood during outdoor exposure

In service, weathering can degrade the performance of WBP, while water uptake is one of the key factors. Moisture distribution is hardly ever homogeneous in WBP during outdoor exposure. Monitoring moisture distribution and detailed structural changes are then essential to improve the performance of WBP when used outdoors.

Chapter 4 explores an adapted electrical MC measurement method to continuously monitor the moisture distribution in WBP. The accuracy of this method is evaluated by comparison with the moisture distribution results obtained with X-ray tomography.

Chapter 5 uses the adapted electrical MC measurement method explored in chapter 4 to monitor the moisture distribution in plywood specimens in service. Combining moisture distribution with the

1

structural changes, the relationship between weathering data and moisture behavior of plywood is attained.

Biological degradation of plywood and MDF

Moisture uptake can induce swelling, lead to fungal decay and consequently decrease the mechanical strength of wood based materials. Understanding the interrelationship of structural changes, fungal decay and the decrease of mechanical strength in moisture conditions is then essential to improve the moisture behavior of WBP.

Chapter 6 studies the mechanical properties variation of WBP after applying in moisture conditions. In order to understand the mechanical strength decrease, mass loss and structural changes of specimens are investigated.

General conclusion and discussion

In chapter 7, I summarize the main findings of this thesis, providing further discussion and give some guidance for future research in this subject.
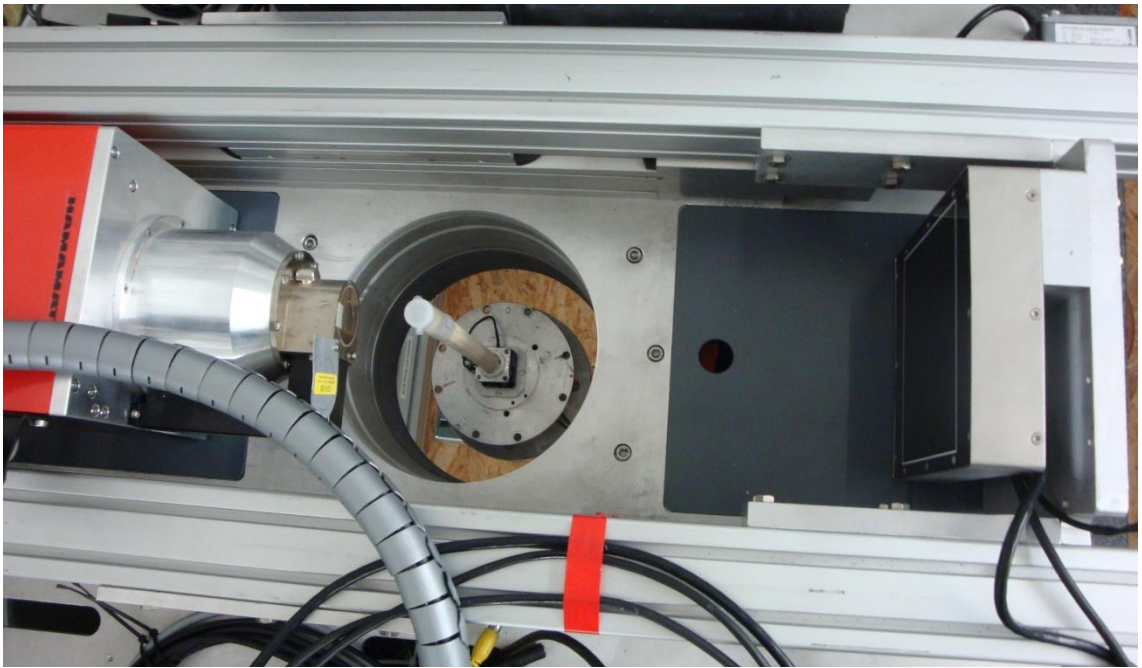
2 Impact of internal structure on water-resistance of plywood studied using neutron radiography and X-ray tomography

2

Abstract

To improve water resistance of plywood, a detailed understanding of the moisture dynamics of plywood and related solid wood is essential. Neutron radiography and X-ray CT were used to monitor water transport and the internal micro-structure respectively. Compared with solid wood, water uptake and release of plywood is, apart from wood species, also influenced by veneer checks and gaps between veneers. Type of adhesive and grain direction of veneers also play a crucial role. According to the findings of this paper and practical requirements, more water resistant plywood can be produced when taking into account abovementioned factors.

2.1 Introduction

Wood is an important construction material with the advantage of being ecologically sustainable and flexible in usage (Issa and Kmeid, 2005). However, as a bio-material, moisture can decrease its physical, mechanical and biological durability. It is thus crucial to understand moisture dynamics in wood products to optimize their usage. The movement of water through wood is complicated by the fact that the coarse capillary system is interconnected via smaller openings. For softwood, tracheids dominate water transport and inter-tracheid pits play an important role on water movement along radial and tangential directions (Comstock, 1970; Domec et al., 2006). Compared with softwood, hardwood has a more complex structure. Water conducting conduits in hardwood are composed of joined vessel elements end to end. Water transport in three dimensions, longitudinal, tangential and radial, of three different softwood species has been investigated by means of neutron radiography before (Sedighi-Gilani et al., 2012). Engineered wood materials, however, can have a different moisture dynamics behavior, obviously still related to the properties of solid wood. Plywood is an important engineered wood material, which is manufactured by gluing solid wood veneers and pressing them together at high temperature. Its mechanical and physical properties are moisture dependent as well (Gerhards, 1982). The water sorption theory in solid wood has been well investigated (Simpson, 1980). Specifically, there are two general forms of water adsorption: part of the water is intimately associated with cellulose molecules and part is distinctly less intimately associated. Sorption isotherms are generally temperature-dependent. As temperature increases, the amount of vapor adsorbed at any given vapor pressure decreases. The water transport theory, however, has been rarely studied in plywood. A thorough understanding of water transport behavior in plywood is valuable to optimize its production and application. The cross layered structure and presence of glue line between layers alters the water movement compared to solid wood. The main water movement directions of plywood are faces and side edges. Hence, it is interesting to investigate the water transport behavior of plywood along these directions and compare it with related solid wood in dynamic water conditions.

To monitor the water distribution in wood products, several approaches have been used. The average MC of plywood exposed outdoors was continuously monitored by weighing (Van den Bulcke et al., 2009c). To further continuously monitor the moisture distribution among layers of plywood, the electrical MC measurement method was introduced by Li et al. (2013). Other state-of–the-art techniques have also been used to monitor water movement in wood and wood-based products, *e.g.* magnetic resonance imaging, X-ray CT scanning and neutron imaging. Magnetic resonance imaging allows monitoring the free water movement in wood materials (Meder et al., 2003). Research with X-ray CT scanning revealed the internal structure and density distribution of wood materials (Chen et al., 2009; De Ridder et al., 2011a). Compared with the above two approaches, neutron imaging is

more suitable to determine moisture distribution due to the high attenuation of the neutron beam by hydrogen nuclei (Mannes et al., 2009; Pleinert and Lehmann, 1997).

The objective of this paper is to investigate the water distribution in plywood and related solid wood during water uptake and air drying in climatized conditions. Several specimens of plywood and solid wood were prepared and scanned with X-ray CT in order to obtain a 3D view of their internal structure. Water uptake and air drying was then periodically monitored by neutron radiography. For solid wood, liquid water uptake in longitudinal, radial and tangential direction of three different hardwood species was monitored. For five different plywood panels glued with PF and UMF, liquid water uptake / air drying from the faces and the side edges was monitored and quantified. To better investigate the difference in moisture dynamics between plywood and solid wood, all plywood panels are uncoated. The relationship between water distribution and the microstructure of the specimens was analyzed by combining the data from neutron radiography and X-ray CT scanning. The classical uptake / air drying test was performed on three replicates of the five plywood panels under study to evaluate the results obtained by neutron radiography and X-ray CT scanning.

2.2 Materials and methods

2.2.1 Preparation of the specimens

Solid wood specimens were prepared from three different hardwood species: poplar (*Populus* spp.), birch (*Betula* spp.) and okoumé (*Aucoumea klaineana* Pierre). For each species, three $25 \times 10 \times 10$ mm^3 specimens were sawn in longitudinal, tangential and radial direction and 25 mm along the water uptake direction. Plywood panels were produced by European plywood companies. Two specimens from each plywood panels (Table 2.1), were cut to the size of $10 \times 30 \times$ (panel thickness) mm^3 and $10 \times 10 \times$ (panel thickness) mm^3 (Fig. 2.1) respectively. For laboratory water dynamics test, three replicates of each plywood panels measuring $50 \times 50 \times$ (panel thickness) mm^3 were prepared. All specimens were without knots, decay or any obvious defects. The four sides of each specimen, parallel to the water uptake direction, were sealed with a two component polyurethane sealant to ensure that water uptake was only possible in a single direction.

Table 2.1

Structure of the plywood panels.

Code	Wood species	Glue	# of plies	Veneers(mm)	Thickness(mm)	Coating
P1	poplar	UMF	7	1.3/2.6/2.6	14.9	no
P2	poplar	PF	7	1.0/2.5/2.8	14.6	no
B1	birch	PF	11	1.4/1.4/1.4	15.0	no
B2	birch	PF	11	1.9/1.4/1.45	15.7	no
O1	okoumé	PF	7	1.3/3.0/2.0	15.2	no

PF: phenol formaldehyde glue; UMF: urea melamine formaldehyde glue.

Veneer thickness: top veneer/inner cross/ inner parallel.
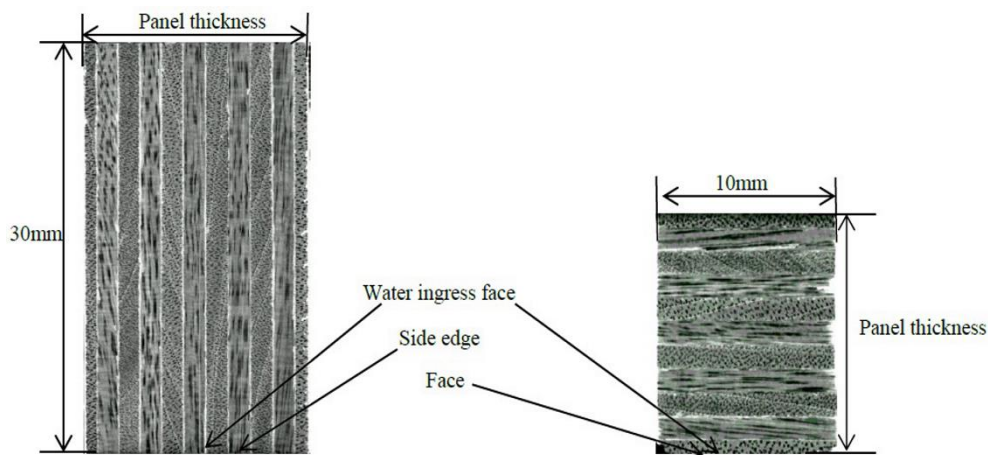
Fig 2.1. X-ray CT cross-section of birch plywood for water uptake testing through side edge (left) and face (right).

Plywood is manufactured by cross-gluing veneers together. The veneers are cut (peeled) perpendicular to the grain with the knife parallel to the grain (Walker, 1993). As such, the water ingress direction of the veneers is longitudinal and tangential when water penetrates from a side edge of plywood. If water is absorbed from the face, the radial direction in veneer is the water ingress direction (Fig. 2.2).

Fig 2.2. Schematic overview of directions in solid wood and plywood. L = longitudinal direction, T = tangential direction, R = radial direction.

2.2.2 Neutron radiography and experimental procedures

For this experiment, the Neutron Transmission Radiography (NEUTRA) beam-line of the Paul Scherrer Institute (PSI) in Villigen, Switzerland was used. The same beam-line was utilized as described in Sedighi-Gilani *et al.* (2012). Fig. 2.3 shows an overview of the experimental setup, in which 4 specimens were mounted in a custom-made aluminum sample holder. The detector consisted of a scintillator CCD camera system and a field of view of 70.5×70.5 mm^2 was applied in this experiment. The distance between specimens and detector needs to be as short as possible to minimize the effect of geometrical unsharpness (Lehmann et al., 2007) . Therefore the specimens were positioned in front of the detector at a distance of approximately 10 mm. The water container underneath the specimens was filled with demineralised water and positioned on a z-translation stage. The height of the water container could be adjusted by remotely controlling the height of this stage. The exposure time was 30 s per radiography with an approximate resolution of 68 μm/pixel.
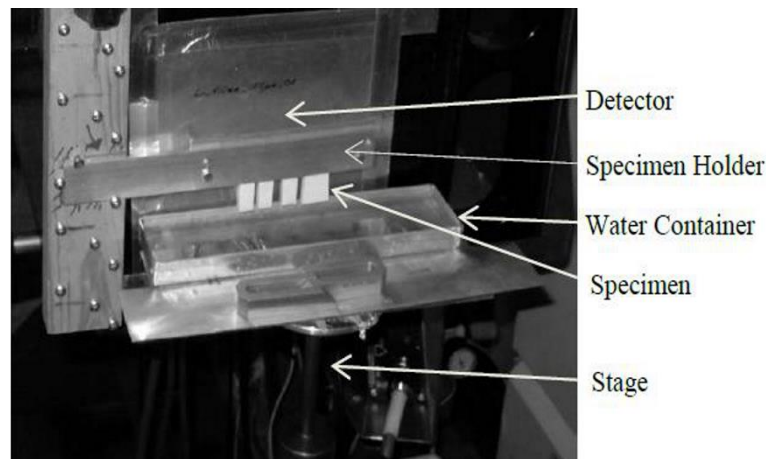

Fig 2.3. Overview of the experimental setup for neutron radiography.

Before water uptake, a neutron radiograph of the specimens was acquired. Next, the water container was lifted such that the bottom of the specimens was in contact with the water surface. Water uptake was monitored for a period of 20 min taking a radiograph every 40 s. The specimens were then removed from the beam line and uptake water continued in a similar setup in an acclimatized room for several hours. During these periods neutron radiographies were taken periodically. Plywood specimens were monitored after approximately 2, 3, 7 hours of water uptake for the side edge experiment and after approximately 1.5, 4.5, 16.5, 25 hours for the face water uptake. For solid wood, specimens were scanned after approximately 1, 3, 5.5, 10 hours of water uptake. After water uptake, all specimens were removed from the water and air drying started. The plywood specimens were scanned after approximately 2, 5, 13.5 hours of air drying for the side edge experiment and 1, 2, 3 hours of air drying for the face experiment respectively.

2.2.3 X-ray scanning and image processing

Before water uptake, all specimens were scanned with HECTOR, the latest system developed by the Ghent University Centre for X-ray Tomography (www.ugct.ugent.be) in collaboration with X-Ray Engineering (XRE bvba, Ghent, Belgium) (Masschaele et al., 2013). The voxel pitch of the reconstructed grid is approximately 30 µm. To acquire further detailed data on the microstructure of a selection of specimens and explain some of the observed phenomena, the Nanowood CT scanner (Dierick et al., 2014), also built at the Ghent University Centre for X-ray Tomography, was used to scan regions of interest of specimens during a second water uptake experiment, after the neutron experiments. The specimens were in contact with demineralized water in the same direction as in the neutron experiments. They were removed from the water after 0, 10, 20, 60 and 120 minutes and scanned. To avoid drying, the scan time was optimized to 8 minutes per specimen. Only the region close to water uptake face was scanned, with a resolution of approximately 20 µm. In order to obtain vessel size of solid wood specimens, the Nanowood CT scanner was also used to scan them with a resolution of approximately 7 µm. Reconstruction of all samples was performed using the construction software Octopus (Vlassenbroeck et al., 2007b).

2.2.4 Water content quantification with neutron radiography

Neutron radiography is based on measuring the intensity of the neutron beam after transmittance through an object. Hence, water content could be calculated using the similar method described in Sedihgi-Gilani *et al.* (2012).

$$I = I_0 \cdot e^{-\Sigma \cdot Z} \qquad (2.1)$$

with I: intensity of the transmitted beam; I_0: intensity of the incident beam; Σ: the attenuation coefficient per unit of material; Z: the total thickness of the object along the beam direction.

In this experiment, to calibrate and evaluate the accuracy of neutron radiography for measuring water thickness, an aluminum water step wedge was always positioned in the field of view during the experiment. The step wedge is composed of aluminum and contains five different water steps, *i.e.* 0.5mm, 1mm, 1.5mm, 1.75mm, and 2mm (Fig. 2.4). The object between the neutron beam and detector consists of wood, water and an aluminum holder. Eq. (2.1) is thus adapted as follows:

$$I_{(wet)} = I_{(dry)} \cdot e^{-\{\Sigma_h \cdot Z_h + \Sigma_a \cdot Z_a\}} \qquad (2.2)$$

The water thickness can be calculated as:

$$Z_h = -\left[\ln(I_{(wet)}/I_{(dry)}) + \Sigma_a \cdot Z_a\right] / \Sigma_h \qquad (2.3)$$

with $I_{(wet)}$: intensity of the transmitted beam with water in water step wedge; $I_{(dry)}$: intensity of the transmitted beam with no water in water step wedge; Σ_h: the attenuation coefficient per unit of water;

$\sum_a$: the attenuation coefficient per unit of aluminium; Z_h: the thickness of water along the beam direction; Z_a: the thickness of aluminum along the beam direction.

$$I = I_0 \cdot e^{-\{\sum_w \cdot Z_w + \sum_h \cdot Z_h + \sum_a \cdot Z_a\}} \qquad (2.4)$$

with $\sum_w$: the attenuation coefficient per unit of wood; Z_w: the thickness of wood along the beam direction.
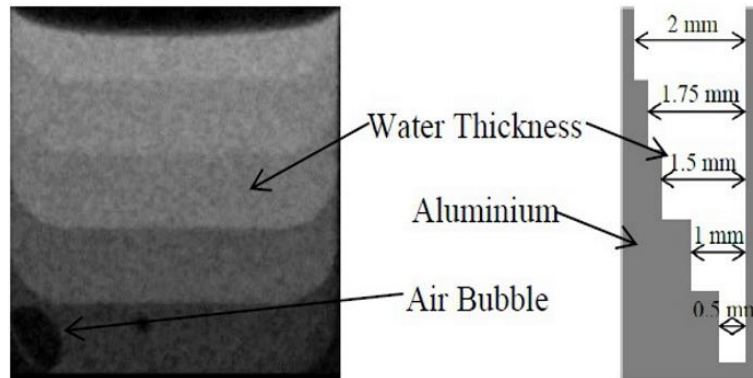

Fig 2.4. Neutron radiography image of step wedge filled with water (left) and illustrated cross-section of step wedge (right).

The change in thickness of the specimens in the direction parallel to the neutron beam was assumed to have little influence on water content calculation. As such, the wood and aluminum between the neutron beam and detector is constant in this experiment. At a certain time t of the experiment, with respect to the initial situation, the variation in beam intensity is ascribed to water ingress. Water content is thus considered as the only change in the specimens, which is equivalent to the water thickness change. In this case, water thickness at a certain moment in time could be calculated by comparison with the initial neutron radiography before the start of water absorption. Eq. (2.4) can be rewritten as:

$$I_{(t)} = I_{(initial)} \cdot e^{-\{\sum_h \cdot Z_{h(t)}\}} \qquad (2.5)$$

with $I_{(t)}$: intensity of the transmitted beam at time t; $I_{(initial)}$: intensity of the transmitted beam before absorption; $Z_{h(t)}$: water thickness in the specimen at time t.

To acquire the water thickness and water content at a certain moment, Eq. (2.5) is changed to:

$$Z_{h(t)} = -(1/\sum_h) \cdot \ln[I_{(t)}/I_{(initial)}] \qquad (2.6)$$

$$W_{(t)} = -[\rho_h/(Z_s \cdot \sum_h)] \cdot \ln[I_{(t)}/I_{(initial)}] \qquad (2.7)$$

with $W_{(t)}$: the water content in the specimen at time t (kg/m^3); ρ_h: density of the water (kg/m^3); Z_s: thickness of the specimen along the neutron beam direction.

The raw neutron images need to be corrected before analyzing due to the artifacts induced by the experimental configuration. The Quantitative Neutron Imaging (QNI) software package was used to correct the images and quantify the water content (Hassanein et al., 2006). To optimize the result, following steps were applied:

1. Image correction by using QNI to decrease artifacts *e.g.* dark current and flat field correction, background scattering and sample scattering correction.

2. Image spot filtering using ImageJ.

3. In order to decrease the error caused by wood swelling and shrinkage, image registration was performed using ImageJ's plugin UnwarpJ (Watanabe et al., 2012). The initial image was applied as the target image.

4. Dividing registered image by initial image using ImageJ.

5. Water visualization and quantification using QNI.

The background of the camera and a hit on the detector by a γ-particle causes noise in neutron radiography. It is thus hard to distinguish small amounts of water. Hence, the grey scale value below 20 kg/m^3 was not taken into account during data analysis.

2.2.5 Laboratory water dynamics test with precision balance

A set of specimens was used to simulate the in-service water uptake and release as well as to compare these data with the calculation of neutron imaging. The specimens were conditioned at standard climate conditions (65% RH and 20℃) until mass constancy was reached. Next, one face of specimens was immersed for 144 hours in a container filled with demineralized water. During this period, the specimens were weighed after 0, 1, 4, 8, 24, 48, 72, 144 hours of immersion. After immersion, the specimens were taken out of water and placed in a conditioning room for 168 hours. The specimens were weighed after 0, 1, 4, 8, 24, 48, 72, 144, 168 hours.

2.3 Results and discussion

2.3.1 Evaluating the water thickness determined with neutron radiography

The water thickness of the step wedge based on neutron radiography was calculated according to neutron radiography images. Fig. 2.5 shows a strong linear relationship ($R^2 = 0.991$) between the actual and calculated water thickness, which proves neutron radiography can accurately calculate

water thickness. This result has also been proven by weighing the specimens before and after a water uptake test by Sedighi-Gilani et al. (2012). In this experiment, we did not weigh specimens because the specimens needed to be fixed in the sample holders. Such fixed position design is helpful for switching the specimens during neutron scanning and processing neutron images afterwards, as well as avoiding change of specimens in the sample holder during long-term recording of water movement. The differences at lower water thickness are more pronounced, probably induced by an imperfect step wedge design due to manufacturing difficulties, which can be enlarged at lower water thickness. A smaller quantity of water could also increase the error caused by a fluctuating beam line, noise correction, *etc*.
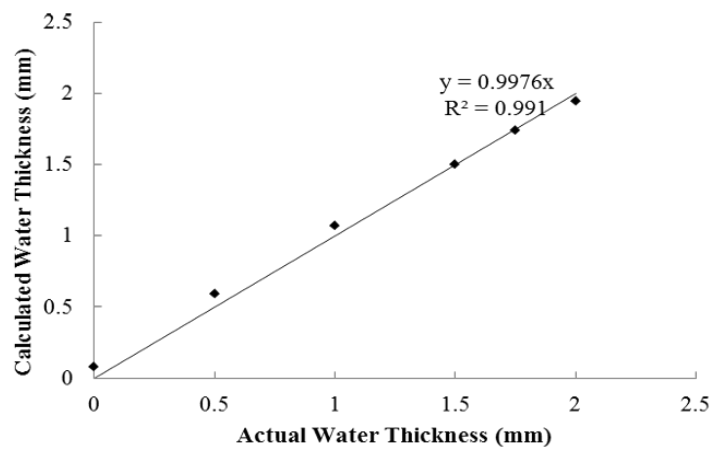

Fig 2.5. Relationship between actual and calculated water thickness of a step wedge.

The water content in the specimens was calculated using the registered radiography image. The registration, however, might induce small errors in the calculated total water content in specimens because the grey scale value of the pixels is not corrected accordingly. The approximate swelling of specimens was calculated according to their width variation in neutron images (Eq. (2.8)). The swelling in both solid wood and plywood specimens is less than 5.5% (Table 2.2). The influence of registration on water content calculation is thus minimal allowing interpretation of water distribution during uptake and release.

$$N = (W_m - W_i) / W_i \qquad (2.8)$$

with N: swelling of the specimen after water uptake (%); W_m: the maximum width of the specimen after water uptake (mm); W_i: the initial width of the specimen before water uptake (mm).

Table 2.2

Swelling of specimens in radial direction (thickness of plywood).

Specimens	Poplar	Birch	Okoumé	P1	P2	B1	B2	O1
Swelling (%)	2.9	3.5	1.5	1.9	3.8	5	5.5	2.2

2.3.2 Comparing water transport in solid wood and related plywood

In order to study water transport behavior in plywood, investigating water transport behavior in solid wood is essential. The water uptake in three wood species under study is discussed here first. Fig. 2.6 shows that the water front moves approximately 2.5 mm into the solid poplar wood specimen after 5.5 hours of water uptake. This result is consistent with the results obtained by using X-ray CT scanning (Li et al., 2013). Water uptake in birch is much faster than in poplar and okoumé, which could be caused by its higher density. Density and moisture uptake are closely interrelated (Christian et al., 2013; Li et al., 2013). The high density, low porosity latewood becomes moisture saturated earlier than earlywood in water absorption test (Sedighi-Gilani et al., 2014). Hardwood species with high density have a high probability to have small cell lumens possibly acting as the preferential pathways for water transport in the longitudinal direction. Water transport through vessels passes from one vessel to another via pores or perforations. These pores are usually aggregated into what is termed a perforation plate that consists of simple perforation plate and multiple perforation plate. These perforation plates increase water flow resistance (Schulte and Castle, 1993). Higher capillary pressure, as expected in wood with small cell lumen, would then promote water transport through vessels that are connected with perforation plate. The consistent results and explanation were also described in Sedighi-Gilani et al. (2012), in which fast water movement was detected in latewood in comparison to earlywood. In addition to vessel size, the anatomy of the perforation plates could influence water movement speed. The perforation plates in birch, poplar and okoumé are scalariform, simple and simple respectively. When water is wicked across the scalariform perforations, continuous gas space is divided into smaller bubbles—one to each vessel element. These smaller packages may dissolve more rapidly than fewer, larger bubbles in refilling vessels with simple perforation plates (S. Sperry, 2003). Therefore, scalariform perforation plates in birch could decrease air pressure and increase water transport speed in vessels. Still, given the complex structure of wood, more experimental work is needed to explain the different phenomena of water transport in wood in detail.
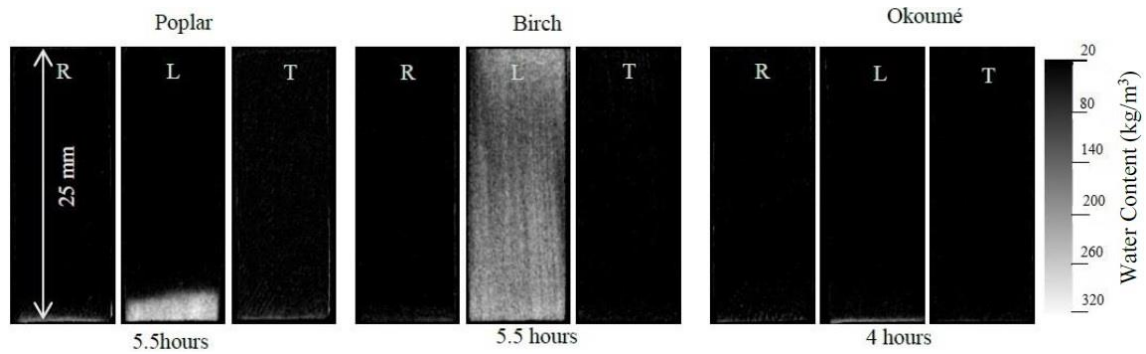
Fig 2.6. Water distribution in three solid wood species along three different directions after several hours of water uptake.

In order to test a possible contribution of capillary pressure, high resolution X-ray CT scanning was used to acquire detailed cross section images of solid wood specimens (Fig. 2.7). Twenty vessels from each wood species were randomly chosen to calculate average vessel size listed in Table 2.3. Because birch has the smallest vessel, water uptake height in birch is higher than poplar and okoumé in the longitudinal direction. As the above analysis shows, water uptake height in hardwood negatively relates with the vessel size. Due to the complex structure of wood, many factors can also influence water uptake rate. The flow of water through the vessel structure in response to the pressure gradient. Water, however, can also migrate across cell walls by diffusion through pits and ray cells (Walker, 1993). The number of vessels of the three wood species was also determined on the X-ray CT scanning (Table 2.3). Poplar has more vessels and larger vessel size than birch, which means more lumen space for free water presence. Hence, for poplar, water content near the water uptake face is higher. For all three wood species, however, little water can move in radial and tangential direction (Fig. 2.6).
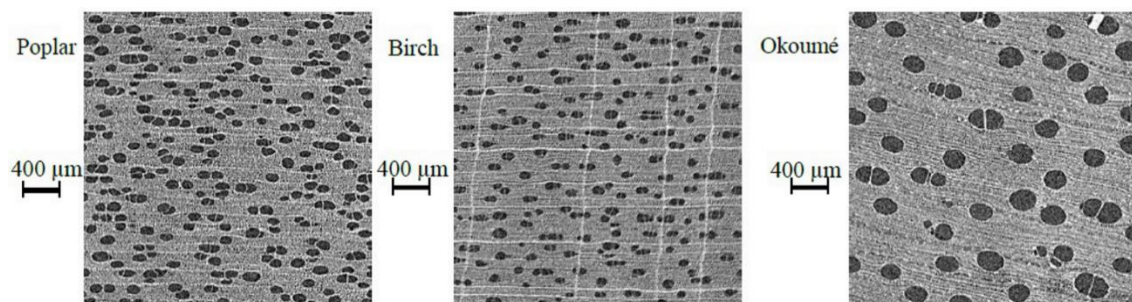

Fig 2.7. High resolution X-ray CT cross section of three different wood species.

Table 2.3

Density and vessel features of the three wood species analyzed (average values).

Wood species	Birch	Poplar	Okoumé
Density (kg/m^3)	620	400	370
Vessel radius/ St. Dev (µm)	56.7/9.2	66.8/14.3	121.4/15.8
Number of vessels	1640	1720	360

Note: The density of the specimens was measured after conditioning at 65% relative humidity and 20 °C. Number of vessels means the amount of vessels per cm^2.

The knowledge of water movement in solid samples can help in explaining differences between plywood specimens under investigation. First, it should be noticed that, as shown in Fig. 2.8, an artefact is seen in the location of the glue lines, caused by an imperfect registration. When performing registration of two images, small positional inaccuracies are pronounced especially at glue layers. The amount of hydrogen nuclei between adhesive and wood substance is different, as such the neutron attenuation coefficient is also different. Hence, a small shift of the glue line could induce an error in comparing the target image to the registered image. This error is then, incorrectly, perceived as water (Fig. 2.8).

Wood species, naturally, plays an important role in water resistance of plywood. Compared with poplar and birch plywood, water uptake in okoumé plywood is minimal (Fig. 2.8). It is obvious that water resistance could be improved by using wood species with good water resistance to produce plywood.

Due to the layered structure, water can easily move along the even layers in this set up and is rarely absorbed by the odd layers of plywood during water uptake alongside edges (Fig. 2.8). Water can penetrate the entire longitudinal layer within approximately two and half hours (Fig. 2.8 P1) while the water front only moves 2.5 millimeters into the solid wood within 5.5 hours (Fig. 2.6 poplar). Several plausible reasons for this difference can be put forward. It is possible that the production process of plywood, *i.e.* pressing at high temperature, increases the permeability of plywood, partially explaining the increased water uptake. Thermal treatment (approximate 6 minutes at 130 ℃), however, can increase crystallinity and hydrophobicity of wood thus decreasing the permeability (Follrich et al., 2006; Yildiz and Gumuskaya, 2007), which is the opposite of higher water uptake.
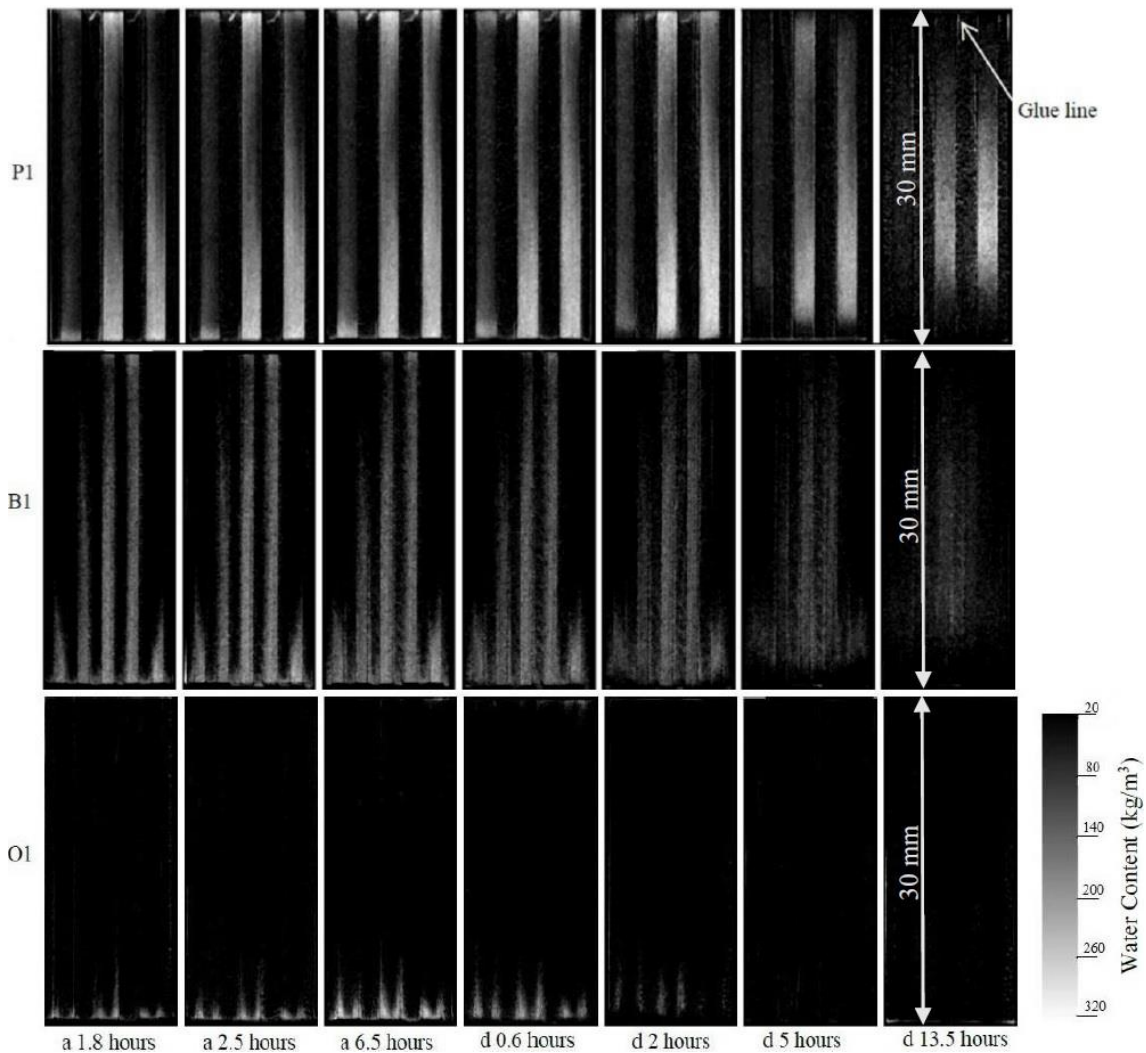
2

Fig 2.8. Water distribution of plywood during water uptake (a) and air drying (d) from the side edge.

The microstructure in plywood can differ from the solid wood microstructure due to the plywood manufacturing process, possibly inducing checks and cracks. Water, therefore, can easily penetrate the longitudinal layers of plywood along these checks. To prove this hypothesis, the microstructure of specimens was investigated using the Nanowood X-ray CT scanner. Compared with poplar solid wood, several distinct checks were found in poplar plywood, which could be induced during veneer peeling or plywood pressing (Fig. 2.9). Since water is the only factor changing the X-ray absorption, the difference before and after water uptake can be seen as whitening of the images. In order to investigate the detailed water distribution, cross sections of entire specimens are shown as well as a magnification of the central region (Fig. 2.9). Most of the water is found in checks or distributed near checks, as shown in Fig. 2.9 for poplar plywood. In solid wood, however, only a small amount of water was found in and nearby vessels. Veneer checks are thus the main reason for an increased water uptake in plywood. Reducing the amount of checks in veneers would be a crucial step to increase water resistance of plywood.

Another phenomenon can be identified when looking at O1 in Fig. 2.8, where water seems to accumulate near the glue line of okoumé plywood. This could be the result of imperfect gluing between veneers. It is indeed hard to combine two separate veneers without any gaps between them. Small gaps near the glue line could induce water uptake. It is well known that the vessel size of okoumé is larger, which makes it difficult for the adhesive to fill them entirely. Gaps, therefore, are present between two veneers as shown in Fig. 2.9 for okoumé plywood. By comparing the X-ray images obtained before and after water uptake, it was found that more water appeared in gaps and nearby vessels. This seems to stress the importance of gluing in order to minimize the gaps between veneers. Veneer checks are also an additional reason for water transport in okoumé plywood (Fig. 2.9).
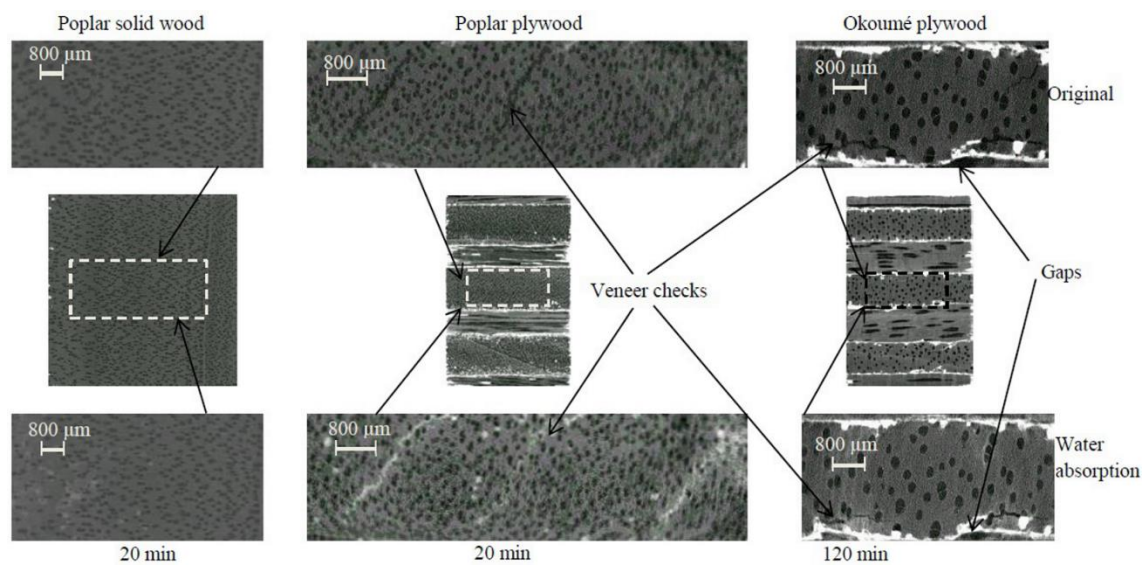

Fig 2.9. Microstructure of poplar solid wood, poplar plywood and okoumé plywood obtained by X-ray CT scanning before (top) and after (bottom) water uptake.

2.3.3 Plywood specific behavior in dynamic moisture conditions

To investigate the plywood specific behavior in dynamic moisture conditions, the water uptake from face and side edge of plywood was studied shown in Fig. 2.10 and Fig. 2.11 respectively. For water uptake from the face, the average water content of the first three layers from face onwards, was calculated based on the neutron radiography experiment. Results are shown in Fig. 2.10. In order to avoid the influence of the glue line, the middle region of each layer was used to calculate the water content.
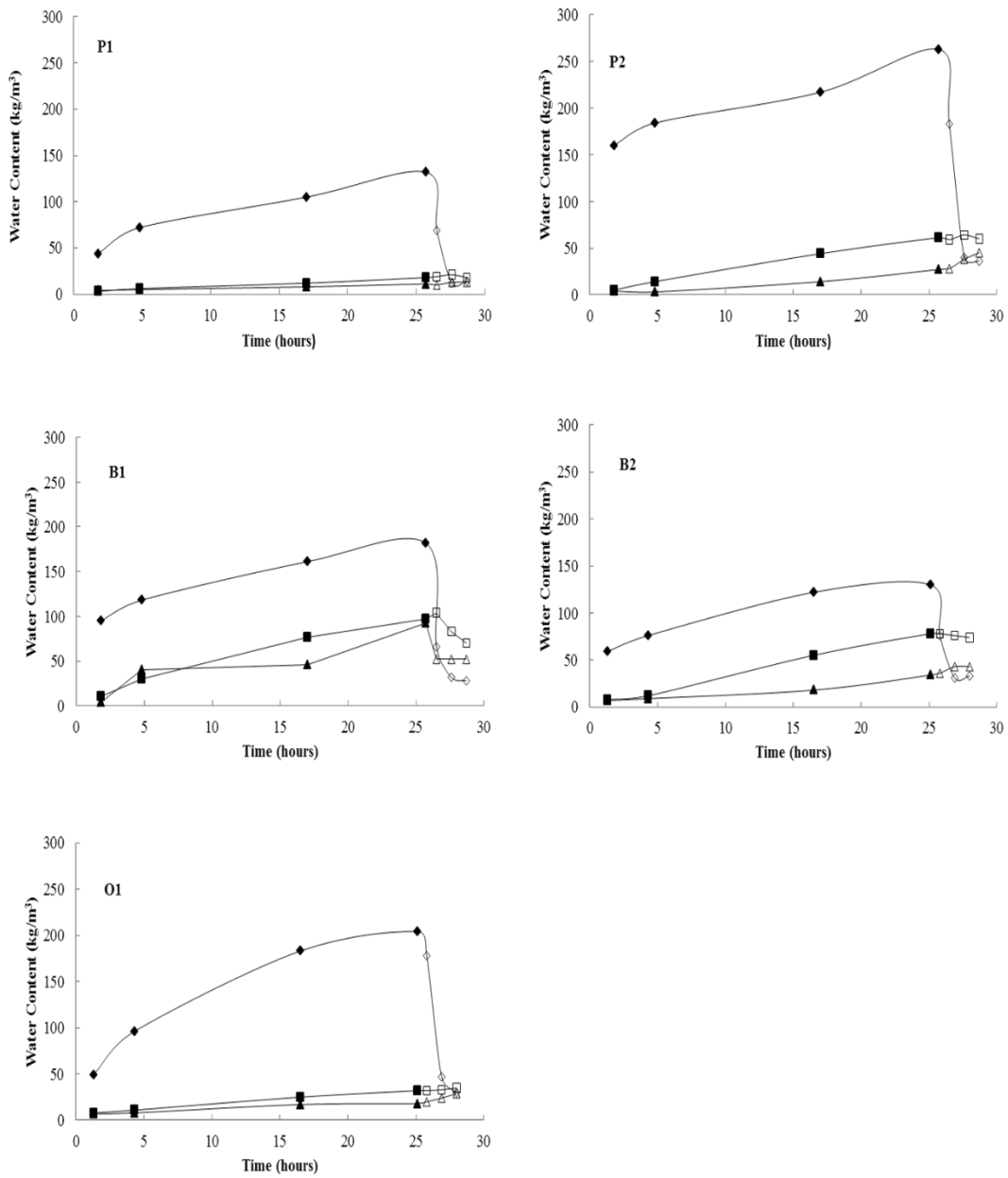
2

Fig 2.10. Water distribution among layers of plywood during water uptake and air drying from the face. ♦ = 1st layer water uptake, ◊ = 1st layer air drying, ■ = 2nd layer water uptake, □ = 2nd layer air drying, ▲ = 3rd layer water uptake, △ = 3rd layer air drying.
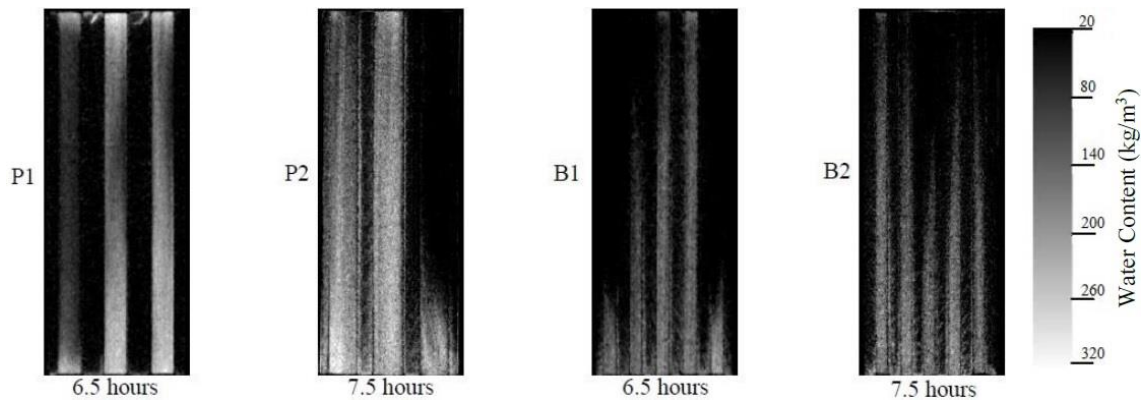
Fig 2.11. Water distribution after uptake from the side edge.

Influence of the top veneer

B1 and B2 are only different in top veneer thickness. The grain direction of the top layer of B1 and B2 was investigated in detail and no clear difference was found. Fig. 2.10B1 and 10B2 illustrate that water content in the layers just beneath the top layer is lower when the thickness of the top layer is higher. The thick top layer acts as a barrier so it takes more time for water to penetrate it and reach the glue line. As is shown in Fig. 2.10, the water desorption rate of the top layer is fast so water can only reach the inner layers of plywood when long-term continuously water uptake occurs. The thick top layer, however, can induce glue rupture in cyclic moisture sorption-desorption, which could increase water uptake. As such, the thickness of the top layer needs to be carefully fit the purpose.

Influence of the adhesive

Compared with other wood-based products, plywood has clear and integral glue lines. The performance of these glue lines plays an important role in the performance of plywood. In this experiment, specimens were selected from panels glued with the two most widely used adhesives, *i.e.* PF and UMF. For the side edge water uptake test, most of the water is trapped in the layers with longitudinal direction (Fig. 2.11P1). Water penetrates glue lines and moves to the nearby layers with lower water content (Fig. 2.11P2). Although the PF glue line is a strong moisture barrier, it is more permeable for water than UMF. Consistent results have been acquired by continuous weighing plywood in outdoor conditions (Van den Bulcke et al., 2009c). It is thus better, in practical outdoor applications, to use UMF as adhesive of face layers. Water uptake can then be hindered more efficiently at the first glue line, which would keep inner layers at a low moisture level.

Water desorption in the second and third layer is much slower than the top layer because of the presence of the glue line, acting as a barrier. Below fiber saturation point, the mechanical strength of wood decreases with increase in MC (Gerhards, 1982). Water entrapment in these layers could thus decrease the mechanical properties of plywood. The risk of delamination of plywood could also

increase in this condition. Layers just beneath the face layer, with moisture content at a high level for a considerable long time, can be subject to fungal decay.

Influence of the grain direction of veneers

Water moves along the radial direction when water uptake is from the face of plywood (Fig. 2.2). As shown in Fig. 2.10, water can cross the first layer of plywood, then reach the second layer and even the third layer. However, according to above results on solid wood, water cannot easily move along the radial direction for all three hardwood species. Veneer checks induced during plywood production could increase the permeability. Furthermore, an imperfect radial direction also could induce an increased water uptake, which is the case for the first layer of P1 and the second layer of B1 (Fig. 2.12). Water is thus transported along vessels and reaches the next layer. Therefore, a carefully selected veneer with parallel grain direction to face could increase the water resistance of plywood.
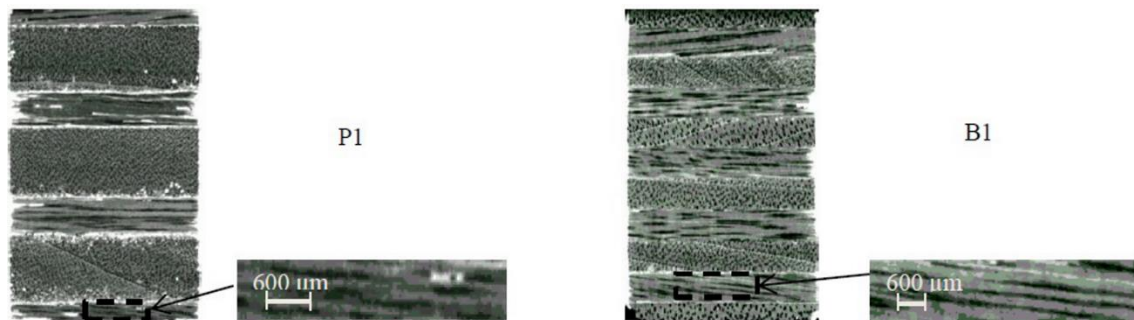

Fig 2.12. X-ray CT cross-sections of plywood and detailed microstructure of veneers.

In general, water can easily move in longitudinal direction, however, the speed of water movement is different (Fig. 2.11). The internal structure of layers with slow water movement was shown in Fig. 2.13 and grain direction of these layers is tilted and not parallel to the glue line. In these layers, therefore, water needs to move along the mixed longitudinal and radial direction, which could decrease the speed of water movement. According to this theory, the water uptake from side edges could be decreased by using veneers with non-parallel grain direction to the face.

It is generally recommended to seal the edges of large plywood panels when applying them in challenging moisture conditions. The fact, however, is that plywood panels are not always sealed properly in practice. It is thus necessary to produce plywood with good water resistance performance on side edges by using veneers with non-parallel grain direction. Such orientation, however, also influences the mechanical strength of plywood. Generally speaking, the mechanical strength of plywood is mainly dominated by the outer layers (Simpson and TenWolde, 1999). Hence, it would be possible to produce plywood panels with qualified strength properties if the grain direction of the outer layers is parallel. The panels with qualified strength properties as well as better water resistance

could be produced by applying parallel and non-parallel grain direction veneers as outer and inner layers of plywood respectively. In practice the veneers could be scanned in-line during peeling or transportation using an X-ray radiography scanner to classify the veneers according to grain direction.
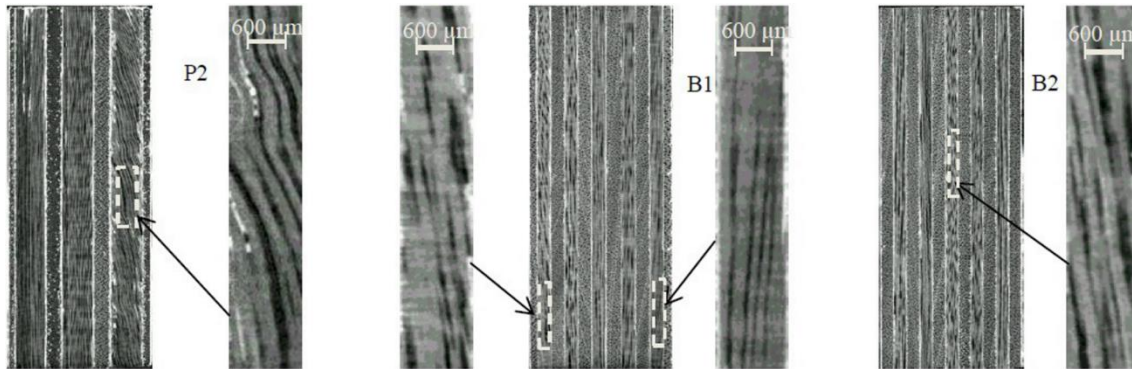

Fig 2.13. X-ray CT cross-sections of plywood and detailed microstructure of veneers.

2.3.4 Laboratory water dynamics test

The results of laboratory water uptake and release test are presented as water content in function of time to keep this comparable with the results of neutron radiography (Fig. 2.14). For the calculation, the specimens' volume is assumed to be constant. As shown in Fig. 2.14, the speed of water uptake in P1 is much slower than the others, which indicates that the glue line plays the most crucial role on increasing water resistance of plywood. With the same PF glue line, O1 absorbs less water so the wood species also plays an important impact on water resistance of plywood (Fig. 2.14). Compared with B2, both water uptake and release in B1 is slightly faster (Fig. 2.14). This result concords with the result from neutron radiography. For B1, the thin top layer and non-parallel grain direction of the second layer causes higher water uptake. Hence, the top layer thickness has an influence on the water resistance of plywood but not as large as glue line and wood species. In current plywood manufacturing, plywood panels may be surfaced with coating metals, plastics, or other materials, or their veneers may be impregnated to achieve resistance against water and microorganisms (George, 1991). Compared with these methods, it is more environmentally friendly and economic to select a top veneer with parallel grain direction, suitable thickness and possibly of a wood species already performing well in dynamic moisture conditions.
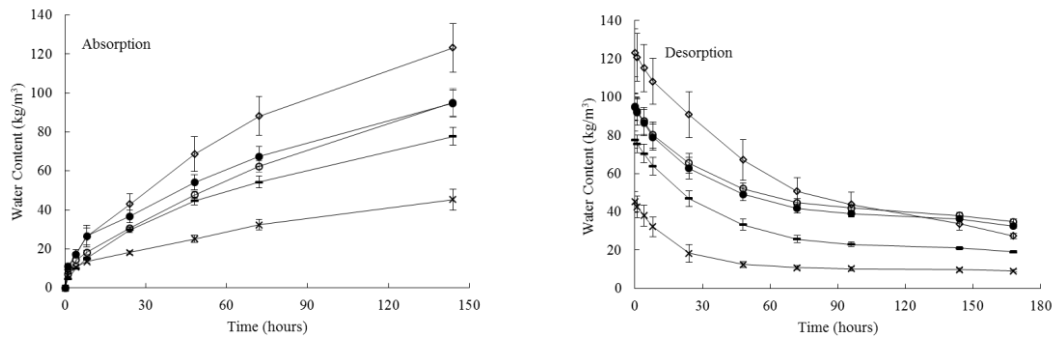
Fig 2.14. Water content of plywood during water uptake and release of laboratory test. × = P1, ◊ = P2, ● = B1, ○ = B2, ▬ = O1.

2.4 Conclusion

Combining neutron radiography and X-ray tomography is an efficient way to investigate water resistance of plywood. Compared with solid wood, the checks in veneers and gaps between veneers could increase water uptake in plywood. Plywood specific factors such as adhesive and grain direction of veneers obviously impact the water resistance. UMF has a better water resistance profile than PF. Veneers with non-parallel grain direction to face can decrease the face water resistance but can increase side edge water resistance of plywood. In-line scanning by means of X-ray radiography could be a helpful means for classification of veneers according to grain direction. To improve the water resistance of plywood, it is helpful to produce plywood by using wood species with good water resistance. The grain direction of the top veneer should be controlled to be as parallel as possible. Using an adhesive with effective water resistance to glue the top veneer to the plywood is important. The findings of this paper have to be combined with practicalities such as the price of the adhesive and wood material, as well as the application requirements.

The relationship between veneer grain direction and the mechanical properties of plywood needs to be investigated especially considering inner veneers. This approach will be used to investigate water distribution in other laminated wood-based panels, *e.g.* MDF (medium density fiberboard) and OSB (oriented strand board). Based on the results of this paper, the first steps towards a moisture kinetics model of plywood will be taken.

Acknowledgment

2

3 Investigating water transport in MDF and OSB using a gantry-based X-ray CT scanning system

Wanzhao Li, Jan Van den Bulcke, Thomas De Schryver, Joris Van Acker. Investigating water transport in MDF and OSB using a gantry-based X-ray CT scanning system. Wood Science and Technology (Under review)

3

Abstract

Both medium density fiberboard (MDF) and oriented strand board (OSB) are important engineered wood products. Water uptake can decrease their physical and mechanical properties as well as induce fungal decay. It is therefore essential to understand the water transport behavior in these products in detail. In this research, a state-of-the-art gantry-based X-ray CT scanner was used to investigate the water transport and the internal micro-structure of the specimens from different types of MDF and OSB during water uptake. The results show that water, obviously, is mainly absorbed from the sides of all specimens during immersion testing. Water can reach the interior of the small specimens within one hour through large fibers and strands. Although water movement through voids is slow, a high water content can be reached when these voids are filled, *e.g.* a moisture content (MC) of more than 100% is found in MDF. A compact structure can effectively decrease water accumulation in voids. Furthermore, presence of a water resistant adhesive, a water repellent additive and acetylated fibers clearly influence water transport behavior in wood fibers and voids, increasing water resistance and improve structural stability of MDF. Moisture dynamics of OSB are different, amongst others influenced by orientation of the strands: grain direction perpendicular to the water uptake direction can protect OSB from water penetration. Furthermore, strands covered with resin have a good water resistance.

3.1 Introduction

Medium density fiberboard (MDF) and oriented strand board (OSB), two of the most important wood-based panels, are widely used in the furniture, flooring and construction industry. MDF is in principle made by gluing wood fibers together and has a typical density between 500 and 800 kg/m^3. OSB is manufactured from cross-oriented layers of thin, long wooden strands bonded together with resin and has a typical density between 600 and 680 kg/m^3. Both MDF and OSB are prone to water uptake, which can impact their physical and mechanical properties as well as biological durability (Ganev et al., 2005b; George, 1991). In order to improve the water resistance and moisture behavior of MDF and OSB, fibers and strands can be treated and process parameters, *i.e.* pressing temperature and time have been optimized (Del Menezzi and Tomaselli, 2006; Li et al., 2009; Ye et al., 2007; Zhang et al., 1998). Sealing or coating with a water repellent material, furthermore, can also effectively protect the panels from water uptake and these approaches are widely used especially for MDF (Walker, 1993). Adding water repellent material on the surface, naturally, increases the cost of such products and could also induce extra environmental impact. Apart from increasing the water resistance, understanding the moisture behavior of MDF and OSB can allow for better guidance on practical applications. For example, predicting the dimensional variation of MDF and OSB during moisture adsorption and absorption (Ganev et al., 2005a; Ozsahin, 2012) provides a possibility of applying specific products according to the practical requirements and intended moisture behavior, thus using different wood-based panel types fit for a certain purpose. Compared to studies focusing on the overall performance of such wood-based panels, only limited research has been carried out on a fiber or strand level to understand the moisture behavior of MDF and OSB. Knowledge of the moisture behavior of fibers and / or strands could contribute to better understand the moisture behavior of the full panels. X-ray tomography, therefore, can effectively reveal the internal structure and density distribution of wood based materials (Chen et al., 2010; De Ridder et al., 2011b; Van den Bulcke et al., 2009a) and moisture distribution can be indirectly calculated (Li et al., 2013). Hence, X-ray tomography is a valuable method to study the moisture behavior of wood-based panels, similar to previous studies on solid wood and plywood (Johansson and Kifetew, 2010; Li et al., 2014). Studying the moisture behavior of MDF and OSB, however, is difficult due to the small size of fibers and fast water uptake accompanied with significant swelling, which means X-ray CT scanning should be fast and at high resolution. A new gantry-based CT system at the Ghent University Centre for X-ray tomography (UGCT) allows such behavior to be investigated in the lab for the first time (Dierick et al., 2014).

The objective of this paper is to investigate the internal moisture behavior of MDF and OSB in dynamic water conditions. Specimens were prepared from different types of commercial MDF and OSB. A unique X-ray CT scanner was used to dynamically map the water transport and structural

variations of specimens. The interrelationship of water transport behavior, structural changes and products' structural characteristics was analyzed. Standard laboratory water sorption and desorption tests were performed as well on three replicates of each panel type to compare with the results obtained with X-ray CT scanning. Finally, suggestions on improving the water resistance and moisture behavior of MDF and OSB by optimizing their characteristics were put forward.

3.2 Method and Materials

3.2.1 Preparation of specimens

The MDF and OSB panels used in this experiment were produced by European companies. Four specimens with the size of $9 \times 9 \times$ (panel thickness) mm^3 from each type of panel, *i.e.* four types of MDF and one type of OSB, listed in Table 3.1, were prepared. All the specimens were conditioned in a conditioning room (65% RH and 20℃) until mass constancy was reached. One specimen and three specimens from each type of panel were used in X-ray CT scanning and laboratory water sorption and desorption testing respectively. The majority of the standard MDF products is meant for internal use in dry conditions. MDF-A is used as a rigid sheathing in roofing and walls and MDF-B is suitable for internal use in humid conditions, *e.g.* MDF based flooring in a bathroom environment. MDF-A contains 11% more adhesive and 20% more additive than MDF-B. MDF-C is considered to have a good durability in service (Suttie et al., 2015). The OSB is commonly used as a structural material.

Table 3.1

Characteristics of the different MDF and OSB types.

Type	Density (kg/m^3)	Thickness (mm)	Glue type	Increased additives and modification
Standard MDF	567	18.0	UF	
MDF-A	612	16.0	MUF	Paraffin emulsion
MDF-B	606	17.9	MUF	Paraffin emulsion
MDF-C	684	14.5	MDI	Wood fiber acetylation
OSB	605	18.0	MDI	

UF: urea formaldehyde glue; MUF: urea melamine formaldehyde glue; MDI: diphenylmethane diisocyanate.

The density of the specimens was measured after conditioning at 65% relative humidity and 20 °C.

3.2.2 X-ray CT scanning and image processing

The specimens were scanned with the Environmental Micro-CT Scanner (EMCT) developed by the Ghent University Centre for X-ray tomography (www.ugct.ugent.be) in collaboration with the Ghent

University (UGent) spin-off company XRE (www.xre.be) (Dierick et al., 2014). This scanner has a rotating X-ray tube and detector and thus the sample remains static, guaranteeing stability during scanning. The scanning duration of a single scan was set to 2 min, reaching a voxel pitch of approximately 18 µm. A piezoelectric XY stage was used to position the specimen precisely in the center of the field of view. In order to avoid movement during water immersion, the specimen was placed in a plastic cylinder, with a lid and a diameter of 15 mm, and stabilized by foam on top and bottom (Fig. 3.1). The cylinder was scanned once before adding water. Subsequently, the cylinder was filled with CsCl water (2.5% concentration) prepared from adding cesium chloride powder to demineralized water. In X-ray tomography attenuation is related, amongst others, to the chemical composition of the specimen. Since the attenuation difference between wood and water is not significant, CsCl doped water was used as a contrast agent in this test. It has been reported to be absorbed readily in stone and wood (Boone et al., 2014; Kuroda et al., 2013) similarly as water. Preliminary tests performed on OSB have confirmed this similar penetration behavior as water. During water uptake, the scan was executed periodically. The standard MDF and OSB were scanned at 5 min, 10 min, 30 min and 60 min respectively. For MDF-A, MDF-B and MDF-C, scans were performed at 1h, 4h, 8h, 24h and 48h respectively. To obtain further detailed data on the microstructure of the specimens, one specimen from the panels MDF-A, MDF-B and MDF-C was scanned with HECTOR, a high-energy CT scanner optimized for research (Masschaele et al., 2013), also built at the Ghent University Centre for X-ray tomography. The resolution is approximately 5 µm. All reconstructions were performed using the software package Octopus Reconstruction (Vlassenbroeck et al., 2007a), licensed by the UGent spin-off company InsideMatters (www.insidematters.be).
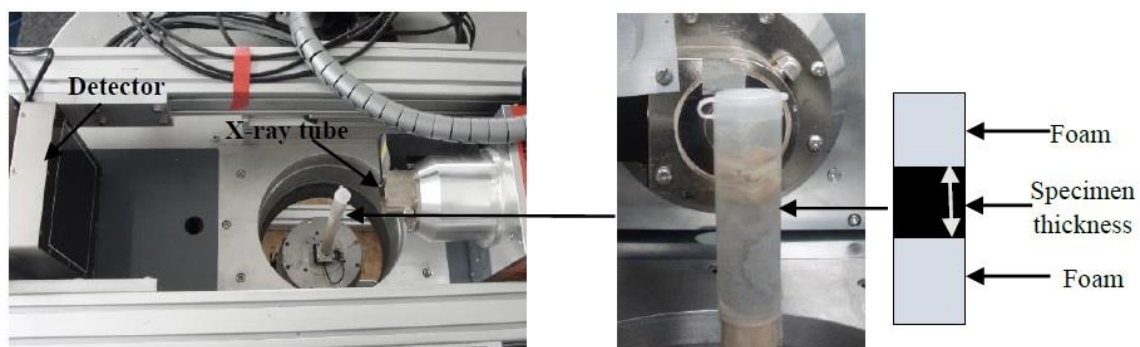

Fig 3.1. Overview of the experimental setup for X-ray CT scanning performed on EMCT.

3.2.3 Mapping water transport in MDF specimens with X-ray tomography

Due to reasons of symmetry, only a representative corner of the specimen was used to calculate the water transport behavior in MDF (Fig. 3.2). Water distribution of this corner was mapped by

averaging the grey scale values of the 50 central slices (white dashed line in Fig. 3.2) in one of the sides and thickness direction respectively. Remark that for visualization the entire sample is used.
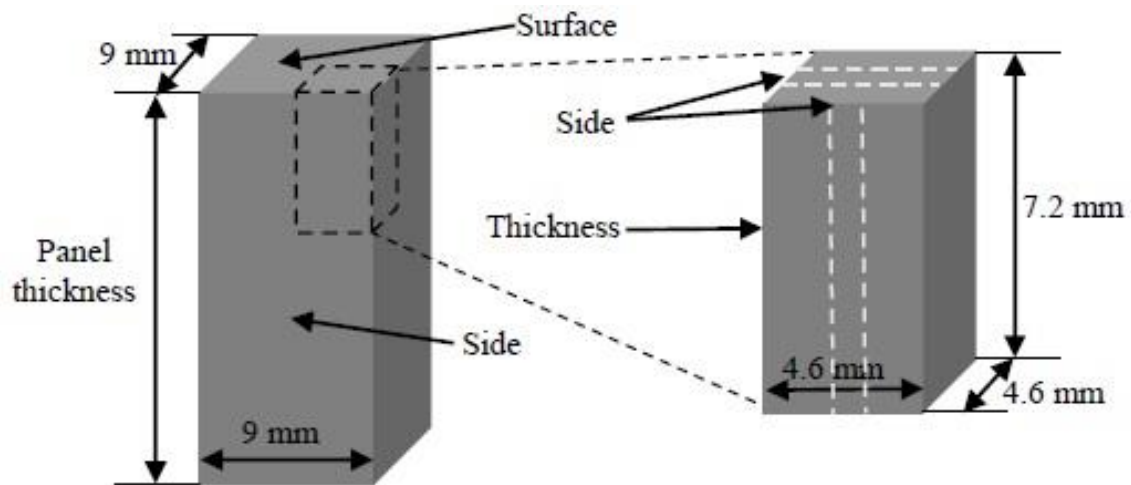

Fig 3.2. Schematic overview of mapping water transport using X-ray CT scanning.

In this experiment, the grey scale value is a result of attenuation by specimen and CsCl water. The water content thus can be calculated according to Eq. (3.1). The density of the CsCl water was 1.1×10^3 kg/m^3 obtained according to the density and ratio of cesium chloride. The swelling of the specimens was not taken into account during water content calculation. It causes an approximate average of 9% and maximum 15% water content decrease in comparison to the real water content in standard MDF. This error, actually is hard to correct due to the emerging of cracks during water uptake. For MDF-A and MDF-B, an approximate average of 7% and maximum 12% water content decrease occurs when there is no volume correction. In MDF-C, the maximally error is around 5%. These small errors, however, have no influence on the general water transport behavior and the conclusions obtained from this research.

$$W_i = [(G_i - G_{air}) - (G_d - G_{air})] \times D_{cs} / (G_{cs} - G_{air}) \qquad (3.1)$$

with W_i: the water content of the specimen at time i (kg/m^3); G_i: the grey scale value of the specimen at time i; G_d: the grey scale value of the specimen before water uptake; D_{cs}: the density of the CsCl water (kg/m^3); G_{cs}: the grey scale value of CsCl water; G_{air}: the grey scale value of air.

3.2.4 Laboratory water dynamics test

The specimens were immersed in a container filled with demineralized water and then weighed periodically according to the schedule of X-ray CT scanning. After immersion, the specimens were taken out of the water and conditioned in a conditioning room for 48 h. During this period, the specimens were weighed after 0, 1, 4, 8, 24 and 48 h. The water content was calculated using Eq. (3.2).

$$W_i = (m_i - m_0) \times 10^6 / (L \times D \times T) \qquad (3.2)$$

with W_i: the water content of the specimen at time i (kg/m^3); m_i: the mass of the specimen at time i (g); m_0: the mass of the specimen before water uptake (g); L: the length of the specimen before water uptake (mm); D: the width of the specimen before water uptake (mm); T: the thickness of the specimen before water uptake (mm).

3.3 Results and Discussion

The density profile along the thickness of the panels obviously influences the water transport behavior (Winistorfer and Xu, 1996). Since grey scale values of absorption CT scanning are related to density, average relative density profiles along the panel thickness were calculated using Eq. (3.3).

$$R_h = (G_h - G_{min}) / (G_{max} - G_{min}) \qquad (3.3)$$

with R_h: the relative density of the specimen at position h; G_h: the grey scale value of the specimen at position h; G_{min}: the minimum grey scale value; G_{max}: the maximum grey scale value.

The relative density difference between surface and core indicates a change in porosity. Low relative density means large porosity and is present in the core region of all four MDF specimens (Fig. 3.3), which is a typical density profile of MDF. This phenomenon in MDF-C, however, is not as clear as in standard MDF, MDF-A and MDF-B. Lower density in the top and bottom faces could be due to surface roughness of the specimens.
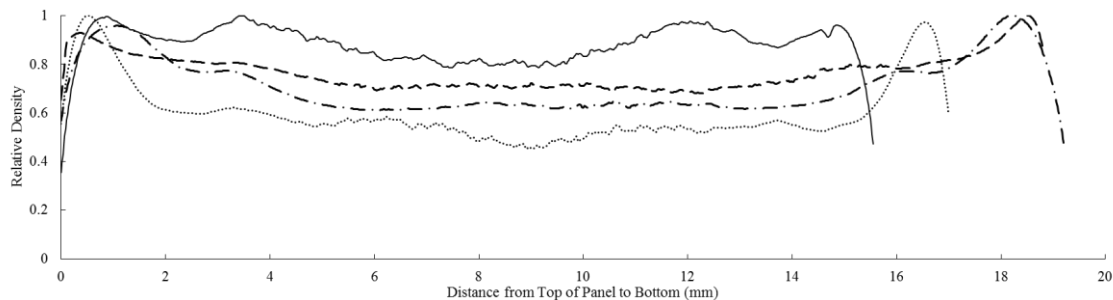
Fig 3.3. Relative density distribution along the thickness of the panels. $-\cdot$ = standard MDF, $\cdot\cdot$ = MDF-A, $--$ = MDF-B, — = MDF-C.

3.3.1 Water transport in standard MDF

Water movement is clearly different in thickness and side direction (Fig. 3.4). After 60 minutes immersion, the water front moves less than 1 mm and almost 2 mm from the surface and the side of standard MDF respectively. The highest water content is approximately 200 kg/m^3 at the surface and around 700 kg/m^3 at the side of the panel. Higher temperature and even higher resin content at the surface during MDF processing gives a solid and tight surface, resulting in more tightly wrapped

fibers embedded in resin. Therefore, water transport through both fibers and voids is hampered. In contrast, fibers in the interior are not interconnected by glue as well as at the surface. The relative loose structure or larger porosity in the core region of the specimen (Fig. 3.3) thus results in a rather large amount of voids and a lower density (Wang et al., 2001). Water entrapment in voids, therefore, induces the high water content at the side of the specimen. In addition, fiber direction is another factor influencing the water transport behavior in MDF. The fiber direction as shown in Fig. 3.5, is generally horizontal and thus water would move along the grain direction of fibers when water is absorbed from the sides.
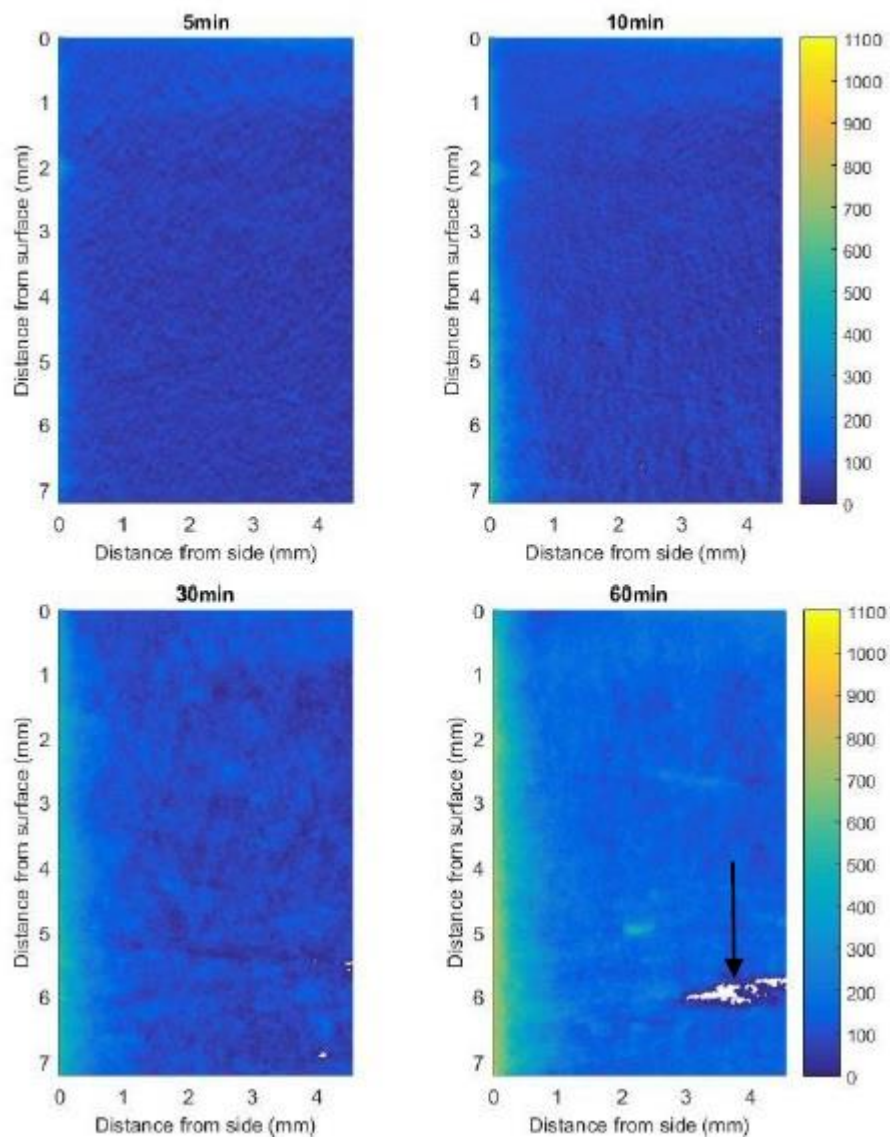

Fig 3.4. Measured water distribution in a representative corner of the standard MDF specimen.

The water movement rate is not uniform as shown by the black arrow in Fig. 3.4, which is consistent with non-homogeneous water movement shown in Fig. 3.5. Fast water movement in a large fiber is indicated with a black arrow in Fig. 3.5 (horizontal cross section through the entire MDF specimen)

and at the same time, cracks emerge. The emerging of cracks result in water content lower than zero shown as white color in Fig. 3.4. These cracks, indicated with white arrows in the vertical cross section, occur exactly where the large fiber is located (Fig. 3.5). This phenomenon is consistent with the results that large wood fibers can increase volumetric swelling and water absorption of wood-plastic composites (Migneault et al., 2008). Fig. 3.5 shows that several cracks emerge in the core of the specimen after 30 min immersion, which is mainly due to the water uptake. Water accumulation weakens the internal bonding between fibers glued with UF. Meanwhile, the tension caused by swelling of fibers can also destroy the adjacent structure. The mechanical properties of MDF panels can be significantly diminished due to emerging of such cracks. This is a key restriction for applying standard MDF in humid conditions. Standard MDF is intended for internal use in dry conditions, so the emerging of cracks is logical.
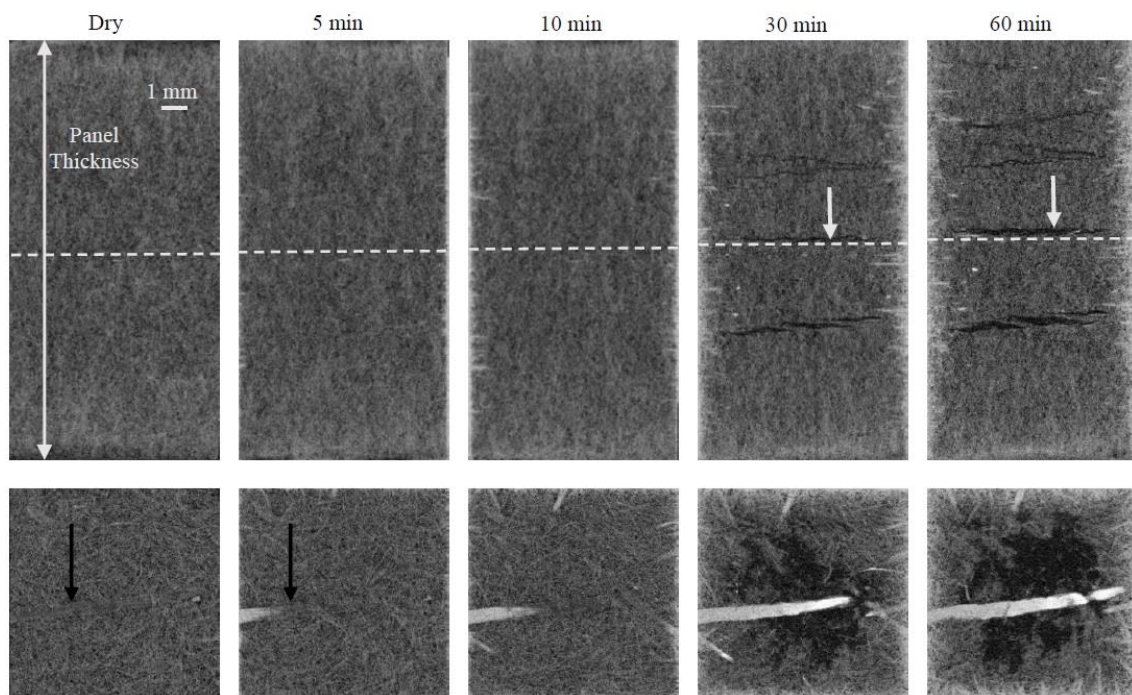
Fig 3.5. Vertical (top row) and horizontal cross section (bottom row) through the entire volume of standard MDF at different time steps obtained with X-ray tomography. The black arrow shows a large fiber along which water is absorb fast while at the same time, cracks emerge at the same height (white arrow).

3.3.2 Water transport in MDF-A, MDF-B and MDF-C

Water transport in water resistant MDF, types A, B and C was investigated by averaging the water content of a selection of 50 slices in side and thickness direction of the representative corner (white dash line in Fig. 3.2). Water enters these three specimens mainly through the sides (Fig. 3.6). Compared to MDF-A and MDF-B, the water content of MDF-C is much lower after 48 hours

immersion test, which is due to the different process technologies. MDF-A and MDF-B are made water resistant by adding paraffin emulsion in the wood fiber mattress and gluing with MUF. MDF-C, however, has acetylated wood fibers and an MDI adhesive.

Water quickly accumulates at the side of the specimens and then slowly moves to the interior for MDF-A and MDF-B. More specifically, the waterfront moves approximately 1.5 mm from the side after 4 hours immersion. Naturally, the accumulated water near the sides could be released quickly in desorption. Hence, MDF-A and MDF-B are suitable for applying in conditions without continuous water exposure. The frequent water desorption keeps the interior water content at a low level, which is key to maintain mechanical strength. The very low water content decrease at 48 hours of MDF-A is attributed to an unexpected decrease of the water level during scanning and possible specimen's top surface water evaporation.

Water absorption from the surface of MDF-C is very low and limited water uptake from the sides of MDF-C mainly occurs at the first 4 hours. Water quickly diffuses to the interior of MDF-C once absorbed at the side, which induces a rather homogenous water distribution. Along with immersion time, water content increase in MDF-C is slow. MDF-C is seemingly suitable to be used in challenging humid conditions, *e.g.* exterior doors and cladding open to all conditions of buildings.
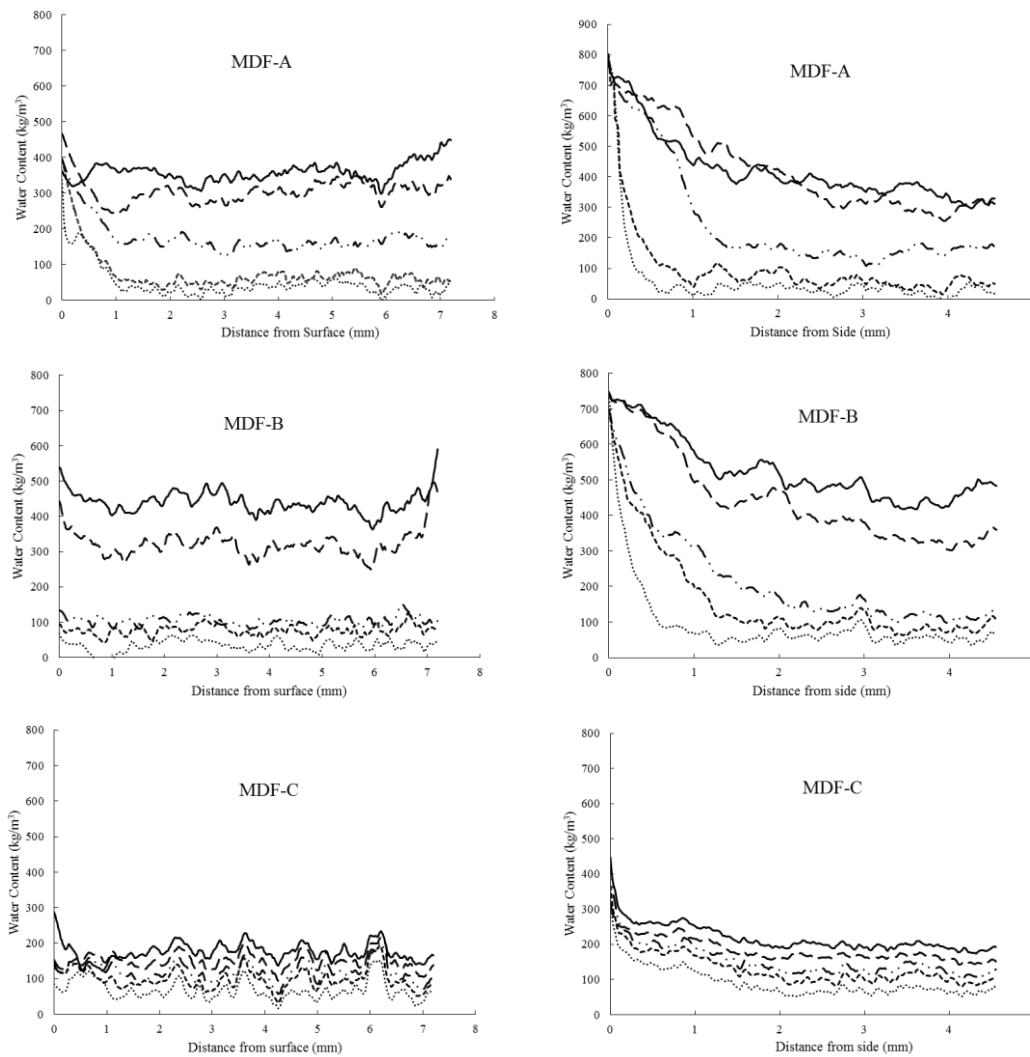
Fig 3.6. Water transport behavior in thickness (left column) and side (right column) direction of the representative corner of MDF-A, MDF-B and MDF-C at 5 time steps during water uptake. $\cdots$ = 1 hour, $--$ = 4 hours, $\cdots-$ = 8 hours, $--$ = 24 hours, $—$ = 48 hours.

To understand the water transport behavior illustrated in Fig. 3.6, water distribution and internal structure of MDF-A, MDF-B and MDF-C were also investigated and shown in Fig. 3.7. The water distribution was obtained by subtracting the image before water uptake from the matching image during water uptake. Due to the linear relationship between the amount of water and the grey scale value, water content could be determined. In MDF-A, MDF-B and MDF-C, no clear cracks were detected, which indicates that the fibers bonded with MUF and MDI can hardly be separated within a 48 hours immersion test.

According to the model described by Cai (2014), water uptake in porous media is influenced by the physical properties of the material, wetting liquid and solid liquid contact angle. In MDF, a porous material, the voids between fibers are similar to the pores of other porous materials such as rock. A

large void size is positively related with water imbibition. Compared to MDF-C, the large void size in MDF-A and MDF-B could thus be an important reason for large amount of water accumulation in voids (Fig. 3.8 arrows). The acetylation decreases the hydrophilicity of wood fibers and then increases the contact angle, which could thus decrease water absorption by voids in MDF-C. The water transport theory in MDF is even more complicated due to the hydrophilicity of the wood fibers and their microstructure. The hydrophilicity of the wood cell wall is mainly due to the presence of accessible hydroxyl groups (Walker, 1993). Formation of hydrogen bonds induces water adsorption and swelling in wood based materials. Acetylation changes part of the free hydroxyls within the wood fibers into acetyl groups and thus the ability of the wood fibers to adsorb water is greatly reduced, rendering the MDF panels more dimensionally stable and durable (Suttie et al., 2015). A wood fiber can be regarded as a hollow cylinder with many pits through the cell wall (Joffre et al., 2013). Free water movement in fibers along the lumen space, therefore, is another way of water transport in MDF. Water reaches the interior of the specimen within one hour through several fibers of MDF-C, which could be generally explained by capillary action (Fig. 3.7) because capillary water uptake reduction caused by acetylation occurs only in a minor extent (Pries et al., 2013). The fast water movement in other mostly smaller fibers of MDF-C, however, is not obvious in Fig. 3.7. The discrepancy could originate from the adhesive and wax that block the cell lumen of these fibers. Compared to MDF-A and MDF-B, water movement in several fibers of MDF-C is much faster, which is due to fiber acetylation and MDI. Hence, possibly, capillary action dominates water transport of these hydrophobic fibers in MDF-C, while a mixture of capillary action and water adsorption controls water movement in fibers of MDF-A and MDF-B.

These findings can impact the interpretation of the European standard EN 317 (1994) since a low swelling of panels is not only the result of good bonding properties, but can also be the result of slow water penetration.
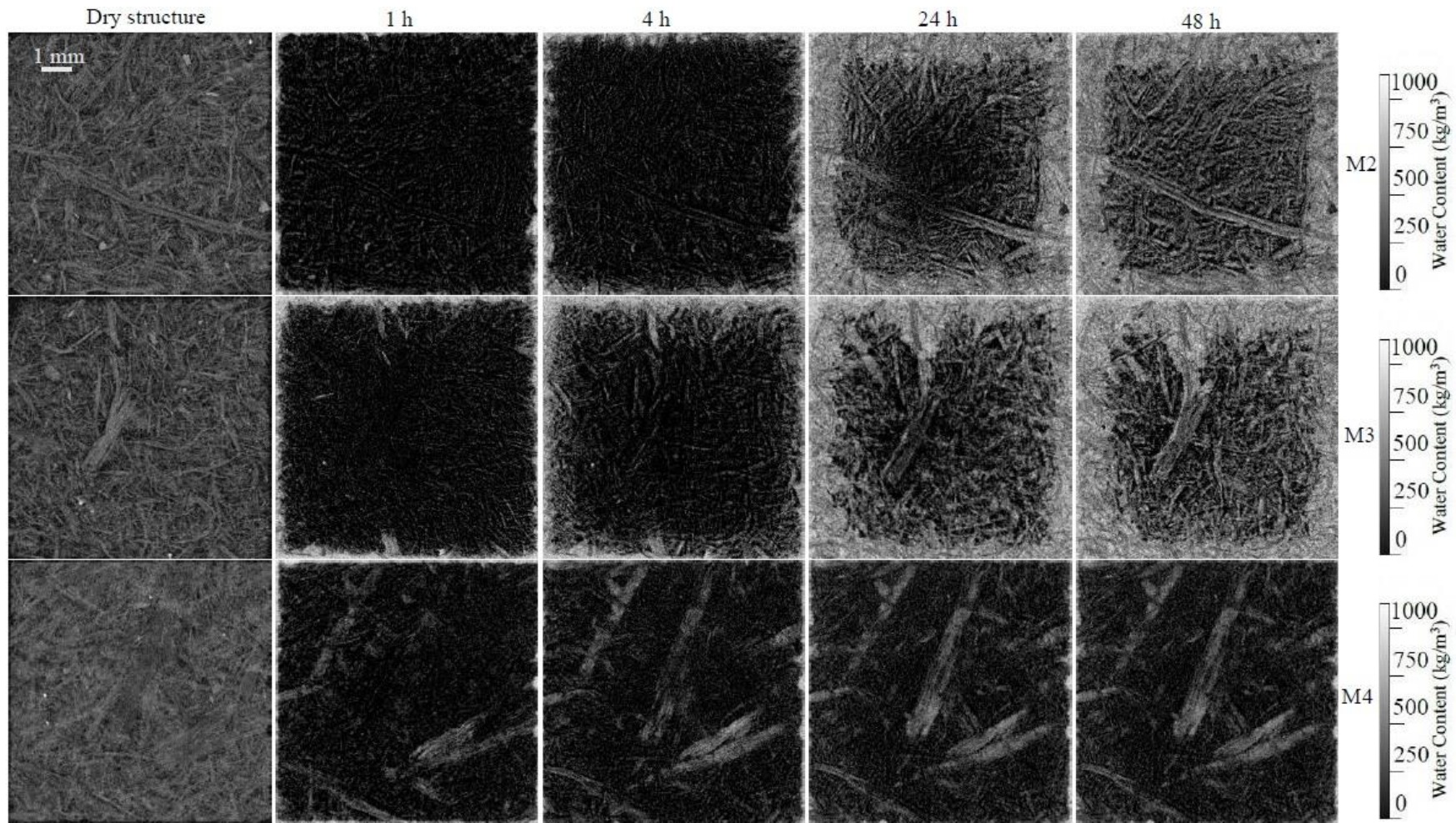
Fig 3.7. The internal structure before water uptake (left) and water distribution of the cross section of the entire specimens of MDF-A (top row), MDF-B (middle row) and MDF-C (bottom row) at 4 time steps during water uptake obtained with X-ray CT scanning by subtracting the image before water uptake from the image after water uptake.
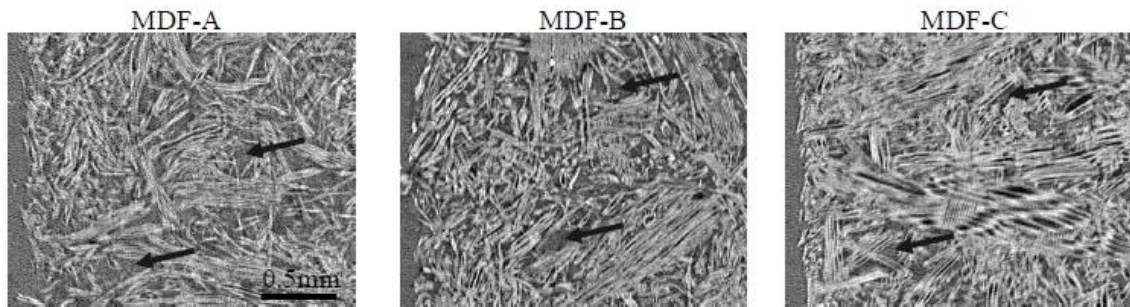
Fig 3.8. Cross-sectional detailed microstructure of different MDF specimens (left side is the side edge) obtained with high resolution X-ray CT scanning.

3.3.3 Water transport in oriented strand board

Oriented strand board (OSB) is a wood-based panel produced by bonding wood strands together. The mixture of resin and strands as well as the randomly distributed voids with different sizes complicate the water transport behavior in OSB leading to a significantly inhomogeneous water distribution in immersion testing (Fig. 3.9). Due to swelling of OSB in vertical direction, water distribution, shown as light grey color in Fig. 3.9, was highlighted by setting a grey scale threshold instead of comparing image after water uptake with image before water uptake. It is feasible because the grey scale value of CsCl water is much higher than wood substance and resin. Generally, water can quickly fill the voids close to the surface and sides of the specimen. Compared to the surface, water prefers entering the interior of the specimen from the sides, which could be due to the low density and loose structure (Wang and Winistorfer, 2000). This hypothesis is consistent with the slow water movement in the regions where strands are pressed tightly (Fig. 3.9 arrow). In these areas, more adhesive accumulation in the small voids and a more continuous glue line increase the water resistance (Evans et al., 2010). In addition to structural factors, the grain direction of strands also impacts water transport. Specifically, the grain direction of strands is parallel and perpendicular to the water uptake direction when water is absorbed from the sides and surface respectively. Hence, after filling the voids, water can hardly penetrate to the interior when entering from the surface. Fig. 3.9 illustrates that the amount of water close to the surface decreases with the immersion time, yet this is due to swelling resulting in an out of field-of-view movement during X-ray CT scanning.
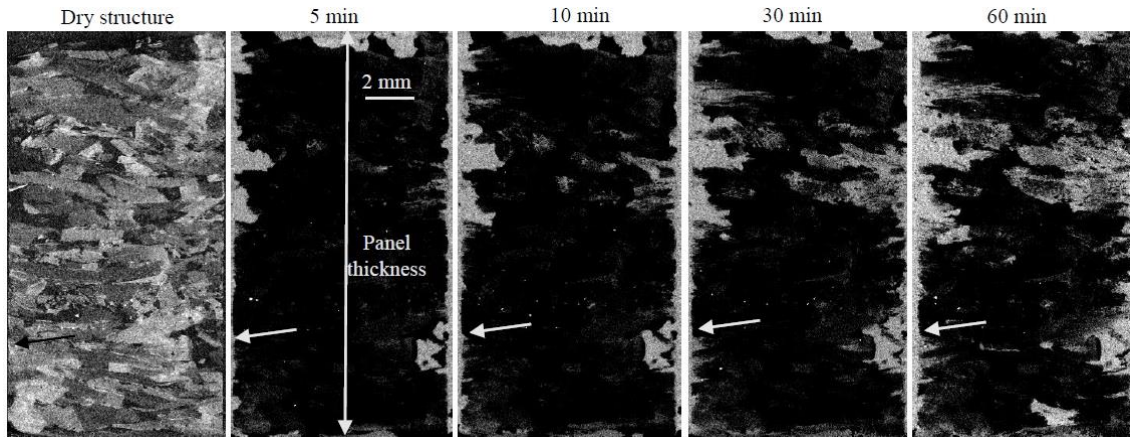
Fig 3.9. Cross-sectional view through the internal structure of the entire specimen before water uptake (left) and water distribution at 4 time steps during water uptake of OSB obtained with X-ray CT scanning.

In order to investigate the relation between structure and moisture transport behavior of OSB in detail, several cross-sections in horizontal direction were selected. Water distribution was further obtained by subtracting the cross-section before water uptake from the one after water uptake (Fig. 3.10). Water content was also calculated according to the linear relationship between the quantity of water and grey scale value (Eq. (3.1)). The results present significant differences in water transport behavior among slices and this difference closely relates to the structural characteristics of OSB, *i.e.* the size and direction of strands, resin distribution and voids. Specifically, water can penetrate the large pieces of strands within 60 min. Resin can prohibit water movement in large strands as well. For example, less water distributes into the region covered with resin, which is indicated with white arrows in Fig. 3.10A. Grain direction of strands can also influence water transport. Fig. 3.10B shows that this cross-section mainly consists of large strands and to a lower extent strands covered with resin, however, only small amount of water enters the interior of the specimen after 60 min water uptake due to the impact of grain direction. Since water moves along the grain direction of the two strands highlighted with an arrow in this cross-section, water is only transported along the edges of the specimen. Hence, water would not penetrate the interior, if the grain direction of the strands could be arranged properly. Compared to the large strands, the small strands can effectively prevent water from penetrating (Fig. 3.10C). The small strands are easily covered with resin (Evans et al., 2010), which can effectively block water movement between strands. If voids are located close to the edge of the specimen, this is detrimental since they could act as a water reservoir (Fig. 3.10D). The entrapped water could then further increase fungal decay risk when water evaporation is slow.
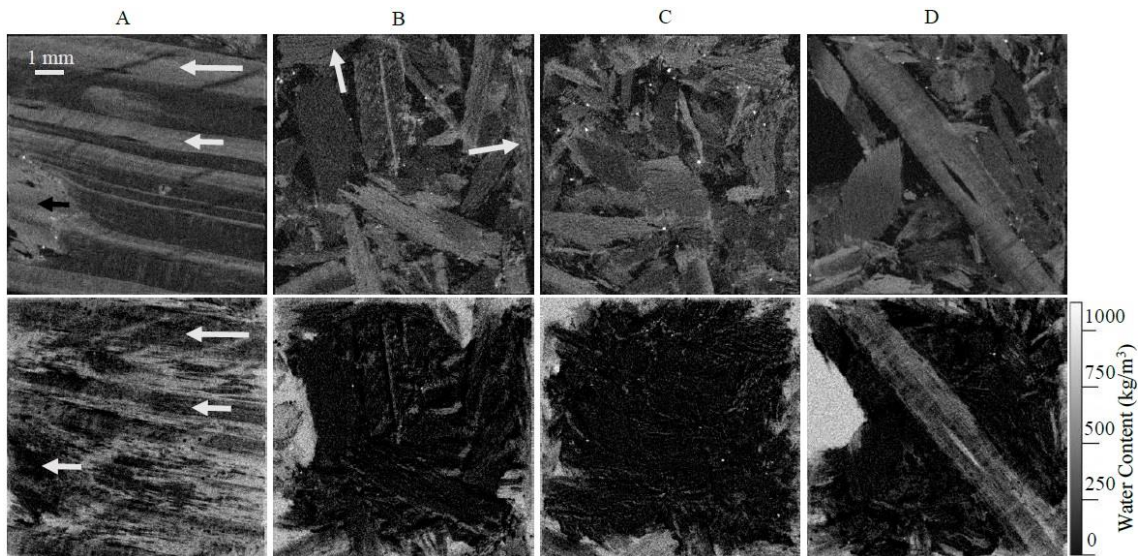
Fig 3.10. The internal structure before water uptake (up) and water (white color) distribution after 60 min of water uptake (bottom) of several horizontal cross sections of the entire OSB specimen obtained with X-ray CT scanning.

3.3.4 Laboratory water dynamics test

The results of the laboratory water uptake test agrees well with the results from X-ray CT scanning (Fig. 3.11). Compared to Standard MDF, the water resistance of MDF-A, MDF-B and MDF-C is better, which is consistent with the description given by the producer. For MDF-A and MDF-B, although water uptake speed is not fast, water content of the specimens is still higher than 350 kg/m^3 when they are immersed in the water for 48 hours, which is over 50% MC. It is thus better to use them in conditions without continuous water exposure. Water resistance of MDF-A is better than MDF-B, which is a result of a higher resin and paraffin emulsion content. Water uptake in MDF-C mainly occurs during the first 4 hours followed by very slow water content increase. Furthermore, the absorbed water can be released quickly. Hence, MDF-C has a potential to be applied in continuous humid conditions, for example, the facade of a building (Suttie et al., 2015). For OSB, the residual water content after 2 days is higher than in MDF, which could be due to water entrapment in the voids. This could decrease the mechanical strength and biological durability of OSB in service.
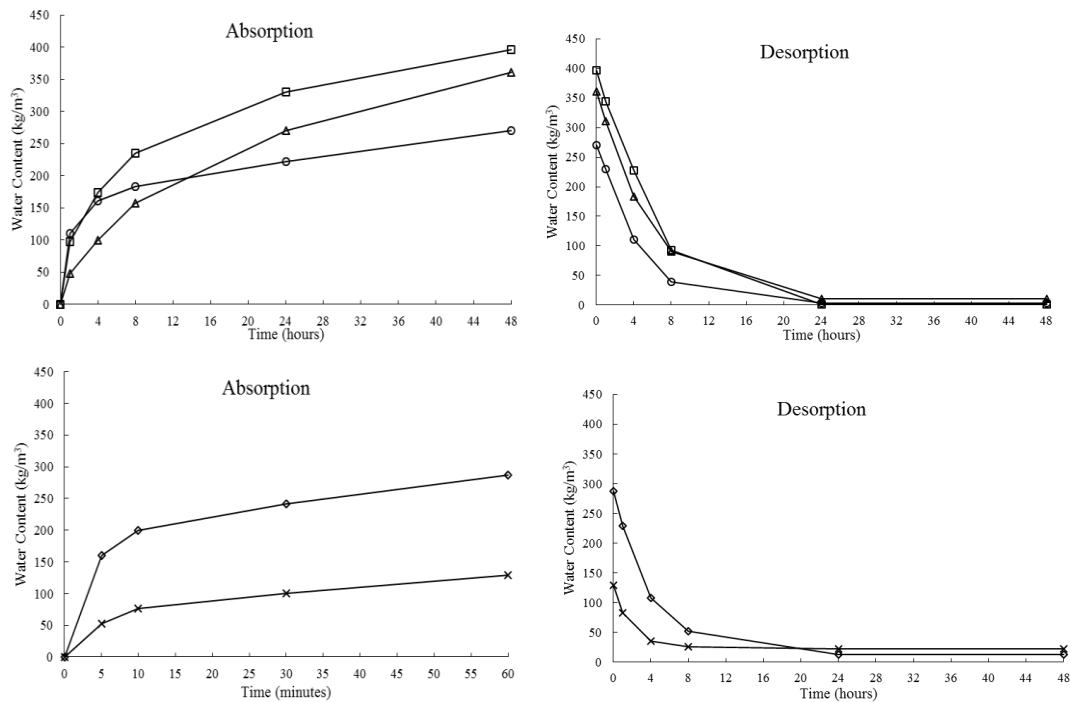
Fig 3.11. Water content of specimens during water uptake and release in laboratory test. ◊ = standard MDF, Δ = MDF-A, □ = MDF-B, ○ = MDF-C, × = OSB.

3.4 Conclusion

The Environmental Micro-CT Scanner (EMCT) is an excellent device to investigate the dynamic water transport in wood-based panels in real-time. Water mainly penetrates from the sides of both MDF and OSB specimens when immersed in water. This dominant entrance pathway was expected. Water mainly moves through the larger fibers or strands and quickly reaches the interior of the specimens. Water transport between voids is slow. A large amount of water, however, can accumulate in voids near the sides of the specimens during immersion wetting, which can be effectively decreased by a compact structure. Compared to UF, MUF and MDI increase water resistance considerably and improve structural stability of MDF. Hence, using a resin with good water resistance and adding a water repellent additive can indeed increase water resistance, as is shown for a selection of samples. However water still can accumulate and move in voids of MDF. Fiber acetylation can significantly decrease water adsorption in the wood cell wall, therefore, the limited water absorption in MDF-C is mainly through the cell lumen of fibers. For OSB, the grain direction of strands influences water movement. Specifically, water uptake can be reduced when the grain direction of a strand is perpendicular to the water uptake direction. Water absorption can be effectively reduced if the strands are covered with a water resistant resin. Different processing technologies can now be evaluated in detail and in real-time using the gantry-based CT system used

in this research. The findings of this paper, however, need to be combined with practicalities such as, the price of adhesives, additives and acetylation as well as application requirements when implemented in factory production.

Acknowledgement

3

4 Combining electrical resistance and X-ray computed tomography for moisture distribution measurements in wood products exposed in dynamic moisture conditions

Abstract

Strength and durability of wood-based products are substantially influenced by moisture. It is, therefore, crucial to monitor the moisture content (MC) distribution in wood products to fully understand their behavior in dynamic moisture conditions. In this paper, we present a combined X-ray CT method and an adapted version of the electrical resistance MC measurement method for detailed studies on MC distribution in wood products. The X-ray CT method is evaluated using the gravimetrically recorded MC of solid wood. Subsequently, the recorded MC of electrical method is evaluated by using an X-ray CT method. Three wood products are used for this purpose, *i.e.* solid wood, plywood and oriented strand board (OSB) panels. It is proven that an X-ray CT method can accurately determine the MC of wood products and thus has great potential for non-destructively measuring the MC distribution in 3D. Furthermore, the results show that the electrical method can effectively record the local MC when the MC distribution in this region is even. Otherwise, the position of the electrodes, with regard to specific wood properties has a substantial influence on its performance. Compared with solid wood and OSB, the electrical method performs best in plywood due to its layered structure. The adapted electrical method as presented here is an effective tool for continuously monitoring the MC distribution of wood products, taking into account that the electrodes should be installed correctly according to the structure of wood products and the research question. In combination with regular X-ray CT scanning, full moisture analysis is possible.

4

4.1 Introduction

Wood is increasingly used as a construction material in the building industry because of its sustainability, renewability and flexible usability. However, as a natural material, wood is prone to the attack by fungi when water is available and environmental conditions favor growth. The optimal condition for decay by most active white and brown rot fungi is the moisture content (MC) above fiber saturation point (FSP). The MC of wood, therefore, is usually considered as the key factor that determines whether or not fungi can grow, and thereby wood rot can occur (Walker, 1993). It is well known that the MC also has an important influence on the physical and mechanical properties of wood based materials (Gerhards, 1982). Hence it is crucial to monitor MC when wood is used outdoors to better understand its behavior when subjected to dynamic outdoor conditions with possible liquid water ingress. Previous study by Van den Bulcke and co-workers (2009c) introduced the CMM method, with continuously weighing of plywood exposed outdoors for calculation of the average MC of the samples. Moisture distribution is a key factor as well. To further monitor this distribution, one could cut the samples into small sections, weighing them individually to reconstruct the moisture distribution (Macindoe and Leonard, 2012), yet this technique is obviously a destructive one, hindering long-term recording. The electrical resistance method is another method to continuously record moisture, being non-destructive and reasonably accurate. Long-term electrical measuring MC of rather large samples, made of pine, spruce and fir, has been tested before as a feasible approach (Brischke et al., 2008a; Brischke et al., 2008b). More advanced techniques exist as well. Magnetic resonance imaging is a non-destructive modality that has been used too as a tool for monitoring the free water movement in wood and wood-based products (Meder et al., 2003; van Houts et al., 2004). Other researchers (Chen et al., 2009; De Ridder et al., 2011a) have proven that X-ray scanning, also as a non-destructive approach, could efficiently reveal density distributions in wood products and wood-based composites. There is a linear relationship between CT number and density of wood containing both wood substance and water (Lindgren, 1991). According to the density in different positions of the wood, moisture distribution was further derived from these scans (Sandberg and Salin, 2010; Watanabe et al., 2008). Neutron imaging is similar to X-ray methods but not as common as the latter. It was also used to test wood density and moisture in previous studies (Mannes et al., 2007; Nakanishi and Matsubayashi, 1997).

Clearly many approaches have been applied for monitoring the MC content and distribution of wood products, but there is not a single method that can simultaneously monitor accurately, continuously and non-destructively the MC distribution in dynamic moisture conditions. Hence, in this research, an X-ray CT method was searched for to accurately map the MC distribution of wood products in three dimensions. This method was then used to evaluate whether an adapted version of the electrical resistance measurement as described by Brischke et al. (2008a) can be the preferred non-destructive and effective method to continuously monitor the water distribution in different wood species and

wood-based panels. Several specimens of solid wood, plywood and OSB were immersed in water for 16 days (384 hours). All specimens were scanned on a regular basis with high-throughput X-ray CT to link the actual local MC inside the specimens and the MC as recorded with the electrical resistance measurements. Furthermore, the relationship between the microstructure of the specimens and the electrical MC measurement performance was analyzed using the volumetric X-ray data.

4.2 Material and methods

4.2.1 Specimens without electrodes

A set of specimens was used to assess the accuracy of X-ray CT method for moisture distribution monitoring. Solid wood specimens measuring 50 x 50 x 15 mm^3, were prepared from four wood species: poplar (*Populus* spp.), Scots pine heartwood and sapwood (*Pinus sylvestris*) and birch (*Betula* spp.). All specimens were without decay, knots and obvious defects. The specimens were conditioned in a conditioning room at 65% RH and 20℃ until constant mass after which all specimens were weighed. The specimens were immersed for 48 hours in a container filled with demineralized water. During this period, the specimens were weighed and scanned after 0, 1, 4, 8, 24, 48, hours of immersion. After 48 hours of immersion, the specimens were oven-dried, weighed and scanned. With each scan also a plastic vial containing demineralized water was scanned along.

4.2.2 Specimens with electrodes

For evaluation of the electrical resistance method, solid wood specimens were prepared from six different wood species: poplar (*Populus* spp.), spruce heartwood (*Picea abies*), Scots pine heartwood and sapwood (*Pinus sylvestris*), okoumé (*Aucoumea klaineana*) and birch (*Betula* spp.), all measuring 70 x 50 x 15 mm^3 and 50 mm along the grain direction. During cutting specimens of polar, okoumé and birch, the materials away from sapwood zone were used. Also PF (phenol formaldehyde) glued plywood, and OSB panels with isocyanate glue, were prepared and sawn to the size of 70 x 50 x (panel thickness) mm^3 (Table 4.1). All specimens were without decay, knots and obvious defects. Two holes of 4 mm diameter were drilled in the specimens. The distance between the centers of the holes was 30 mm orthogonal to the grain. Inside the 4 mm drill hole, another small hole with 1 mm diameter was drilled starting from the bottom of the former drill hole (Fig. 4.1). Then, these specimens were conditioned in a conditioning room at 65% RH and 20℃ until constant mass after which all specimens were weighed. After weighing, all sides of the solid wood specimens except one end grain face (cross section) were sealed, while, for plywood and OSB panels, only four sides were sealed. This way, the water was allowed to enter the specimens in one direction only. Next, the wires were glued in the predrilled holes with conductive and isolating glue as described in Brischke et al. (2008a).

Table 4.1

The details of the wood based panels.

Type	Wood species	# of plies	Thickness [mm]
Plywood	Pine	7	18
Plywood	Spruce	5	15
OSB	Spruce+Pine	−	17

These electrodes were made of stripped commercial wires. In order to avoid beam hardening and metal artefacts in X-ray CT scanning, thick metal wires such as described in Brischke et al. (2008a), are not suitable. Hence, wires with plastic cover having a diameter of 0.2 mm were used in this experiment. Furthermore, in order to decrease possible noise, the following protocols had to be followed: the wires in the small holes at the bottom of the large drill holes were fixed using conductive glue to make sure these electrodes could effectively test the MC at the region of interest (further called ROI, see Fig. 4.1). We assume that the measurements are mainly influenced by the MC in this region. As is well known, water movement in wood mainly takes place along the grain direction and the speed of movement is not identical for different wood species. Hence, for solid wood, the distance (X) between end grain face and the electrodes is different according to the anticipated absorption of the different wood species (Fig. 4.2). These distances are listed in Table 4.2. All electrodes were positioned at the same depth, *i.e.* 7 mm from the top face. It is the aim of electrical resistance method to measure the general MC distribution instead of accurate regional MC of different wood products. Electrical loggers (Materialfox Mini), with the same formula to convert electrical resistance to MC, were used for reading out the MC values of all specimens from different wood species. The formula is specifically applied to calculate MC of pine and spruce species. We assume that the influence of wood species is rather small.
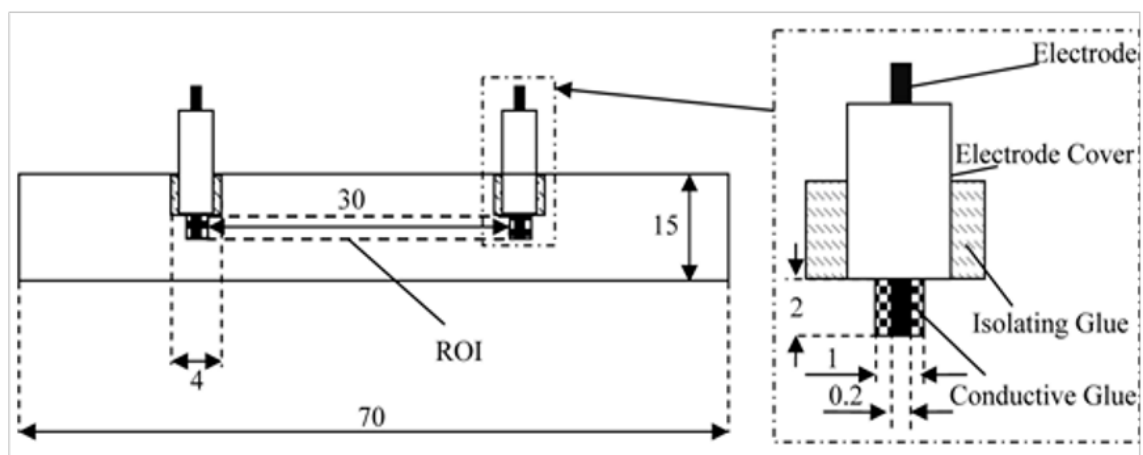
Fig 4.1. Detailed view of electrodes (all dimensions in mm).
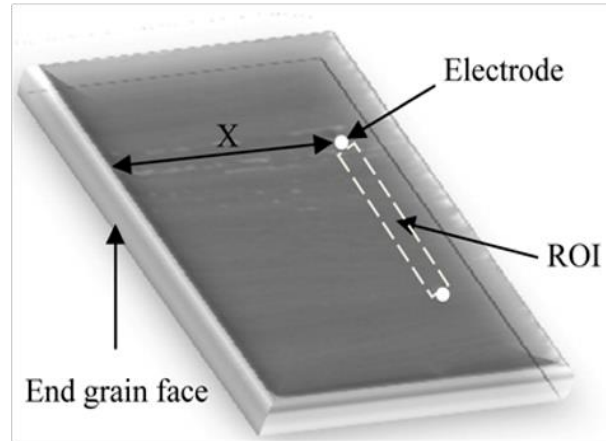
Fig 4.2. Overview of solid wood specimen.

Table 4.2

The distance between end grain face and electrodes.

Wood species	Poplar	Spruce	Pine heartwood	Pine sapwood	Okoumé	Birch
X(mm)	40	20	10	40	10	35

For plywood and OSB, two pairs' of electrodes were installed in each specimen at different depths to record the MC distribution in vertical direction (Fig. 4.3). The depths for each pair of electrodes are listed in Table 4.3 and were carefully controlled and adjusted if necessary using X-ray radiography.
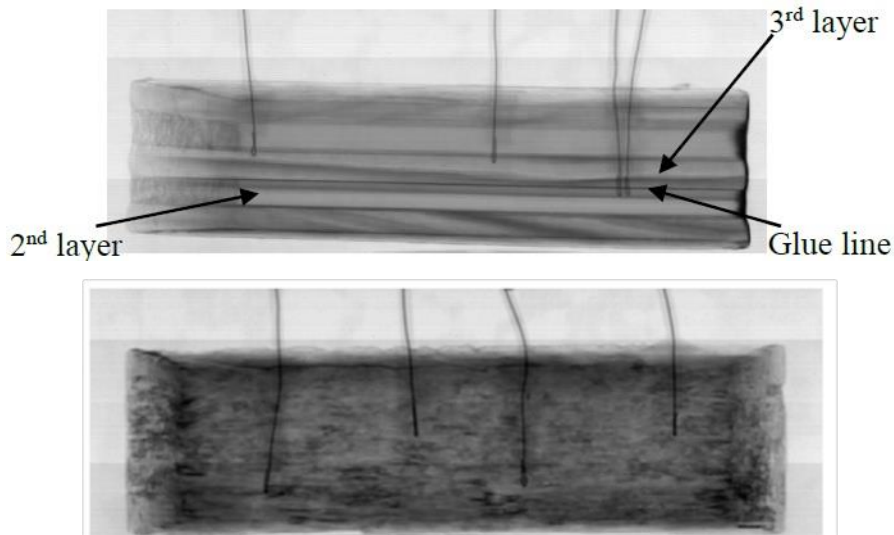
Fig 4.3. X-ray radiographies of electrodes in spruce plywood (up) and OSB (bottom).

Table 4.3

Depth of electrodes, measured from the bottom face of the panels, in plywood and OSB.

Panels	Pine plywood (Layer)	Spruce plywood (Layer)	OSB (mm)
Depth	4th	2nd	8
	5th	3rd	3

Finally, the specimens were conditioned again until constant mass and weighed. Subsequently they were positioned with the appropriate face / end grain in a container and immersed in demineralized water in the conditioning room. For plywood and OSB, the specimens were put in the container horizontally allowing water to move from the bottom face up. All specimens were mounted on stainless steel grids to avoid complete submersion and placed in the water for 16 days (384 hours). During this period, the electrical MC was recorded every 24 hours and the specimens were scanned after 0, 24, 48, 96, 168, 216, 264, 336, 384 hours of immersion. Electrical measurements were recorded after specimens were taken out of the water and remained in a conditioning room for 30 min with removal of the liquid water of the immersed face to avoid incorrect measurements.

4.2.3 Gravimetrical method

All specimens were weighed before scanning. The average MC could be obtained with following formula:

$$MC^i_x = (m^i_x - m^i_0) / m^i_0 \times 100 \tag{4.1}$$

The calculations are adjusted to correct for the weight of edge sealant and wires. The sealant and wires are considered having a constant weight and as such the average MC of the specimens could be calculated using the following:

$$MC^i_x = (m^i_x - m^i_0) / [m^i_0 - (m^i_2 - m^i_1)] \times 100 \tag{4.2}$$

with MC^i_x: the average moisture content of specimen i at time x (%); m^i_x: the mass of specimen i at time x (g); m^i_1: the conditioned mass of specimen i with holes (g); m^i_2: the conditioned mass of specimen i with glue and wires (g); m^i_0: the oven-dry mass of specimen i (g).

4.2.4 X-ray scanning

All specimens were scanned with the CT scanning set-up built at the Ghent University Centre for X-ray Tomography (www.ugct.ugent.be). The scanner is similar to the one as described in Masschaele et al. (2007) and used in Van den Bulcke et al. (2009a; 2009b). It has a generic in-house developed CT scanner control software platform (Dierick et al., 2010) that allows full control of the scanner hardware. The scan settings and test set-up were optimized to limit scan time to 6 minutes per

specimen and avoid drying. 16 bit projection images were obtained. Reconstruction was performed with Octopus, a tomography reconstruction package for parallel, cone-beam and helical geometry (Vlassenbroeck et al., 2007b). An approximate voxel pitch of 100 μm was obtained. Both hard- and software filtering was necessary to reduce the remaining metal artefacts.

4.2.5 Data processing

Converting greyscale values to actual MC is a non-trivial procedure. In X-ray absorption tomography the attenuation is dependent of the chemical composition of the specimen, the density of the material and the energy of the X-ray beam. The latter is assumed equal for all experiments and thus not influencing the results. When a specimen consists of different constituents, the ratio of these constituents influences the attenuation coefficient. Hence their greyscale value, in this case of water and wood, should be obtained independently. The general relationship between a constituent and its greyscale value can be expressed as following:

$$G = \mu' \times \rho \qquad (4.3)$$

$$\mu_{wood} = G_{dry} / \rho_{dry} \qquad (4.4)$$

$$\mu_{water} = G_{H2O} \times 1 \qquad (4.5)$$

$$G_{sum} = G_{wood} + G_{water} \qquad (4.6)$$

$$G_{wood} = \mu'_{wood} \times \rho_{wood} \qquad (4.7)$$

$$G_{water} = \mu'_{water} \times \rho_{water} \qquad (4.8)$$

with G: the average greyscale value of the material; μ': the attenuation coefficient per unit mass of material (cm^2/g); ρ: the material density (g/cm^3); G_{dry}: the average greyscale value of oven-dried wood; ρ_{dry}: the density of oven-dried wood (g/cm^3); μ_{wood}: the attenuation coefficient of wood (1/cm); μ_{water}: the attenuation coefficient of water (1/cm); G_{H2O}: the average greyscale value of pure water; G_{sum}: the total greyscale value of the material; G_{wood}: the greyscale value of the wood; G_{water}: the greyscale value of water; μ'_{wood}: the mass attenuation coefficient of wood (cm^2/g); ρ_{wood}: the mass of wood substance per unit volume of material (g/cm^3); μ'_{water}: the mass attenuation coefficient of water (cm^2/g); ρ_{water}: the mass of water per unit volume of material (g/cm^3).

As is well known, the standard gravimetrical MC is calculated by using Eq. (4.11). Measuring MC by application of X-ray CT method is, however, an indirect approach as the greyscale value is related to the density of wood and water rather than to the MC only. Hence, by substitution of Eq. (4.6), Eq. (4.7) and Eq. (4.8) into Eq. (4.11), the MC can be obtained using Eq. (4.12). The attenuation coefficient of H_2O obtained by scanning pure demineralized water is assumed to be constant because

the same X-ray scanning setup was used for all specimens. The attenuation coefficient of wood is acquired by scanning the oven-dried specimens.

$$G^i_{ROI\text{-}sum} = G^i_{ROI} \times V^i_{ROI} \tag{4.9}$$

$$G^d_{ROI\text{-}sum} = G^d_{ROI} \times V^d_{ROI} \tag{4.10}$$

$$MC^i = \rho_{water} \times V^i_{ROI} / (\rho_{wood} \times V^i_{ROI}) \tag{4.11}$$

$$MC^i = (G^i_{ROI\text{-}sum} - G^d_{ROI\text{-}sum}) \times \mu'_{ROI\text{-}wood} \times 100 / G^d_{ROI\text{-}sum} \times \mu'_{water} \tag{4.12}$$

with $G^i_{ROI\text{-}sum}$: the sum of all greyscale values within the ROI at time i; G^i_{ROI}: the average greyscale value of the ROI at time i; V^i_{ROI}: the volume of the ROI at time i (cm^3); $G^d_{ROI\text{-}sum}$: the sum of the greyscale values of ROI of the oven-dried specimen; G^d_{ROI}: the average greyscale value of the ROI of the oven-dried specimen; V^d_{ROI}: the volume of the ROI of the oven-dried specimen (cm^3); MC^i the moisture content of the ROI at time i (%); $\mu'_{ROI\text{-}wood}$: the mass attenuation coefficient of wood of the ROI (cm^2/g).

The software package Morpho+ was used to obtain the average greyscale values of the different constituents (Brabant et al., 2011). Preprocessing of the volumes included bilateral filtering to remove noise and preserve edges. By plugging the average greyscale value of water, wet and dry wood in abovementioned formulae, the MC of a specimen can be calculated. For the scanned volumes of the specimens without wires, thresholding was applied to segment the specimen and to calculate the average greyscale value. The ROI in this case equals the entire specimen to enable comparison with the gravimetrically determined MC. The volume of the specimens, therefore, was derived from the amount of voxels the sample consists of. The density of oven-dried specimens is acquired from dividing weight by volume. For the specimens with wires, the ROI was demarcated manually and MC was calculated within this specific region. In order to obtain the oven-dried density of this region, reconstructed volumes were converted to density values with Matlab, as a reference material with known density was included in each scan. By using the average greyscale value of this reference material and air (zero density), greyscale values of reconstructed specimens can be converted to densities (De Ridder et al., 2011a).

4.3 Results and discussion

4.3.1 Evaluating the MC determined with X-ray CT method

The X-ray CT derived MC was obtained using Eq. (4.12). As the specimens were not edge sealed and had no electrodes, the gravimetrical MC was calculated according to Eq. (4.1). Fig. 4.4 illustrates the strong linear relationship (0.994) between the X-ray CT method and gravimetrical MC. The slight difference between them was induced by the moisture adsorption and desorption during scanning as

well as an imperfect segmentation of background and sample due to remaining beam hardening artefacts. It indicates that the X-ray CT method can accurately monitor the MC and its distribution in specimens.
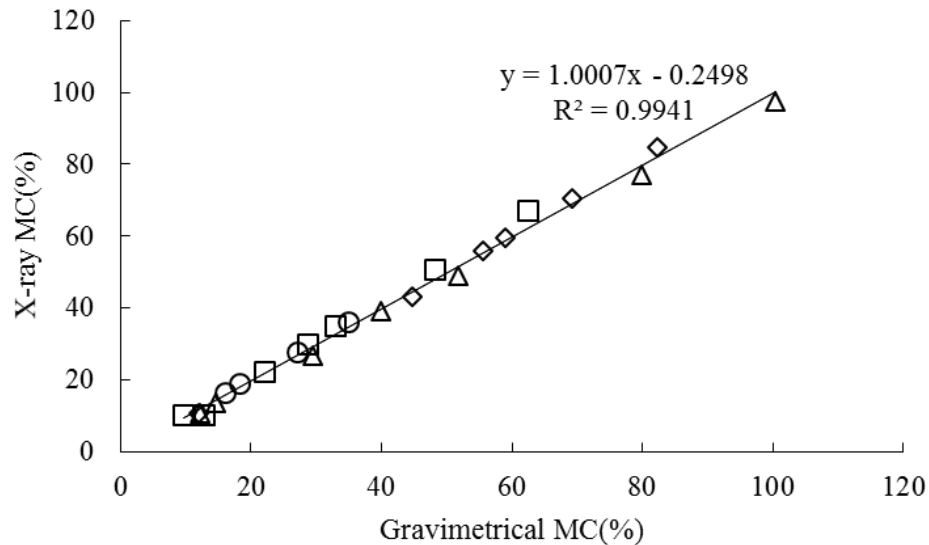
Fig 4.4. The relationship between the MC measured with X-ray CT and measured gravimetrically. □ = birch, △ = poplar, ○ = pine heartwood, ◇ = pine sapwood.

4.3.2 Optimizing X-ray scanning of specimens with electrodes

A first adaptation of the electrical resistance method is the thickness of the wires used. Fig. 4.5 shows that thick wires cause serious beam hardening, especially between the two electrodes, which can influence the MC calculation in this region. Thin wires were used for this reason to minimize beam hardening and metal artefacts in X-ray scanning and a small hole was drilled at the bottom of the large hole, as explained in the Materials and Methods section (Fig. 4.1). The small hole was filled with conductive glue in which the thin wire was installed, as such ensuring proper contact between the thin wire and the surrounding wood material and a proper measurement of the MC in the ROI.

Fig 4.5. CT image obtained from thick wires (left) and thin wires (right).

Wood swells and the volume of the specimens changes during water absorption. If an unchanged volume is used to calculate the MC, it might cause an incorrect estimation of the MC. However, due to the uneven swell in different areas, volume change of the entire specimen cannot represent the regional volume change. Therefore, three specimens were selected to investigate the relationship between entire and regional volume change. As shown in Fig. 4.6, the entire volume, obtained by r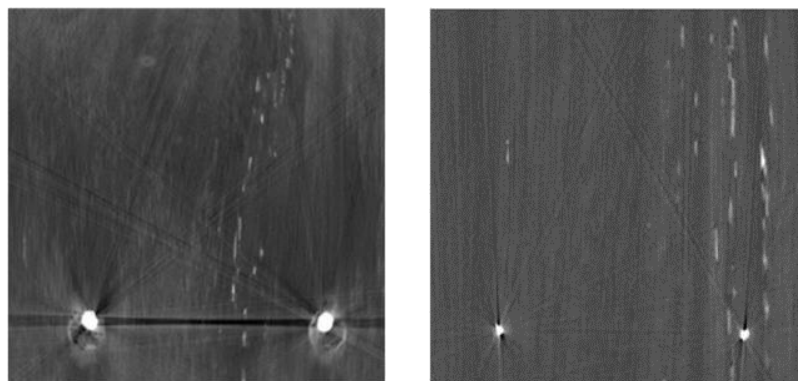ecording the number of voxels of the entire specimen, is larger than the ROI volume change. Therefore, the local volume was used to calculate MC of the ROI in between the electrodes. For solid wood and OSB, the volume of the ROI can be obtained from the distance between the two electrodes and the height of the small holes (Fig. 4.1). For plywood, the volume is obtained from the distance of the two electrodes and the height from the bottom of the small hole to the nearest glue line. Swell along the grain is negligible, compared to that of other directions.
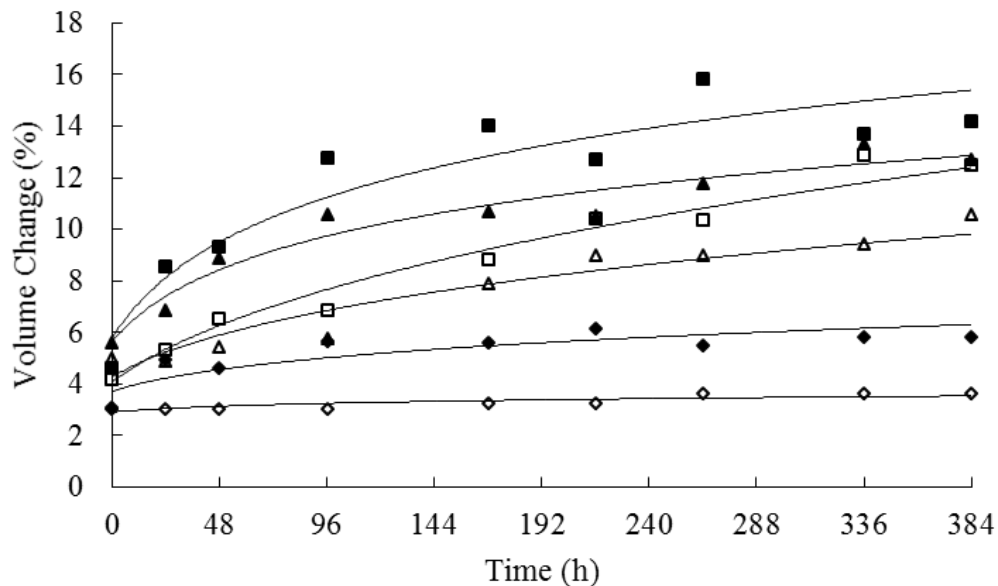
Fig 4.6. The volume change of the entire specimen and the ROI. ■ =birch, □ = birch ROI, ▲ = poplar, △ = poplar ROI, ◆ = pine plywood, ◇ = pine plywood ROI.

4.3.3 MC of solid wood

An example of X-ray CT scanning of a specimen with electrodes, illustrating the grey value distribution in the specimens as water is absorbed, is shown in Fig. 4.7. In this experiment, since water is the only factor that causes the greyscale value to increase, these changes can be converted to MC changes. The highest MC is noted a few millimeters into the wood from the end grain surface as the water moves longitudinally into the specimens. The MC decreases with increasing distance from the end grain surface. The MC increases along with immersion time and obviously the edge region absorbs more water than the core. The moisture absorbed into the wood takes place due to the

capillary force and presence of accessible hydroxyl groups when the MC is below the fiber saturation point (FSP). Above the FSP, free water moves into wood as a result of capillary forces (Haygreen, 1996; Mounji et al., 1991). This pressure force is related to a moisture and air gradient of nearby cells. Generally speaking, the air near the edge is easy to be forced out and consequently the air pressure gradient should be higher. Hence the water prefers to penetrate along with the edges. This result has also been found in spruce timber tested by Sandberg and Salin (2010).
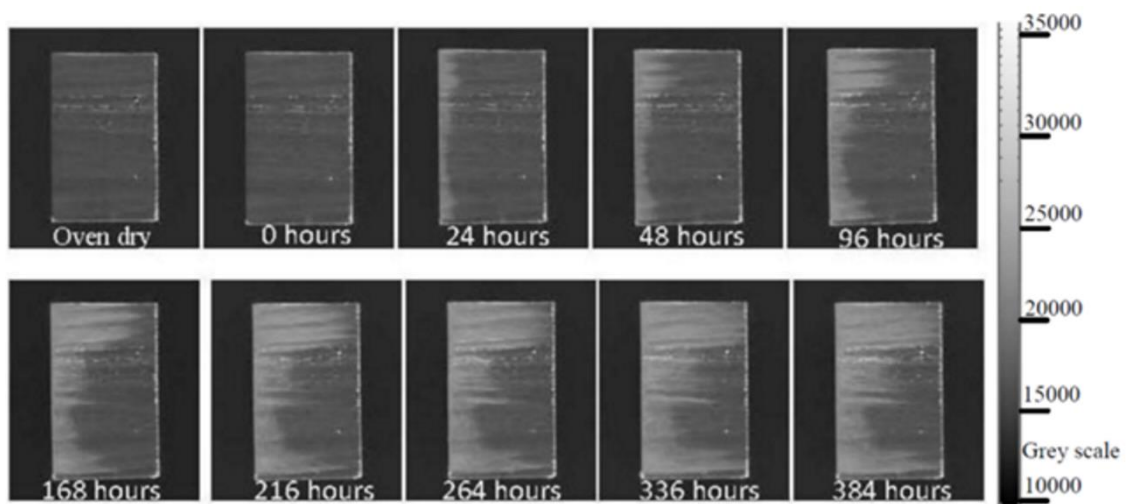
Fig 4.7. CT slices of water ingress in poplar after immersion.
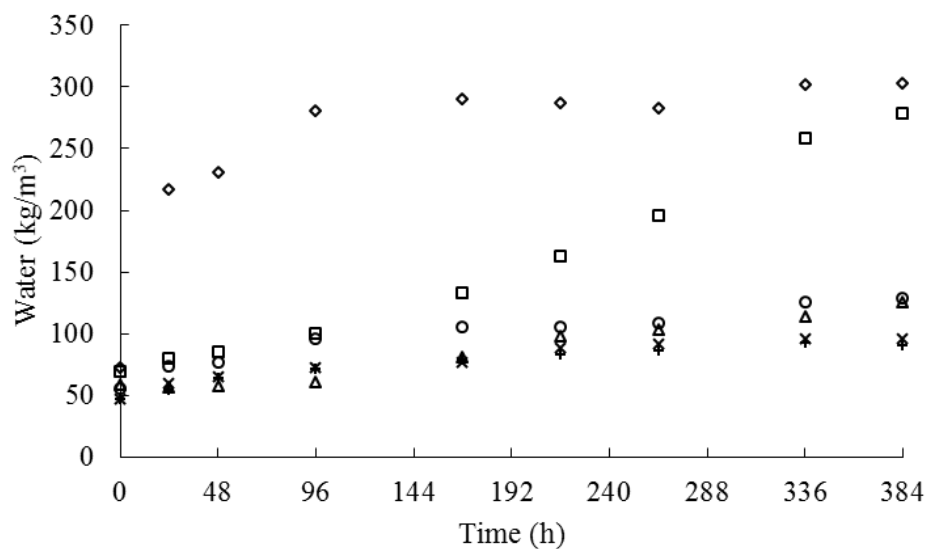
Fig 4.8. The amount of water in the ROI of 6 wood species. $\diamond$ = pine sapwood, $\square$ = birch, $\bigcirc$ = pine heartwood, $\triangle$ = poplar, $\times$ = spruce, $+$ = okoumé.

Fig. 4.8 illustrates the water volume calculated by using X-ray MC in the ROI of several wood species. It is obvious that pine sapwood and birch absorb much more water than other wood species

despite the fact that the distances between ROI and the end grain face are 40 and 35 mm. On the other hand, pine heartwood, spruce and okoumé can effectively prohibit water from penetrating (Fig. 4.8). Although poplar easily absorbs water, there is only a small amount of water in the ROI. This result is consistent with the MC profiles in Fig. 4.7.

Fig. 4.9 gives a graphical overview of the comparison of electrical and X-ray MC of the ROI as well as the average gravimetrical MC of the specimens. These results are obtained for different wood species. It is obvious that there is a substantial difference between the MC of the ROI and the average MC, which indicates that the average MC cannot represent the regional MC in dynamic moisture conditions. These results are consistent with the findings of Sandberg and Salin (2010). The MC for poplar determined with the electrical and X-ray method is equal except for the last measurements. In these last measurements, the increase of electrical MC is higher than X-ray MC, which means that the electrical resistance tested by the logger is smaller than the actual electrical resistance of the ROI. Reason for this phenomenon is that electricity follows the path of the least resistance rather than the shortest distance between two electrodes. From the MC profiles in Fig. 4.7, there is no obvious water in the area between the two electrodes, while other positions are filled with water, as such making electricity flow around the ROI from which the X-ray derived MC is calculated. This explanation also holds for the last measurement of birch.
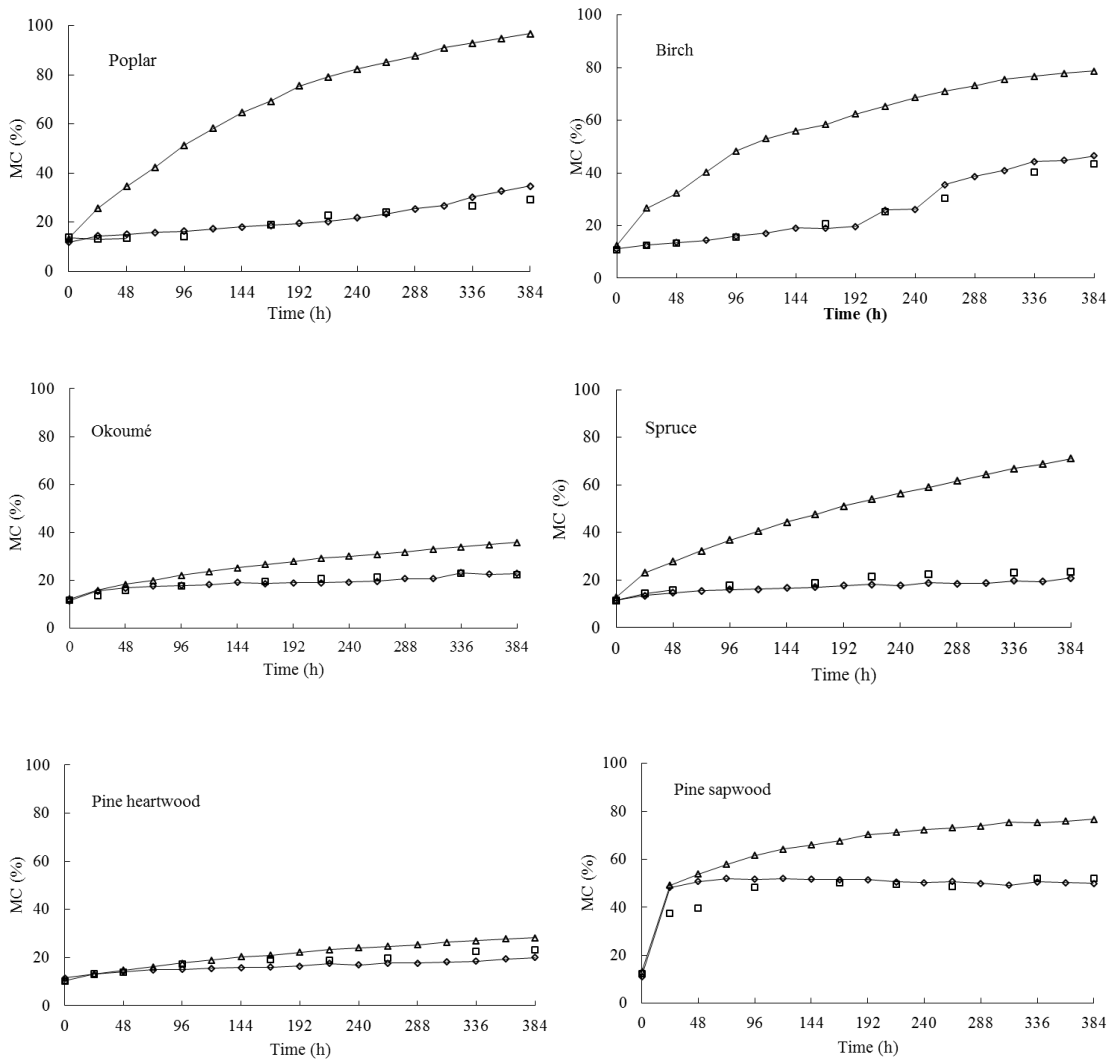
4

Fig 4.9. The MC of solid wood tested by three methods. ◇ = electrical ROI MC, □ = X-ray ROI MC, △ = gravimetrical average MC.
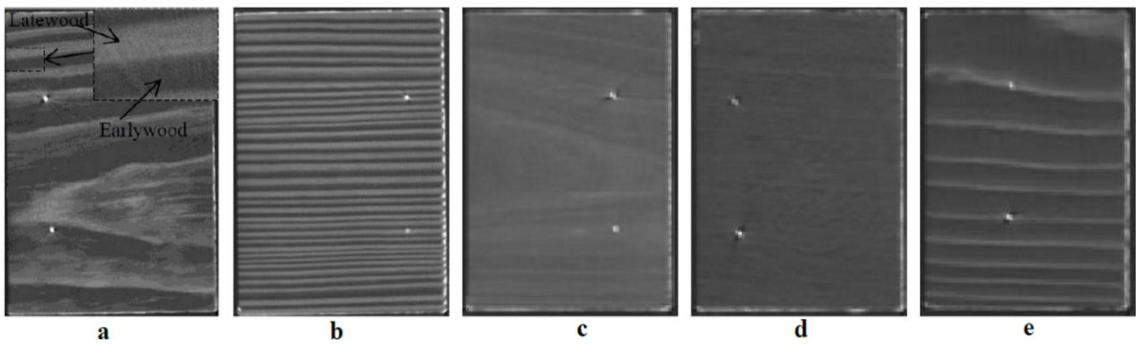

Fig 4.10. The macroscopic structure of 5 wood species: (a) pine heartwood; (b): pine sapwood; (c): birch; (d): okoumé; (e): spruce. The lighter colors represent high densities and the dark colors represent lower densities.

Fig. 4.9 also shows that the X-ray MC is slightly higher than the electrical MC in spruce and pine heartwood. To explain this phenomenon, the macroscopic structure of these wood species is studied. Fig. 4.10 shows the differences in density between the two electrodes of these wood species. The distinction of earlywood and latewood in softwood is obvious and much clearer for pine.

Latewood cells play a more significant role in water uptake than earlywood cells because latewood tracheids have smaller cell lumens. Hence water flows preferably along the latewood in longitudinal direction (Sedighi-Gilani et al., 2012). When there is free water in these cells, the structure of latewood cells, with smaller tracheids and thicker cell wall, can act as a boundary to free water movement (Meder et al., 2003). Therefore, to prove if this characteristic would influence the MC distribution, the MC values of adjacent earlywood and latewood of pine heartwood (Fig. 4.10a), from end grain face to the electrode are calculated. As shown in Fig. 4.11 the MC of both earlywood and latewood is around 10% before immersion. After immersion, MC in latewood increases faster than in earlywood when the MC is below 30% (FSP). Later on, obviously, most of the free water is found in the earlywood. The waterfront in Fig. 4.11 also illustrates that water is absorbed from end grain face to the internal regions of the specimen and the decrease of the MC near the end grain face is caused due to drying during scanning, although scan time was shortened significantly by fine tuning the protocol. Because the electricity has to flow across latewood and earlywood and there is a negative relationship between MC and electrical resistance, the section with lower MC dominates the electrical resistance between two electrodes. Hence, the measured electrical MC is slightly smaller than the actual MC of ROI.

4
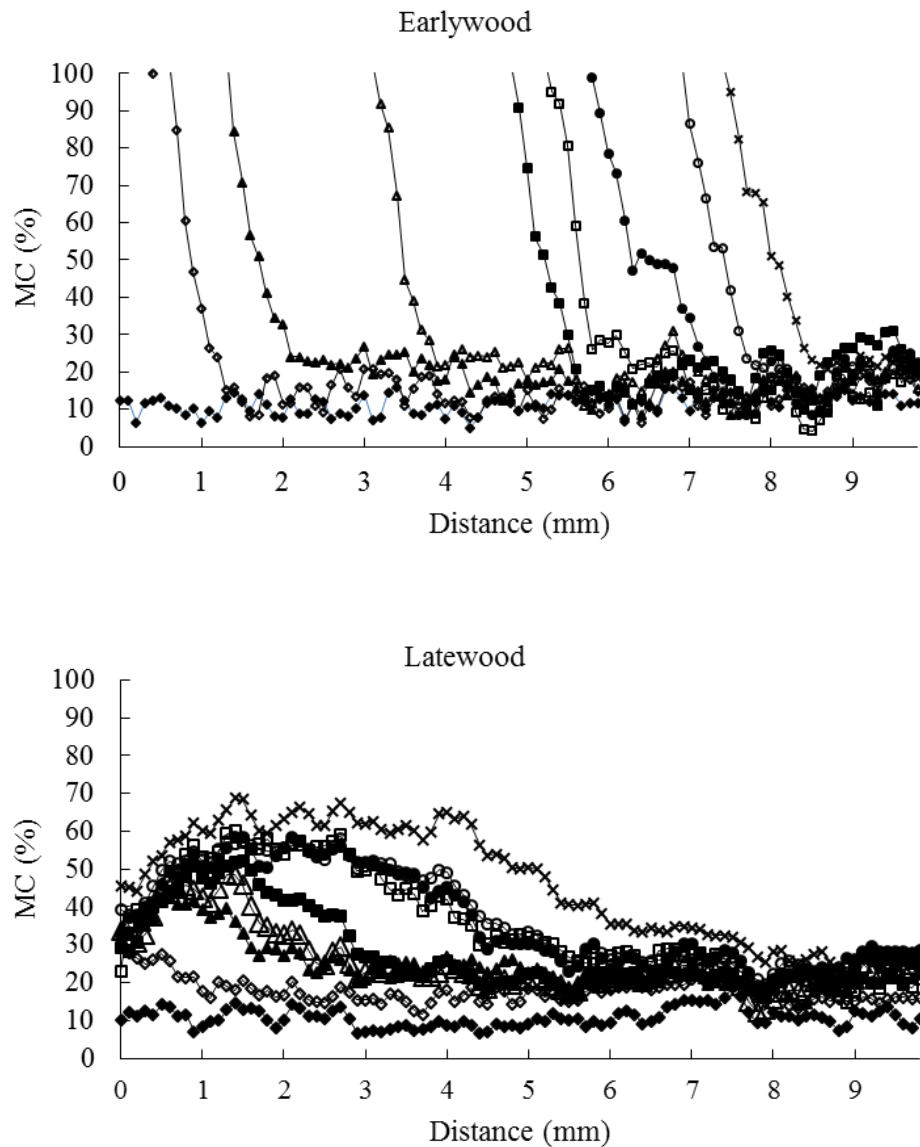
Fig 4.11. MC changes in earlywood and latewood of pine heartwood at different distance from the end grain face. ◆ =0 hours, ◇ = 24 hours, ▲ = 48 hours, △ = 96 hours, ■ = 168 hours, □ =216 hours, ● = 264 hours, O = 336 hours, ×= 384 hours.

As shown in Fig. 4.9, the MC in the ROI of pine sapwood is higher than FSP at the first measurement. Based on above analysis, the MC of earlywood should be much higher than the MC of latewood, which would cause the electricity to flow along the earlywood. Hence, the measured electrical MC is higher than its real MC. Later on, due to the position of the electrodes and the wood structure of ROI, the electrical MC generally equals the actual MC of the ROI in the last measurements.

Similar electrical resistance MC measurements were performed by Brischke *et al.* (2008a; 2008b). The structure of the wood did not influence their results as specimens were conditioned to equilibrium MC before measuring electrical MC or rather large specimens were used in outdoor conditions. Taking into account these conditions, the MC distribution in the core of the specimens is more or less even and the MC value of high and low density zone is close to each other when the MC is below FSP (Pang and Herritsch, 2005). Therefore, the electrical MC is in a good agreement with the gravimetrical MC especially when the MC is below 30% (Brischke et al., 2008a). However, our experiments show that results can be heavily influenced by the absorption of liquid water; therefore electrical MC measurements should always be interpreted with proper knowledge of the material structure, including the specific anatomy and the position of the electrodes within the structure, especially when working with materials of much smaller dimensions, such as wood-based panels (cf. infra). Combining these measurements with X-ray tomography is an ideal situation.

4.3.4 MC of plywood

Plywood is an important engineered wood material in the building industry and therefore monitoring its water distribution is essential. Contrary to solid wood, the glue lines separate the veneers and hamper water movement between them. Fig. 4.12 gives evidence that the gravimetrical average MC of the plywood specimens cannot be applied to evaluate the MC of the different layers. To investigate the moisture distribution, electrical and X-ray MC measurement methods are used for measuring the moisture distribution in each layer of the plywood. It should be noted that it is difficult to select exactly the same ROI in such a small volume for each scan, therefore, the results can show a slight up-and-down movement, although the general trend is clear. The slight fluctuations of the electrical MC can be caused by little remaining liquid water at the bottom face, decreasing the electrical resistance between the electrodes slightly. In Fig. 4.12b, 12c and 12d, the MC values as obtained with the electrical and X-ray method are comparable. However, Fig. 4.12a shows that the electrical MC is much higher than X-ray MC when the MC exceeds 25%. To explain this phenomenon, we take a closer look at the structure of plywood. Plywood is manufactured by gluing together veneers which are cut perpendicular to the grain with the knife parallel to the grain (Walker, 1993). Hence, a single veneer can consist of both earlywood and latewood layers. As above analysis shows, water has a fast uptake by latewood when there is no free water whereas expressed in absolute values most of the free water is present in earlywood. Hence if the region with the electrodes contains earlywood and latewood layers, the electrical method might measure the MC of the layer with higher MC, with a smaller electrical resistance at that moment, while the X-ray method would measure the average MC of earlywood and latewood. Therefore, the recorded electrical MC is higher than the X-ray MC. On the contrary, if the electrodes are positioned in a region consisting of earlywood or latewood only, the electrical MC should be equal to the X-ray MC. This hypothesis is proven by the structure of

spruce plywood in which the whiter region represents latewood and the darker region earlywood (Fig. 4.13). As shown in Fig. 4.13b, the region between the two electrodes in the 3rd layer is basically entirely earlywood. Fig. 4.13a shows that in the 2nd layer, the electrodes just enter the earlywood layer then the electrical MC corresponds with the MC of the layer with higher MC. The water is absorbed from the bottom and has to penetrate the earlywood layer and then the latewood layer. Hence, the MC distribution is more or less even before free water gets in and the electrical method records the same MC as the calculation based on the X-ray CT method. After that, the electrical MC corresponds with the MC of the earlywood layer at the bottom of the electrodes. The electrical MC is thus much higher than the average MC of ROI measured by X-ray CT method (Fig. 4.12a). Overall, the electrical MC measurement method is suitable for measuring the MC distribution in plywood thanks to its layered structure. Although the electrical MC can be higher than the average MC of a veneer, this method can effectively monitor the maximum MC of this veneer, which can play a key role in assessing its influence on strength properties as well as potential decay.
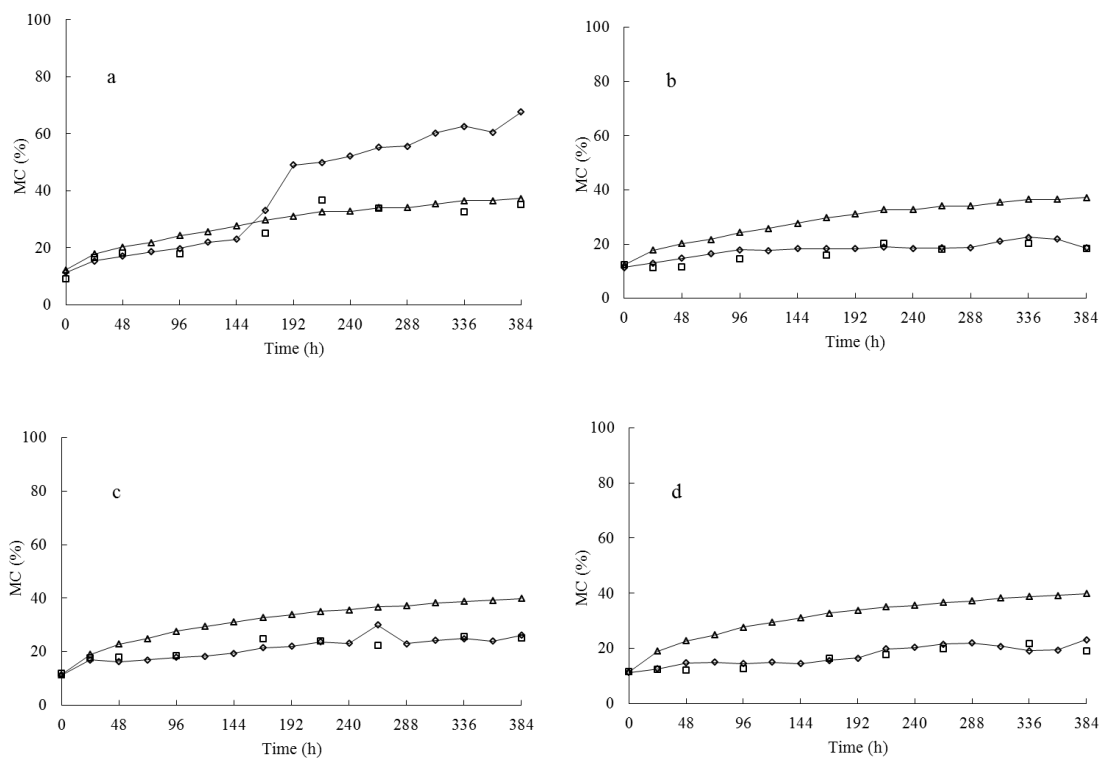

Fig 4.12. The MC of plywood tested by three methods. (a): the 2nd layer of spruce plywood; (b): the 3rd layer of spruce plywood; (c): the 4th layer of pine plywood; (d): the 5th layer of pine plywood. ◇ = electrical ROI MC, □ = X-ray ROI MC, △ = gravimetrical average MC.
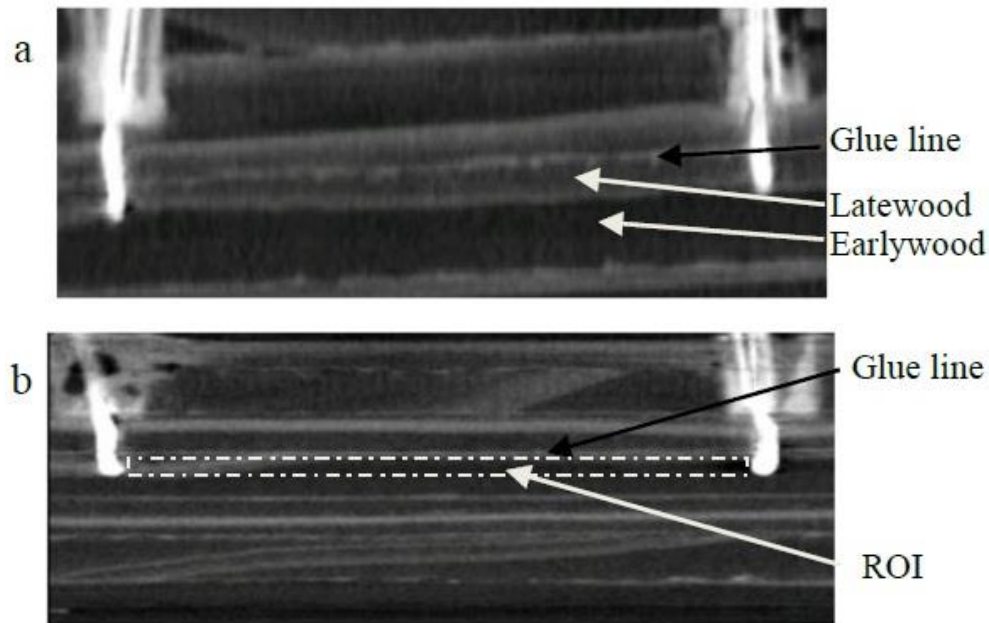
Fig 4.13. The internal structure of spruce plywood: (a) the 2nd layer; (b) the 3rd layer.

4.3.5 MC of oriented strand board

Oriented strand board (OSB) is a wood-based panel made from strands of wood bonded together with a binder under pressure and heat. The strands in the core layer can be randomly oriented, or aligned. Its internal structure is more complex than solid wood and plywood panels. As illustrated in Fig. 4.14a, the MC measured by both electrical and X-ray CT method is less than 15%, which indicates little water can penetrate across 8 mm thick OSB after 16 days immersion because presence of paraffin wax can increase hydrophobicity of OSB. Fig. 4.14b also shows that there is a good agreement between these two MC measurement methods when the MC is below 20%. However, the electrical MC differs from X-ray MC in the last two measurements. As is well known, the glue distribution in each "layer" of OSB is not equal, causing an uneven water distribution. Because the uneven glue distribution, water will probably move at a different speed. If there is sufficient water between the electrodes and only little water close to the electrodes, a higher electrical resistance and thus a lower MC would be recorded than expected. On the contrary, if both electrodes are in contact with a volume with high MC, the electricity could follow the path of least resistance instead of the ROI of interest. The electrical MC would then be higher than the actual MC of the ROI. This hypothesis is visually supported by Fig. 4.15 in which the water is concentrated under the dashed line. It is obvious that the water distribution near these two electrodes can differ considerably. In Fig. 4.15a, there is little water around the right electrode, in Fig. 4.15b both electrodes are actually in contact with water. The electrical MC, therefore, is smaller than X-ray MC at 336 hours measurement and higher than X-ray MC at 384 hours measurement. Overall, the electrical MC measurement

method could be used in testing the MC of OSB if the water distribution is not important, but best in combination with X-ray CT scanning.
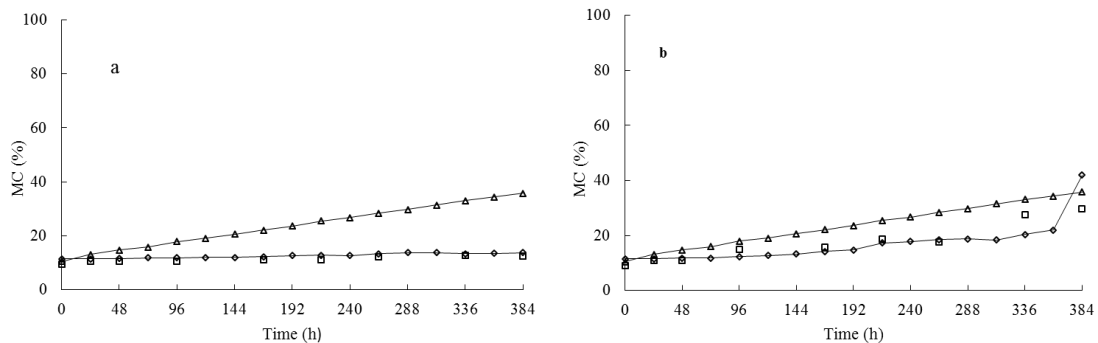
Fig 4.14. The MC of OSB tested by three methods. (a): the depth of 8mm; (b): the depth of 3mm. ◇ = electrical ROI MC, □ = X-ray ROI MC, △ = gravimetrical average MC.
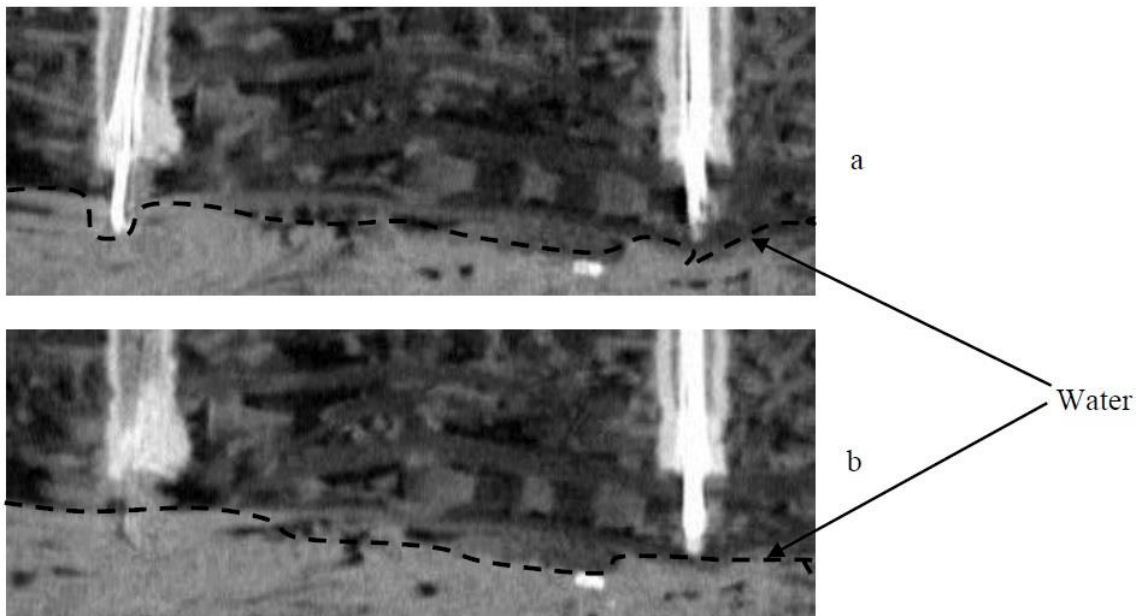
Fig 4.15. X-ray images of the internal structure of OSB at a depth of 3mm: (a) after 336 hours; and (b) after 384 hours of immersion.

4.4 Conclusion

The X-ray CT method presented here can accurately measure the MC and its distribution of wood and wood-based products. The electrical MC measurement method in its turn is an efficient approach to continuously monitor the moisture distribution of wood and wood-based products. This method can be used to measure the MC between the two electrodes if the MC is evenly distributed in this region. If not, it is difficult to reveal the actual MC of this region. To optimize this method, the microstructure and the position of the electrodes should be analyzed and checked carefully using X-

ray CT scanning during set-up. More precisely, the density distribution between the two electrodes plays a crucial role in the performance of the electrical MC measurement method on solid wood. The study shows that wood species with a uniform density distribution and especially plywood panels are very suitable to use this method. X-ray CT method is anyhow a necessary complementary technique if full moisture analysis is aimed at. This way, the position of the electrodes can be checked and the reliability of the recorded data can be analyzed, as well as interpreted correctly in function of the structure. Furthermore, accurate water distribution can be mapped and visualized non-destructively in addition to electrical MC measurements.

In future research, the electrical MC measurement method, combined with periodically X-ray tomography scanning, will be used to continuously monitor the MC distribution of wood specimens exposed outdoors. To measure the MC distribution more accurately using the electrical resistance method, the formula to convert resistance to MC will be adjusted in terms of the wood species specific resistance characteristics. In addition, the MC distribution will be used to assess decay risk. To optimize these MC measurement methods, new scan and reconstruction methods will be elaborated on to reduce metal artefacts. Also image processing software will be used to correct for dimensional changes (semi-)automatically.

Acknowledgement

5 Moisture behavior and structural changes of plywood during outdoor exposure

Abstract

Plywood is an important wood-based construction material yet prone to water uptake, as such potentially decreasing mechanical properties and increasing decay risk. It is, therefore, essential to understand the moisture behavior and structural changes of plywood in service. In this research, several plywood specimens were exposed in outdoor weathering conditions for approximately one year. During this period, the average moisture variation of and moisture distribution in different veneer layers of a set of plywood specimens and detailed field weather information were recorded continuously. The internal structure of the specimens was also monitored by periodically scanning using X-ray CT. Measurements indicate that moisture distribution in plywood is not homogeneous in outdoor conditions. The second layer can, in some plywood types, accumulate a significant amount of rain, and long rainy periods and cloudy weather can keep the moisture content of the inner layers of plywood significantly high. Moisture accumulation and moisture dynamics, in combination with wood species, are the main factors causing structural changes, mainly occurring as cracks, of the plywood veneers in service. The glue line between the veneers, however, is not ruptured after one year of outdoor exposure. Plywood with layers having a slow water sorption and fast water desorption could effectively avoid internal moisture accumulation and cracks in service. Based on the knowledge of the interrelationship of weather data, internal moisture behavior and structural changes in service, fit-for-purpose design of plywood could be improved and service life prediction is at hand.

5

5.1 Introduction

Plywood is a highly valued construction material which is used, more than other wood-based panels, in class 3 situations where it is subjected to natural weathering (Van Acker and De Smet, 2007). However, as a wood based material, moisture influences its physical and mechanical properties (Drow, 1957; Lee and Biblis, 1976). In practice, weathering conditions with alternating wetting and drying cycles could obviously decrease the mechanical properties of plywood (River, 1994). Knowledge on moisture behavior is thus essential to protect plywood panels and predict their changing properties in service. To obtain the average moisture content (MC) of wood samples and from wood derived materials, a continuous moisture measurement (CMM) set-up was developed, which can continuously weigh specimens' mass and simultaneously record the local climate (Van den Bulcke et al., 2009c). Based on the data from this CMM set-up, the relation between weather data and the amount of days with an average MC higher than 20% or 25% was further analyzed (Van den Bulcke et al., 2011). In addition to the average MC, other studies reported on continuously recording of the internal MC of solid wood samples by using electrical moisture measurements (Brischke et al., 2008a); decay in those monitored wood samples was further investigated as well and linked to the MC and local climate (Brischke et al., 2008b). With a similar set-up, an adapted electrical moisture measurement method was introduced by Li and co-workers (2013) to measure the internal moisture in plywood. This method allows to map the moisture dynamics of the different layers of plywood, which is especially valuable for in-service testing. With the data of the moisture distribution at hand, the influence of moisture on the performance of plywood in service can be investigated better and compared to using either only the value of the average MC or only the single-point internal MC. Non-uniform moisture distribution naturally leads to non-homogeneous variation in the properties of plywood in service. Studying moisture distribution in function of local properties of plywood is therefore valuable. X-ray CT scanning has been used to investigate the internal structure and density distribution of wood materials (Chen et al., 2009; De Ridder et al., 2011a; Lindgren, 1991). Hence, this method is well-suited to monitor the structural changes of plywood, which is essential to understand the influence of moisture distribution on local structure and vice versa. Although plenty of research reports on plywood, limited information is available on studying layer based properties of plywood in service (Antikainen et al., 2015; Gillespie and River, 1976; Kojima and Suzuki, 2011a, b; Reinprecht and Kmet'ova, 2014).

The objective of this paper is to highlight the moisture behavior, *i.e.* average moisture variation and moisture distribution, as well as structural changes of plywood specimens in outdoor weathering conditions. The specimens were subjected to two different exposure conditions, namely under cover and uncovered, for approximately one year. The cover can limit the impact of rainfall, sunshine and wind. Weather data was also recorded using a weather station consisting of a solar radiation sensor,

5

a tipping bucket rain gauge, a relative humidity probe and a thermometer. According to the results obtained with the techniques above, *i.e.* weather data logging, average moisture variation, moisture distribution mapping and mapping of structural changes, the relationship between weathering, moisture behavior and structural changes of plywood panels in service was analyzed.

5.2 Method and Materials

5.2.1 Preparation of the specimens

Specimens were prepared from uncoated plywood panels produced by European plywood companies. Two specimens from each plywood panel (Table 5.1) were cut to the size of $100 \times 100 \times$ (panel thickness) mm^3. In order to investigate the detailed performance of specimens, limited plywood types were used. All side edges of the specimens were sealed with a two component acrylic polyurethane sealant. Electrodes were carefully installed in the different layers of the specimens to monitor the MC of these layers (Table 5.1) according to the method described in Li et al. (2013). Afterwards, all specimens were conditioned at 65% relative humidity (RH) and 20 ℃ until constant mass prior to outdoor exposure on the CMM set-up as described in Van den Bulcke et al. (2009c). Specimens were put in two different exposure conditions on the CMM set-up to sheltered and non-sheltered situations. More specifically one set of specimens was covered with a textile sheet supported by two transparent hard plastic walls on south and north side with the surface of the specimens facing north while another set of specimens was not covered facing south (Fig. 5.1). Approximately 25% of rainfall and 25% of solar radiation could penetrate the cover used to shade the specimens. All specimens were installed at an angle of 45°. Adjacent to the CMM set-up, a weather station recorded precipitation (mm), relative humidity (%), solar radiation (W/m^2) and temperature (℃). For solar radiation measurement, the type of sensor is D-PYRPA-CA and it can measure total shortwave solar radiation. Electrical data loggers (Materialfox mini), all programmed with the same formula to convert electrical resistance to MC, were used to record the MC of all specimens. The electrical MC data was not corrected considering that the three wood are more or less similar and species correction is usually less than 2 percent (James, 1988). For other wood species, however, this could be different. The measurements started on 29th October 2013 with recordings of weather data and CMM weighing every 5 min, whereas electrical MC was measured every 10 min. The default minimum value of electrical MC measurement data logger is 11%. This study contains the data of approximately one year of outdoor exposure. Missing data, because of periodically removal of the specimens for scanning or due to temporary power failure, were excluded from the analysis.

Table 5.1

Plywood type, structure and position of electrodes (exposed face of the specimen = 1st veneer).

Code	Wood species	Glue	# of plies	Veneers (mm)	Thickness (mm)	Oven dry density (kg/m^3)	Electrodes (veneer number)
P1	poplar	UMF	7	1.0/2.6/2.6	14.9	0.34	2nd, 3rd, 4th
P2	poplar	PF	7	0.8/2.5/2.8	14.5	0.43	2nd, 3rd, 4th
B1	birch	PF	11	1.1/1.4/1.4	14.8	0.61	2nd, 4th, 6th
B2	birch	PF	11	1.5/1.4/1.4	15.7	0.63	2nd, 4th, 6th
O1	okoumé	PF	7	1.1/2.5/2.7	15.1	0.46	2nd, 3rd, 4th

PF: phenol formaldehyde glue; UMF: urea melamine formaldehyde glue.

Veneer thickness: top veneer/inner cross/ inner parallel.
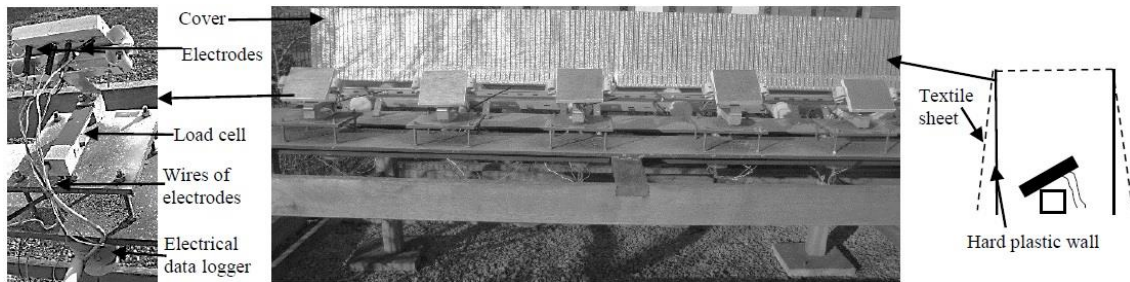
Fig 5.1. Set-up of the specimens in two different weathering conditions at CMM.

5.2.2 X-ray CT scanning and flatbed scanning

All specimens were periodically scanned with HECTOR (Masschaele et al., 2013), a high-energy CT scanner optimized for research, developed by the Ghent University Centre for X-ray tomography (www.ugct.ugent.be) in collaboration with the Ghent University (UGent) spin-off company XRE (www.xre.be). The approximated voxel pitch of the reconstructions was 80 µm. The specimens were scanned before outdoor exposure and on the 28th of November 2013, the 5th of February 2014, and the 5th of June 2014 and the 4th of October 2014. To ensure the similar conditions for all specimens, they were conditioned at 65% RH and 20 ℃ for one week before scanning. In addition to these periodic scans with moderate resolution, high resolution scans with an approximate voxel pitch of 20 µm of a region of interest of all specimens were obtained at the end of experiment. Reconstruction was performed using the software package Octopus Reconstruction (Vlassenbroeck et al., 2007b), licensed by the UGent spin-off company InsideMatters (www.insidematters.be).

The surface of all specimens was also scanned at the same time intervals using an Epson Perfection 4990 Photo Scanner with a resolution of approximately 50 µm.

5

5.2.3 CMM data processing

In order to obtain the MC of specimens after conditioning, 6 control specimens of $50 \times 50 \times$ (panel thickness) mm^3 for each plywood type were used (Eq. (5.1) and Eq. (5.2)). In this experiment, the part of the wires of the electrodes close to the specimen were attached to the CMM set-up, such that both mass of the specimen and the wires was measured. Since specimens were periodically removed for scanning and it is difficult to re-attach the wires at the exact same position, the average MC of specimens during exposure was calculated according to Eq. (5.3). The influence of wind on free-hanging wires was taken into account during data analysis also.

$$MC_c = (m_c - m_d) / m_d \qquad (5.1)$$

with MC_c: the moisture content of control specimen after conditioning (%); m_c: mass of the control specimen after conditioning (g); m_d: oven dry mass of the control specimen (g).

$$m_1 = m / (1 + MC_c) \qquad (5.2)$$

with m_1: oven dry mass of the specimen (g); m: mass of the specimen after conditioning (g);

$$MC_i = MC_c + (m_i - m_0) / m_1 \qquad (5.3)$$

with MC_i: the average moisture content at time i (%); m_i: the mass of the specimen and wires at time i; m_0: the initial mass of specimen (g).

5.3 Results and Discussion

5.3.1 Specific moisture behavior of specimens

The original 10 min electrical MC data and 5 min CMM data were converted to daily means by averaging as presented in Fig. 5.2 and Fig. 5.3. Specifically, precipitation and other weather data were recalculated by summing and averaging respectively. The moisture distribution between veneer layers is not always homogenous during weathering (Fig. 5.2 and Fig. 5.3). The moisture sorption and desorption is faster in the outer layers, as seen for P2 during the period of the 25th of December 2013 to the 6th of January 2014 highlighted with an arrow in Fig. 5.2. Both the average MC and MC in the inner layers of specimens, in general, is quite high from the 7th to the 27th of November 2013, which could be due to the cool and wet weather. During this period, heavy rainfall was registered nearly every day while temperature and solar radiation were approximately 10°C and 30 W/m² respectively (Fig. 5.2 weather data), which can induce water accumulation in specimens. Periods, such as the end of July 2014, without significant rainfall and high temperature combined with a high amount of solar radiation dry the specimens and decrease their MC. The MC in the second layer and fourth layer of P2 under cover between the 21st and the 31st of March 2014 is as high as 26% (Fig.

5.2 arrow b). Heavy rainfall (9.8 mm) on the 21st of March 2014 and slow moisture desorption in covered condition could be the cause of such high moisture content. Compared to the second and the fourth layer, the MC of the third layer of P2 under cover is lower. Possibly water accumulated mainly between the electrodes of these two layers, given the fact that the overall average MC is not significantly high. This could be a result from the position of the electrodes in layer P2 under cover, *i.e.* electrodes of the second and fourth layer are at the side close to the edge facing precipitation and the electrodes of the third layer are at the other side. Small amounts of water penetrating from above thus possibly induced an increased MC in the second and fourth layers of P2 under cover. The MC of the second layer of B2 between the 3rd and the 7th of March 2014 is also pronounced (arrow c in Fig. 5.3). Probably the electrical current, following the path of minimal resistance, could cross the glue line and flow along the top layer that was saturated with water after raining.

Relationship between average MC and moisture distribution of specimens in service

The influence of rainfall events on moisture dynamics in specimens is clearly distinguishable. Almost each rainfall event causes an average MC increase and a similar result was obtained by Van den Bulcke *et al.* (2009c). Compared to the average MC, the MC of the inner layers is also related to rainfall events but does not increase after each rain event, given that during a rainfall event water mainly accumulates in the outer layers and evaporates afterwards. Only heavy rainfall can result in an increase in the MC of the inner layers of all test specimens. The peak of MC in the inner layers (dashed arrow d) appears later than the peak of average MC (solid arrow d) after raining at the start of the exposure period (Fig. 5.3 B2 under cover), due to the slower process of water diffusion. This lag effect becomes small when exposure time increases, which could be caused by structure changes, *i.e.* crack formation, increasing the speed of water movement into specimens.

5

Fig 5.2. Daily moisture behavior of plywood specimens and weather data (from the 29th of October 2013 till the 4th of October 2014). ○= MC of the 2nd layer, Δ= MC of the 3rd layer, □= MC of the 4th layer, ◊ = average MC of specimens. Weather data: bar graph= precipitation, solid line= solar radiation, dashed line= temperature, dotted line= relative humidity. The amplified image relates to the image highlighted with nearby arrows.

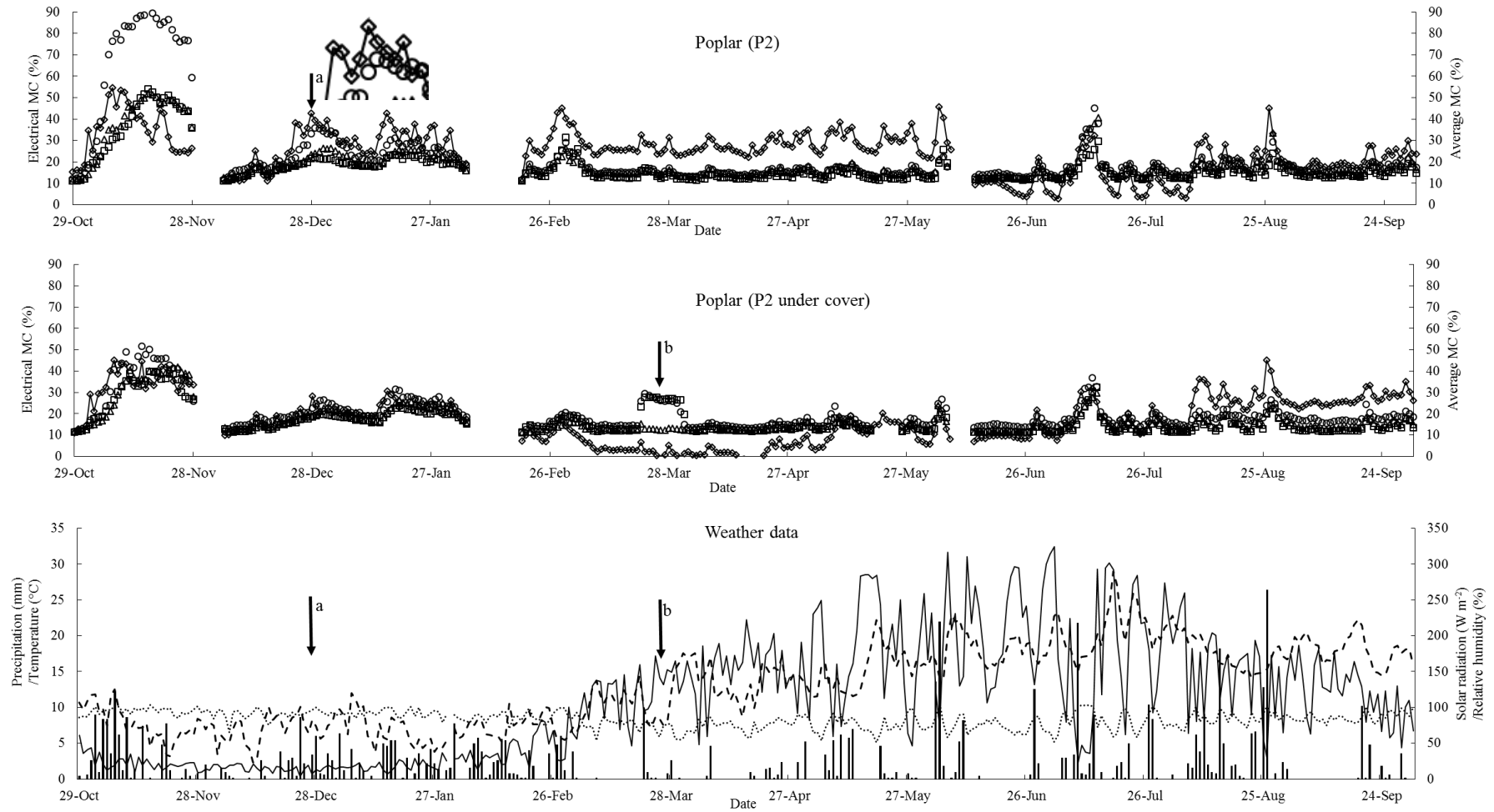Fig.5.3. Daily moisture behavior of plywood specimens and weather data (from the 29th of October 2013 till the 4th of October 2014). ○= MC of the 2nd layer, Δ= MC of the 4th layer, □= MC of the 6th layer, ◊ = average MC specimens. Weather data: bar graph= precipitation, solid line= solar radiation, dashed line= temperature, dotted line= relative humidity. The amplified images relate to the images highlighted with nearby arrows.
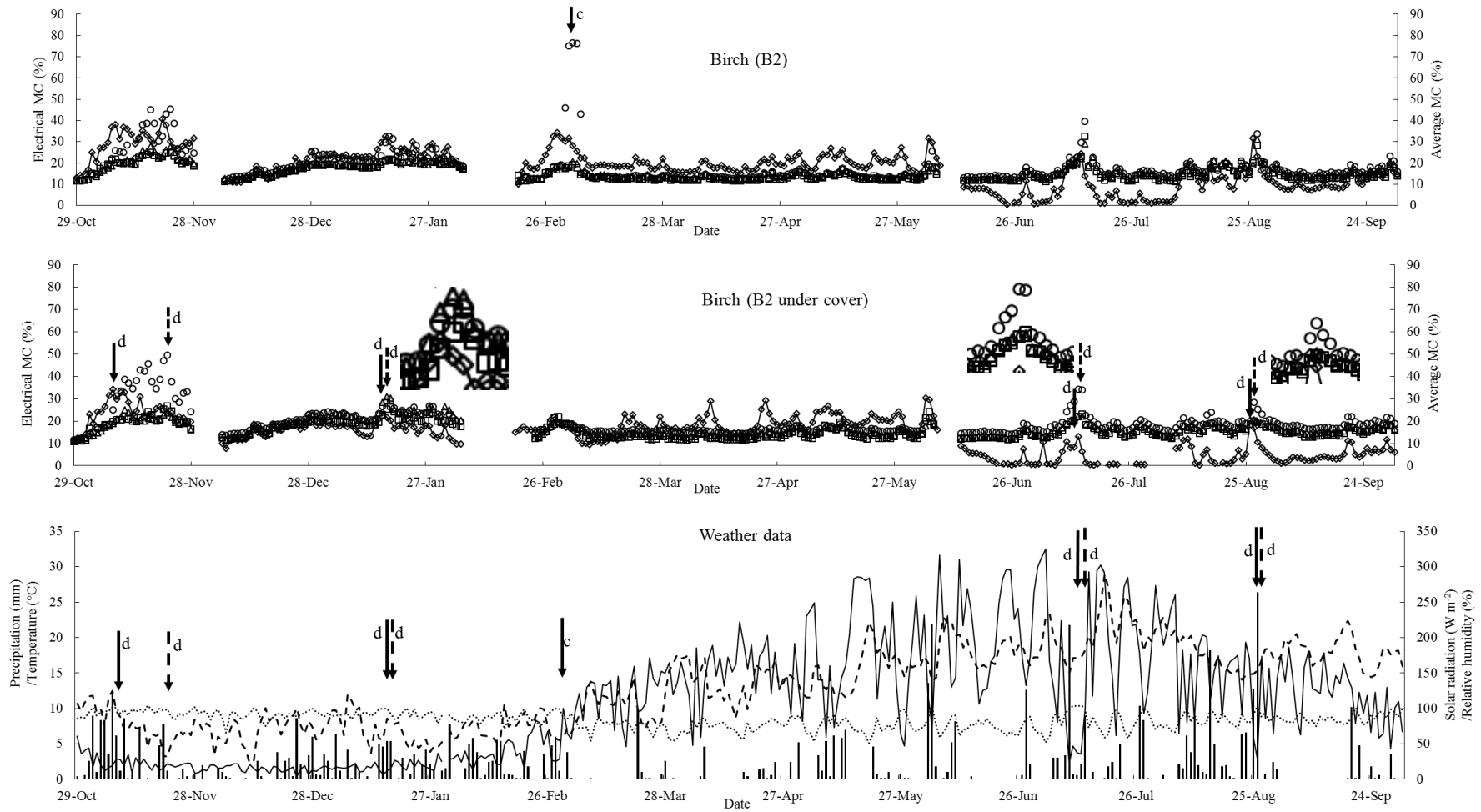
Moisture behavior in different exposure conditions

Specimens were subjected to two different exposure conditions, *i.e.* under cover and uncovered. The cover, partially protecting the specimens from rainfall, solar radiation and wind, is comparable to a partial shelter in practice. The influence of the cover on moisture distribution in the inner layers of the specimens is well correlated with average MC (Fig. 5.2 and Fig. 5.3). Both the average MC and inner MC of sheltered specimens is, in general, lower since part of the precipitated water is blocked by the sheet used to cover the specimens. There is, however, one exception. During the last 100 days of exposure (July, August and September of 2014), the average MC in uncovered P2 is slightly lower than in P2 under cover. It is possibly because water desorption is faster due to higher temperature and stronger solar radiation for the uncovered sample. The influence of a cover on the moisture dynamics of P2 is larger compared with B2. Poplar porosity is rather high, as such acting as a strong capillary reservoir of water. A rather large amount of water, therefore, is needed to saturate the poplar plywood specimens. Since the cover decreases the amount of precipitation, it has a significant influence on moisture dynamics of P2. Compared to B2, a larger amount of water and shorter sorption time is required for P2 when water reaches the inner layers as reported in Li et al. (2014) investigating moisture distribution on the same batch of specimens using neutron radiography. The cover decreases the amount of water absorbed by the specimen. Simultaneously, since solar radiation is reduced this results in slower water evaporation and thus longer wetting time. The cover, therefore, could have a larger influence on the MC in the inner layers of P2 than B2. This hypothesis is consistent with the results in Fig. 5.2 and Fig. 5.3. Specifically, the MC of the inner layers of P2 under cover is obviously smaller than P2 especially in the beginning of the exposure. The MC in the inner layers of uncovered B2 and B2 under cover are similar. This proves that the impact of a cover on the moisture behavior is different for different plywood types. This difference is mainly determined by plywood characteristics, *e.g.* wood species and glue line. During March and April of 2014, a low average MC and default minimum electrical MC of P2 under cover could be caused by water evaporation (solar radiation) in combination with only little water absorption.

Influence of weathering on the moisture distribution of specimens

The internal MC of specimens increased due to intensive rainfall events, however, the increase is not only concordant with the amount of precipitation (Fig. 5.2 and Fig. 5.3). This phenomenon is studied in detail by selecting two periods (from the 9th to the 14th of July 2014 and from the 24th to the 29th of August 2014). The amount of precipitation during these two periods is 34.4 mm and 40.0 mm respectively. The hourly MC and weather data were calculated and shown in Fig. 5.4 and Fig. 5.5. The inner layers of the specimens had an increased MC for a longer time in the first period compared to the second period, although a smaller total amount of precipitation is recorded (Fig. 5.4 and Fig. 5.5). This difference is caused by dissimilar weathering conditions. The weather in the first period is

cloudier with continuous rain and low solar radiation for most of the time. More water is absorbed when there is almost continuous rainfall, and in combination with low solar radiation, and thus low water evaporation, this increases the MC. In the second period, several separate heavy rainfall events were registered which caused an obvious increase in MC even in the inner layers of the specimens. The moisture, however, could quickly evaporate because of intensive solar radiation after rain. The short and non-continuous rain and cloudless weather could thus hardly increase the MC of the inner layers of the specimens. Similar results were obtained on average MC of plywood in weathering by Van den Bulcke et al. (2009c), which could be well explained by the moisture distribution obtained in this experiment. The average MC is significantly high in the night especially when rainfall events occur in the evening of the day before. This is based on low temperatures and only limited solar radiation resulting in higher MC. Rainfall events occurring in the middle of the day cannot increase the average MC significantly because high temperature and intense solar radiation are the main reasons of moisture desorption in such conditions (Fig. 5.4 hour 110). When taking a closer look at the cyclic MC in the second layer, it correlates with the alternation of day and night especially when there is no heavy precipitation. Specifically, the MC starts to decrease in the middle of the day (arrow in Fig. 5.4 and Fig. 5.5) and reaches a minimum around midnight. This phenomenon is not clear in the third and fourth layer that are less sensitive to such influences. The discrepancy between average MC and MC in the second layer could be due to the delay of moisture ingress and also the influence of temperature on the electrical MC measurement. According to the moisture distribution obtained by using neutron radiography in the same batch of the specimens, it takes approximately 15 hours for water to penetrate to the second layer of P2 (Li et al., 2014). During outdoor exposure, the emerging of micro cracks could increase water penetration. Hence, the peak of MC in the second layer of P2 occurs around 12 hours later than the peak of average MC. High temperature can also decrease electrical resistance of wood, which increases measured MC value. The temperature compensation factors calculated according to the formula provided by Brischke et al. (2008a) are listed in Table 5.2. Hence, intense solar radiation in the middle of day increases the temperature of specimens and then increases MC values measured with the electrical resistance method.

5

Fig 5.4. Hourly MC and weather data from the 9th to the 14th of July 2014. ○= MC of the 2nd layer, Δ= MC of the 3rd layer, □= MC of the 4th layer, ◊ = average MC of specimens, bar graph= precipitation, solid line= solar radiation, dashed line= temperature, dotted line= relative humidity.
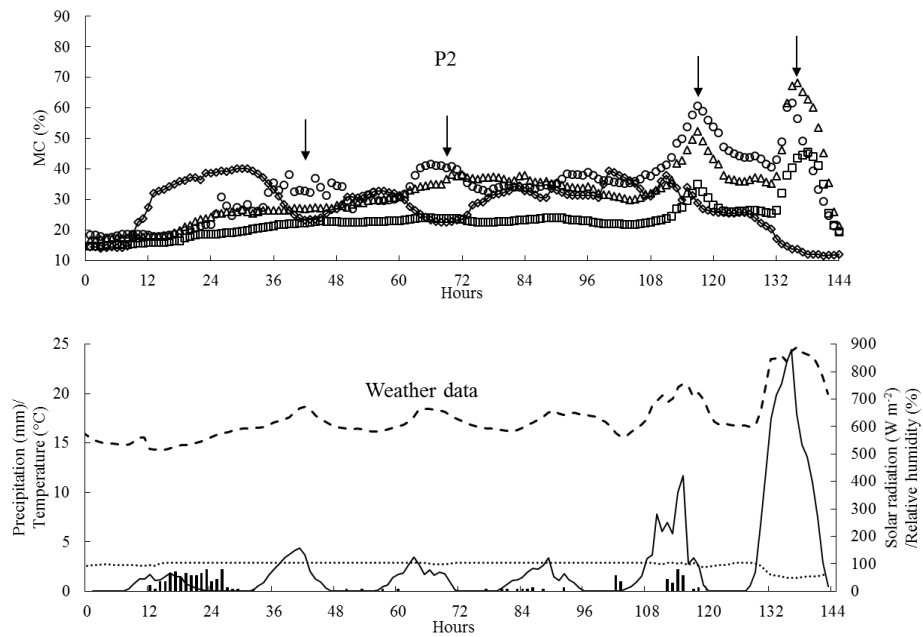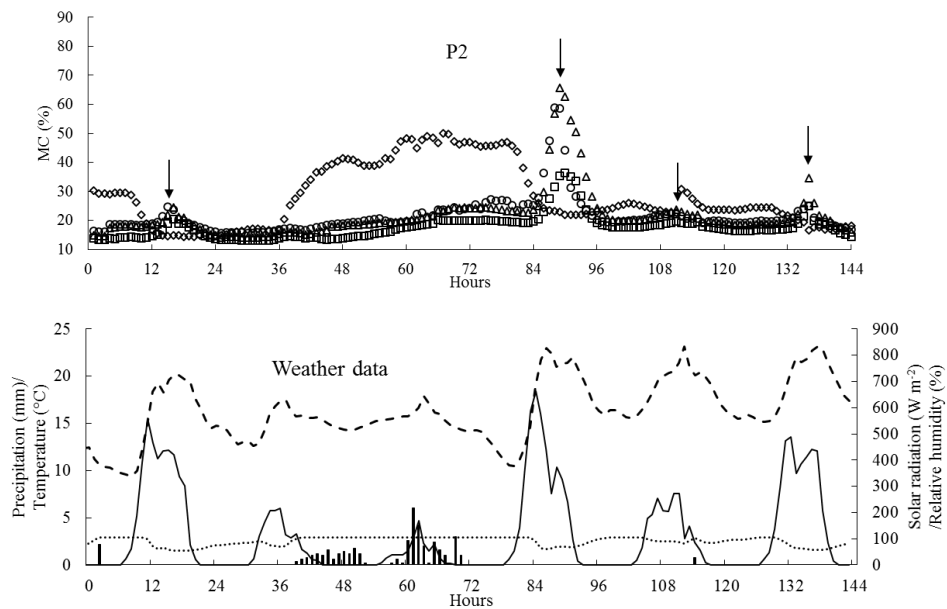

Fig 5.5. Hourly MC and weather data from the 24th to the 29th of August 2014 ○= MC of the 2nd layer, Δ= MC of the 3rd layer, □= MC of the 4th layer, ◊= average MC of specimens, bar graph= precipitation, solid line= solar radiation, dashed line= temperature, dotted line= relative humidity.

Table 5.2
Temperature compensation for a temperature difference of 20°C for Scot pine sapwood at different moisture content levels, with moisture content measured at 20°C.

Moisture Content (%)	65	48	30	23
Temperature compensation (%)	13.4	11.2	8.4	5.7

5.3.2 Relationship between moisture distribution and plywood characteristics

Temperature and moisture are the most important factors for fungal growth in wood based materials (Viitanen, 1997). Generally, the MC threshold for decay is influenced by wood and fungal species as well as the type of wood treatment (Meyer and Brischke, 2015). In this research, 20% MC was used as the reference value for calculation of time of wetness (TOW) in different layers of the exposed plywood panels.
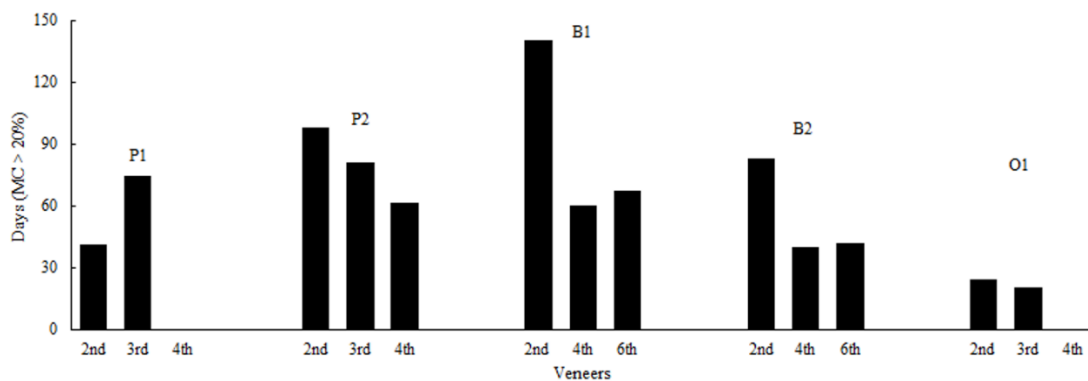
Fig 5.6. Amount of days with an MC higher than 20% (TOW) in different layers of the specimens.

Moisture accumulated for most of the specimens in the second layer causing a high TOW (Fig. 5.6). For P1 with UMF glue, however, most of the water accumulated in the third layer, which is possibly due to water re-distribution resulting in water accumulation in the third layer or water penetration partially via the voids of the drilled holes to the region between the electrodes of the third layer of P1. The TOW in each layer of P1 is smaller compared to P2, which means UMF could efficiently protect plywood from water penetration. This result is consistent with the results obtained with neutron radiography and standard laboratory absorption testing (Li et al., 2014).

Compared with the TOW of poplar (P) and birch plywood (B), the TOW of okoumé plywood (O) is much lower. Consequently, okoumé, a wood species with high water resistance, could be effectively used as water barrier although low durability. The PF glue used in O1 also allowed a high moisture desorption rate. Thus plywood similar in behavior to O1 could be suitable for outdoor application.

B1 is identical to B2, except the latter has a thicker top veneer. Fig. 5.6 illustrates that the TOW in the inner layers of B1 is larger than in the inner layers of B2. Investigating the distribution of days with MC higher than 20% shows that, compared to B1, the lag of moisture accumulation in the

monitored layers of B2 occurred before the 6th of March 2014 (Fig. 5.7). This difference could be explained by the top layer acting as a water reservoir. More water and a longer wetting time is needed for the moisture to cross the top layer and to reach the second layer. During this period, the TOW of the monitored layers in B1 and B2 is similar, which indicates that a thicker top veneer in B2 cannot effectively prevent the inner layers from water uptake. The higher TOW of B1 in the last exposure period (after the 1st of May 2014) could be the result of a structural change of the top veneer. Fig. 5.8 shows that compared to B2, the cracks in B1 are wider and closer to the glue line. Hence, water can easily reach the glue line and penetrate to the next layer, which induces a higher TOW in the inner layers of B1.
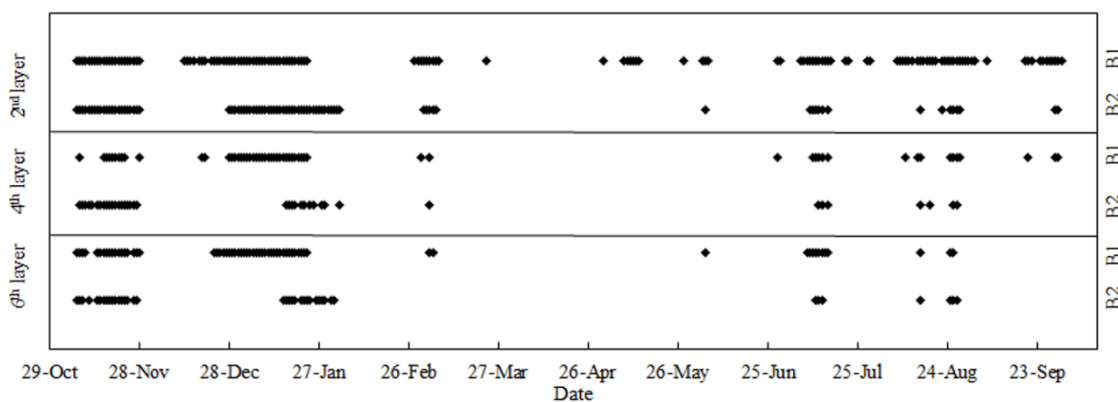
Fig 5.7. Days with MC higher than 20% (TOW) in the different layers of B1 and B2.
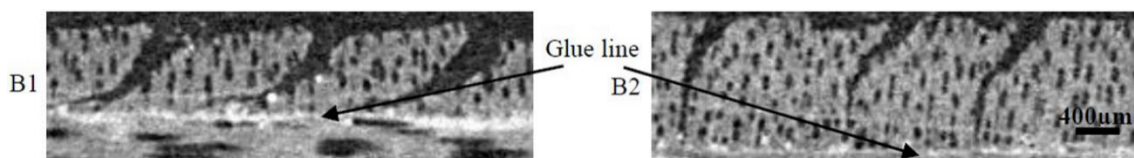
Fig 5.8. Structure of the top veneers (top layer in the images) of B1 and B2 after approximately one year exposure obtained from X-ray CT scanning with high resolution.

5.3.3 Structural changes of specimens during weathering

Surface appearance of the specimens

The surface of the specimens clearly changed as function of exposure time. The most apparent changes are cracking and darkening (Fig. 5.9).

Cyclic sorption-desorption and related swelling-shrinkage can lead to significant changes. The surface scans in Fig. 5.9 illustrate the variation in surface appearance among wood species. Birch plywood has a high amount of rather deep cracks compared to poplar and okoumé plywood. The amount of swelling-shrinkage, generally speaking, positively relates to the density of wood (Walker,

1993). In weathering conditions with repeated wetting and drying, large shape variation occurred in birch plywood due to its high density and thus significant structural changes, mainly cracks, in birch plywood appeared.

Darkening and even degradation of the surface could be induced by fungi decomposing the carbohydrates and lignin, surface oxidation, generation of new chromophoric groups and other processes described in depth in literature (George, 1991; Hon and Feist, 1986). Wood degradation in weathering is initiated primarily by solar radiation (Williams, 2005). The significant amount of solar radiation in summer time (between the 5th of June and the 4th of October 2014) is thus an essential factor for wood discoloration and degradation shown as obvious visible changes in appearance in this period (Fig. 5.9).
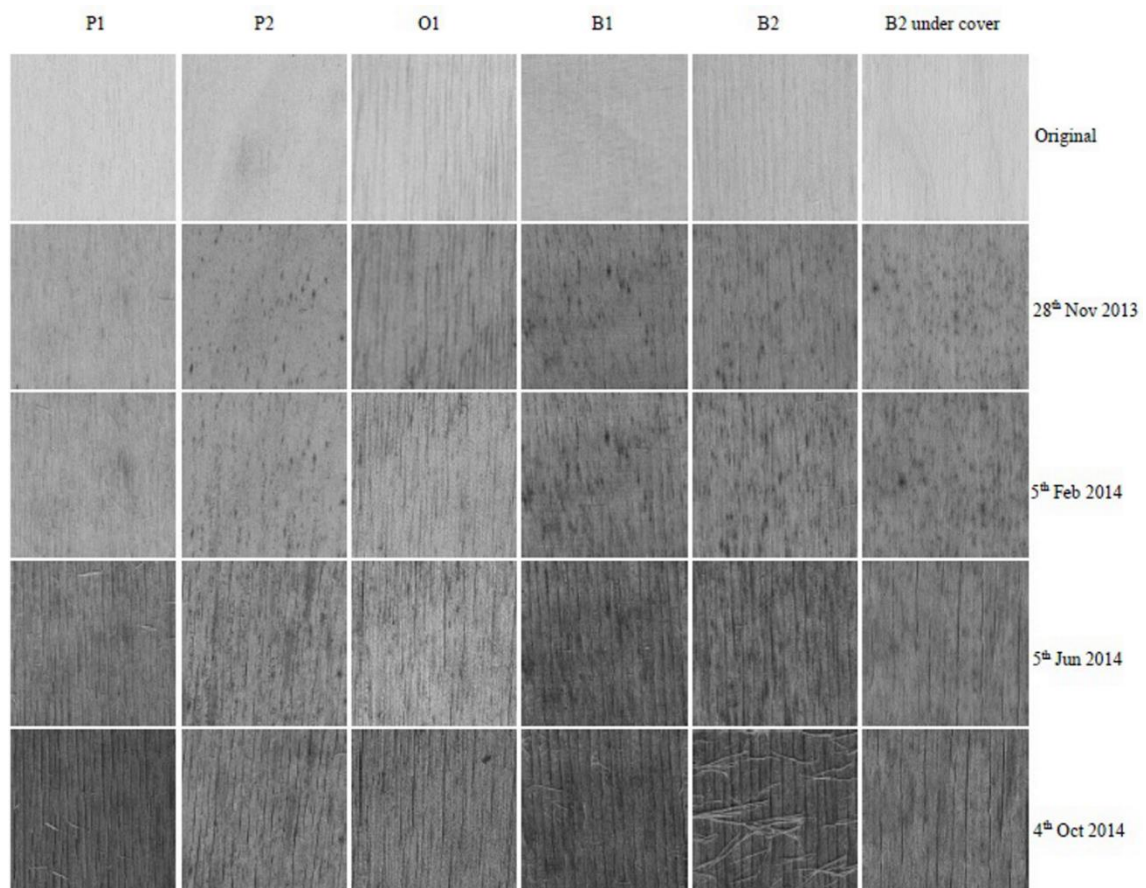
Fig 5.9. Surface of the specimens imaged with a flatbed scanner.

Fig. 5.9 shows that, in general, after approximately one year exposure, the effects are much less pronounced for specimens under a cover, although the surface of B2 under cover also darkens and has cracks. Nevertheless, compared with B2 uncovered, these changes are much smaller.

Changes in the veneers

Surface discoloration and structural variations, which are visible on the surface, are used to assess the durability of wood-based products (Evans et al., 1996; Kropf et al., 1994). The internal structural changes, however, are difficult to take into account. Changes in the internal structure during long-term exposure can definitely influence properties. One can visualize these changes by X-ray CT scanning. P2, B1 and B2 all show distinct cracks appearing in the second layer (Fig. 5.10). Their low water resistance even increases moisture dynamics and causes cracks in the second layers. Water can easily penetrate along veneer checks of plywood (Li et al., 2014), the emerging of cracks during outdoor exposure is thus possibly due to the enlargement of veneer checks. The difference between the original scan and the scan after approximately one year is, however, small for P1 and O1. The third and fourth layer of specimens were also investigated, showing no obvious structural changes.
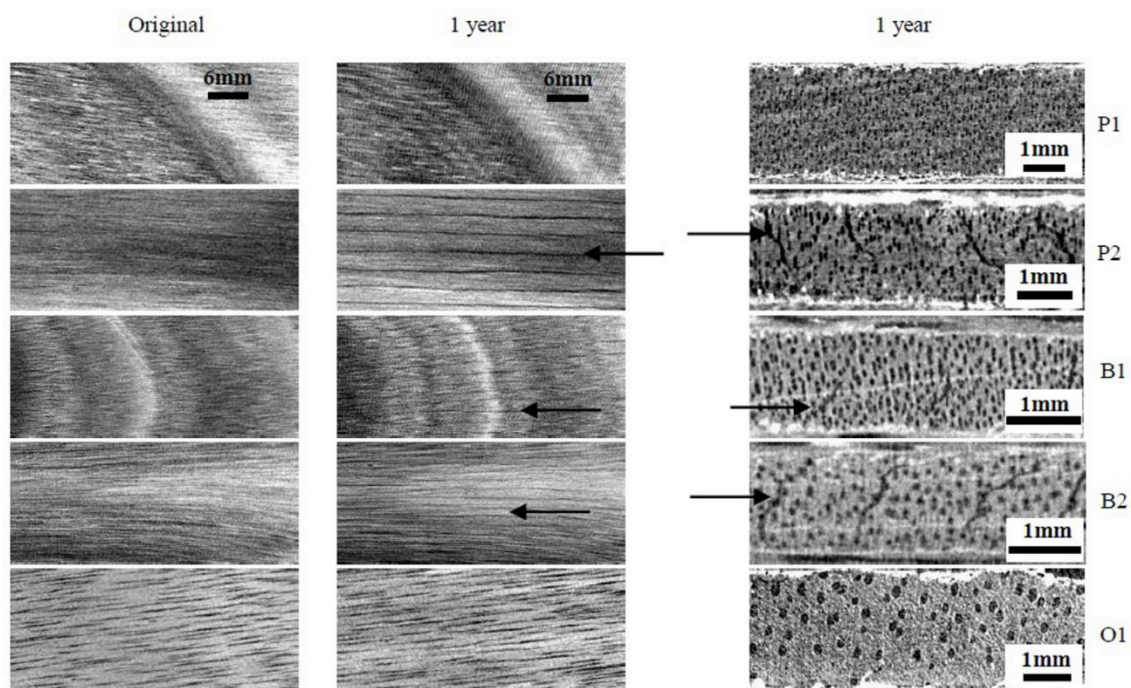
Fig 5.10. Horizontal cross-sections (left two columns) and vertical cross-sections (right column) of the second layer of specimens obtained with moderate resolution at periodic intervals and final high resolution X-ray CT scanning respectively.

Changes in the glue line

Compared to other wood-based materials, plywood clearly benefits from a clear and integral glue line as an effective barrier against water uptake. A durable glue line is thus essential for the performance of plywood panels in outdoor application. Fig. 5.11 is a single slice through the plywood volume scanned with high resolution (20 μm) X-ray CT at the end of the experiment. Within the resolution limit, no clear rupture in the glue lines of all specimens is detected after one year of outdoor

exposure. The cracks in the top layer of the specimens are clear and several severe cracks even reach the glue line (Fig. 5.11 B1 and B2). It was shown that cracks also appear in the second layer of B1 and B2. These cracks, however, are not causing rupture of the glue line between them. Although cracks occurred in the veneers during weathering, the intact glue line still could act as water barrier. A strong glue line is crucial to improve the durability of plywood and can be influenced by glue type, pressing parameters and veneer wood species. These results, however, are after 1 year of exposure, yet rupture of the glue line can occur after longer exposure: Van den Bulcke et al. (2011) found cracks crossing the glue line of plywood specimens after two years of outdoor exposure in a similar outdoor climate.
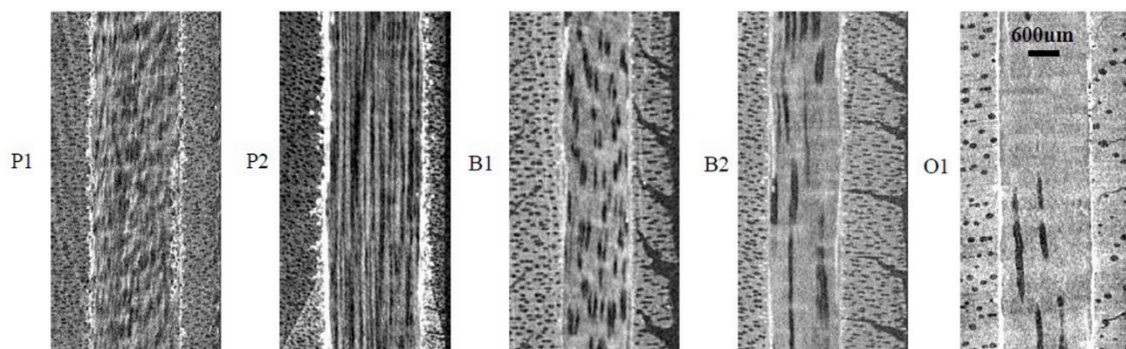
Fig 5.11. Detailed microstructure of the three top layers (right layer is the top layer) of the tested specimens after approximately one year outdoor exposure obtained with high resolution X-ray CT scanning.

5.4 Conclusion

Moisture distribution in plywood specimens is not homogenous during outdoor exposure. Continuous raining, thus implying long term cloudy weather, even increases the moisture accumulation in the inner layers of the plywood specimens. High temperature and intensive solar radiation, on the other hand, are the major factors for moisture evaporation. Short-term MC changes in the second layer correlate with the alternation of day and night. In addition to weathering conditions, the characteristics of plywood specimens significantly influence the moisture accumulation in inner layers. For specimens glued with PF, the second layer is prone to water accumulation giving rise to a high time of wetness (TOW). A UMF glue line can effectively limit water uptake. Wood species absorbing only little water are key for decreasing the risk of high TOW in inner layers of plywood. Thick top veneers can lag the moisture accumulation in inner layers. After approximately one year outdoor exposure, the structural changes occur and the moisture behavior of specimens was influenced accordingly. The cracks appear in the top layer of all specimens and the second layer of specimens with low water resistance. Cracks emerging in top veneers during exposure can increase moisture accumulation in the inner layers. The glue lines of all specimens are

not ruptured after approximately one year of exposure. Based on the above findings, plywood including layers with slow moisture sorption and fast moisture desorption could effectively avoid moisture accumulation in the inner layers. Veneers made of wood species with good water resistance, like okoumé, could be more suitable as top veneer of plywood aiming at outdoor application. During plywood production, it is however difficult to prepare each layer with these properties. Hence, carefully preparing outer layers is the main focus. Optimizing the combination of wood species, glue line and veneer thickness is essential. In future research, it would be interesting to study the effect of water vapor diffusion, water liquid flow, and heat transfer on the electrical MC measurement method. Combining the TOW and temperature of different layers, service life prediction of plywood could be predicted. It is also important to relate the TOW with real fungal decay (mass loss) of layers. To improve service life prediction of solid wood, investigating moisture distribution is thus essential.

Acknowledgement

6 Relating MOE decrease and mass loss due to fungal decay in plywood and MDF using resonalyser and X-ray CT scanning

Wanzhao Li, Jan Van den Bulcke, Imke De Windt**,** Nele Defoirdt, Jelle Dhaene, Manuel Dierick, Hugo Sol, Joris Van Acker. Relating MOE decrease and mass loss due to fungal decay in plywood and MDF using resonalyser and X-ray CT scanning. International Biodeterioration & Biodegradation (Under review)

Abstract

Both plywood and medium density fiberboard (MDF) are important engineered wood products or at least specifically often intended to be applied in service conditions with fungal decay risk, which can lead to a decrease in physical and mechanical properties. It is thus essential to understand the detailed performance over time of the panels under fungal decay using non-destructive techniques. The specimens were exposed to wet vermiculite inoculated with *Pleurotus ostreatus* for 14 weeks. A flexural vibration method (resonalyser) was used to measure the modulus of elasticity (MOE) of the specimens, whereas the internal structure and mass loss distribution were monitored with X-ray CT scanning. Resonalyser is proven to be a reliable method to measure the MOE of plywood and MDF products when compared with static bending test results. The significant MOE decrease of standard MDF, fit for non-humid conditions, is a result of internal cracking. MDF produced with acetylated fibers had only a 1.5% mass loss and 10% MOE decrease after fungal decay testing. Plywood specimens exhibit a MOE decrease of approximately 12% at incipient fungal decay partially resulting from water dynamics and structural changes such as cracks. There is a linear relationship between MOE decrease and mass loss, yet different for different types of plywood. Most mass loss occurs in the surface layers causing significant MOE decrease of entire plywood specimens, whereas the mass loss of the inner layers is influenced by the structure of the veneers such as grain direction.

6

6.1 Introduction

Wood based products are intensively used in the building industry as a construction material. They are flexible in use, have a high strength to weight ratio and are sustainable materials, which are clear advantages compared to other alternative materials such as plastic, metals and cement (George, 1991; Issa and Kmeid, 2005). Wood based products, however, are prone to water uptake and biological degradation in service, which can decrease their mechanical strength (Schirp and Wolcott, 2005). Understanding the impact of biological degradation on the mechanical strength of wood based products is important from a construction point of view. At the incipient stage, fungal decay causes changes in the chemical composition of wood and induces a measurable strength decrease before measurable mass loss (Winandy and Morrell, 1993). From then on, there is a direct relationship between strength loss and mass loss of wood (Curling et al., 2002). Plywood is an important representative of the wood-based panels group and widely used in class 3 situations (Van Acker and De Smet, 2007) and the only WBP considered suitable for load bearing application. Currently, several medium density fiberboard (MDF) products produced with treated fibers are also considered to have a good durability in service (Suttie et al., 2015). The mechanical strength of plywood and MDF during several years of outdoor exposure was studied by other researchers by periodically measuring the modulus of rupture (MOR) and internal bond strength (IB) (Kojima et al., 2011; River, 1994). The use of accelerated aging to evaluate mechanical strength decrease of wood-based panels was also investigated to compare with outdoor exposure (Kojima and Suzuki, 2011b). Fungal decay of plywood in outdoor exposure was further studied by Van den Bulcke et al. (2011; 2009c) reporting on the importance of glue type on the biological durability of plywood. Although substantial research on the overall biological degradation of plywood and MDF has been performed, there is a need for non-destructive measurements of strength and structure in function of decay time. Investigating the internal structure, mass loss and strength decrease due to fungal decay can provide valuable knowledge on understanding the mechanics of decay. X-ray CT scanning is a valuable method to non-destructively monitor the internal structure and density distribution in wood based materials (De Ridder et al., 2011b; Herve et al., 2014). Flexural vibration has been used to non-destructively measure the mechanical strength of wood based materials (Haines et al., 1996). A so-called 'Resonalyser' technique was further developed to determine the elastic properties of orthotropic plates from resonance frequencies (Lauwagie et al., 2003). These methods are thus feasible to non-destructively visualize and quantify the biological degradation of plywood and MDF.

The objective of this paper is to investigate fungal decay of plywood and MDF by monitoring strength decrease and mass loss of the specimens in a laboratory test. The specimens were prepared from several types of plywood and MDF available on the market. Modulus of elasticity (MOE) of the specimens was measured using resonalyser and static bending as validation test. The specimens

were scanned with X-ray CT to obtain information on the internal structure. They were put in culture boxes for 14 weeks to test for fungal decay. During this period, three replicates were removed from the culture vessels after 6 weeks, 10 weeks and 14 weeks respectively and internal structure, MOE and mass loss of these specimens were then recorded. Based on the interrelationship of MOE decrease, mass loss, mass loss distribution and internal structure, the influence of fungal decay on the mechanical strength of plywood and MDF was analyzed.

6.2 Method and Materials

6.2.1 Preparation of the specimens

Beam-shaped specimens, measuring $30 \times 360 \times$ (panel thickness) mm^3, were prepared from each type of panel (Table 6.1) from different European suppliers. Three replicates were used to evaluate the flexural vibration technique with static bending and nine replicates were used for fungal decay testing. Three replicates from plywood panels and MDF-C were used as reference specimens to evaluate the influence of the experimental setup without fungal growth on the mechanical strength of the specimens. The grain direction of the odd and even layers of the plywood specimens is shown in Fig. 6.1. Standard MDF is a product aiming at internal use in non-humid interior use conditions. MDF-C is considered to have a good durability in service and is produced using acetylated wood fibers (Suttie et al., 2015). Virulence control specimens measuring $15 \times 25 \times 50$ mm^3 were prepared from beech (*Fagus*). A flow chart of the different tests performed is shown in Fig. 6.2.

Table 6.1

The type, structure and characteristics of plywood and MDF panels.

Code	Type of panels	Wood species	Glue	# of plies	Veneer thickness (mm)	Thickness (mm)
P1	Plywood	poplar	UMF	7	1.0/2.6/2.6	14.9
P2	Plywood	poplar	PF	7	0.8/2.5/2.8	14.5
B1	Plywood	birch	PF	11	1.1/1.4/1.4	14.8
O1	plywood	okoumé	PF	7	1.1/2.5/2.7	15.1
Standard MDF	MDF		UF			18.0
MDF-C	MDF		MDI			14.5

UF: urea formaldehyde glue; MUF: urea melamine formaldehyde glue; MDI: diphenylmethane diisocyanate.
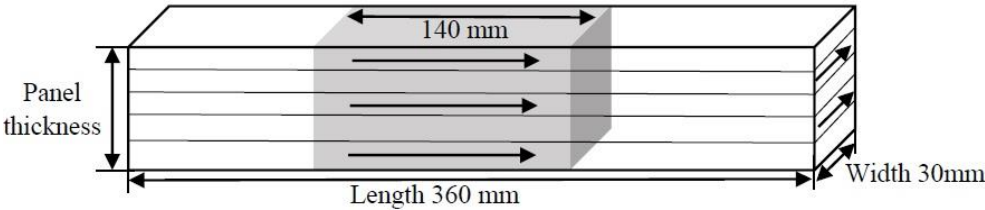
Fig 6.1. Schematic overview of the plywood specimens with indication of grain direction (arrow). Selected zone with grey color is for X-ray CT scanning.
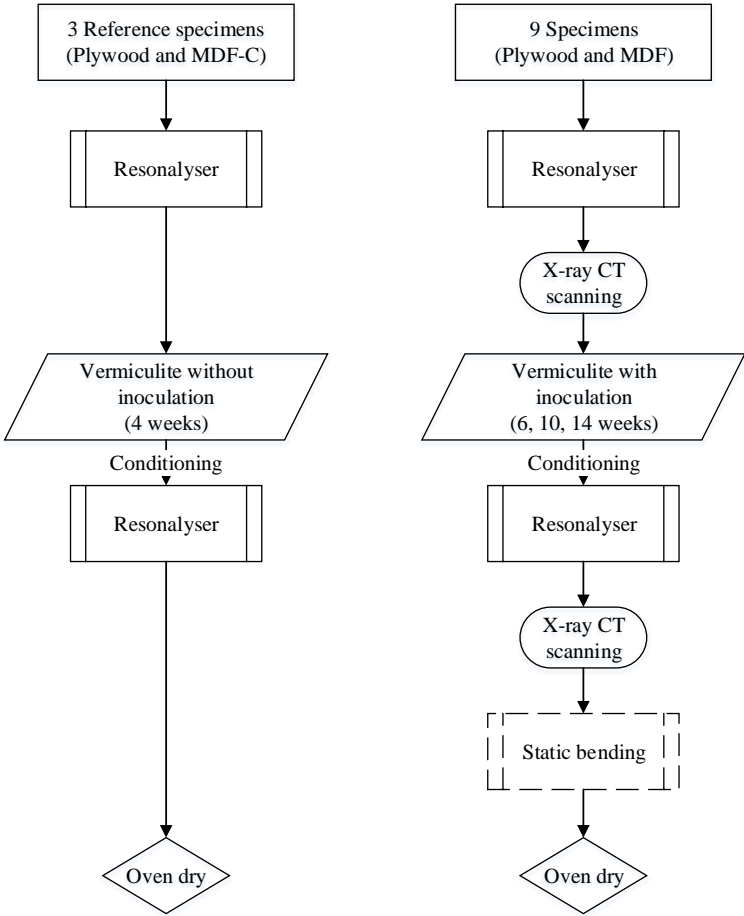
Fig 6.2. Schematic overview of the different experimental steps.

6.2.2 Fungal decay testing

Specimens

All test panels were with aging for more than one year. All specimens were conditioned in a conditioning room at 65 ± 5 % relative humidity (RH) and 20 ± 1 ºC until constant mass before recording. The beam-shaped specimens were then surface-sterilized by immersing in disolol containing 97% ethanol and 3% isopropyl alcohol (IPA) for two seconds, subsequently swiping them through the flame of a bunsen burner and extinguishing the flame within five seconds, as such

limiting the impact on the mechanical strength of the specimens. It is similar with the method for sterilizing the surface of plants (Akgul et al., 2014). All sterilization was performed aseptically in a laminar flow chamber. The virulence control specimens were sterilized with steam based on CEN/TS 12038 (2002).

Culture vessels

As culture vessels transparent, plastic boxes, measuring $390 \times 330 \times 150$ mm^3, with a lid were used. The boxes were sterilized using disolol.

Vermiculite and fungal inoculation

Vermiculite was prepared and sterilized with steam according to CEN/TS 12038 (2002). A buffer solution was prepared using 50 ml HCl (0.1 mol/L) + 950 ml KCl (0.1 mol/L) + 40 g of malt extract and autoclaved. Next, 840 g of vermiculite was mixed with 1600 ml buffer solution. After soaking with the buffer solution for 2 hours in aseptical conditions, vermiculite was inoculated with *Pleurotus ostreatus* that is more often present in hardwood and glue non-sensitivity (De Smet and Van Acker, 2006). The inoculated vermiculite was then transferred to glass bottles and placed in a conditioning chamber at 65 ± 5 % and 20 ± 1 ºC for two weeks. Also some vermiculite were soaked with steam sterilized demineralized water for 2 hours and not inoculated.

The fungal test set-up is intended to invoke homogeneous decay through the overall surface presence of vermiculite particles covering with water and the test fungus. Hence, nine specimens from the same panel type and six virulence control specimens were put in one culture vessel and immersed in inoculated vermiculite. All reference specimens from plywood panels were put in one culture vessel and immersed in non-inoculated vermiculite. The gap between the box and lid was sealed with parafilm. All above was also performed aseptically. Finally, the culture vessels having inoculated vermiculite were put in a conditioning room for 14 weeks. During this period, three specimens were removed from each culture vessel after 6, 10 and 14 weeks respectively. The objective of selecting maximum 14 weeks experimental time is to assure moderate mass loss and avoid destructive structural changes. The reference specimens in the culture vessel having non-inoculated vermiculite were removed after 4 weeks to avoid possible fungal decay. These specimens were cleaned by removing vermiculite at the surface and conditioned in a conditioning room at 65 ± 5 % and 20 ± 1 ºC for 4 weeks.

6.2.3 X-ray CT scanning and image processing

The specimens were scanned with HECTOR (Masschaele et al., 2013), a high-energy CT scanner optimized for research, developed by the Ghent University Centre for X-ray Tomography (www.ugct.ugent.be) in collaboration with the Ghent University spin-off company XRE

(www.xre.be). The central 140 mm region of the specimens was scanned before and after fungal decay (Fig. 6.1 grey color). Twelve specimens were scanned at once using a custom-made sample holder also containing reference material and water-filled tubes (Fig. 6.3). One scan takes approximately 34 min and creates 18 GB volume of X-ray images. The approximated voxel pitch of the reconstructions was 80 µm. To obtain further detailed information on the structure of the specimens, a selection of specimens after fungal decay was scanned with a resolution of 20 µm using a central 3 mm region of two specimens for each scan. Reconstruction was performed using the software package Octopus Reconstruction (Vlassenbroeck et al., 2007b), licensed by the UGent spin-off company InsideMatters (www.insidematters.be).
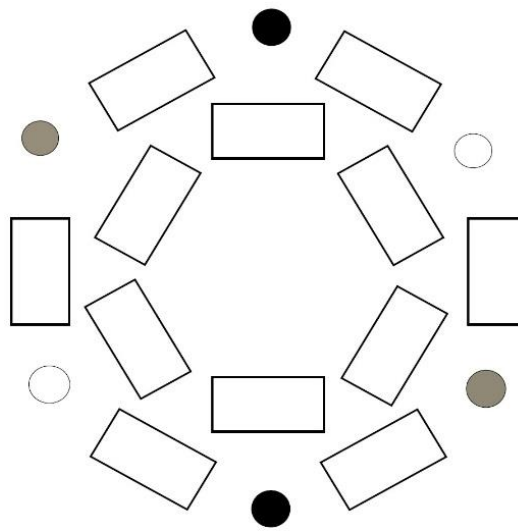
Fig 6.3. Schematic cross section through the custom-made sample holder for X-ray CT scanning. ⬜= the specimens, ○ = air, ● = water, ● = reference material.

6.2.4. Modulus of elasticity

Modulus of elasticity (MOE) was measured using both a non-destructive and a destructive technique, respectively resonalyser and four-point static bending. Resonalyser requires a free hanging specimen (see Fig. 6.4). A sensor was glued centrally on one side of the specimen. The resonance frequency was acquired by tapping the specimen with a hammer at the opposite side of the sensor.

6
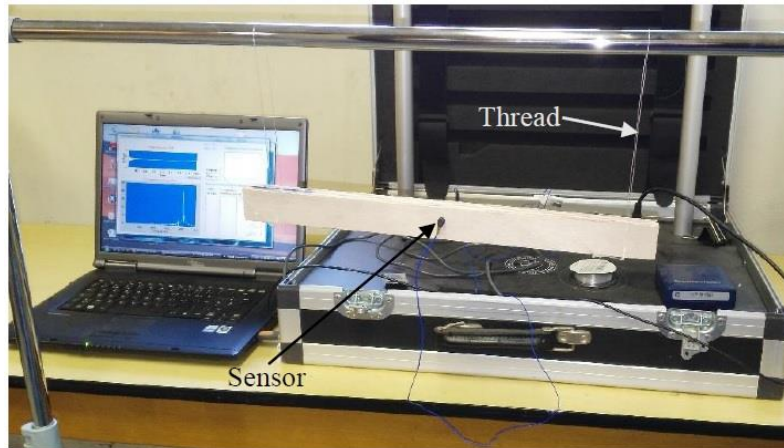
Fig 6.4. Overview of resonalyser setup.

The MOE was calculated according to the formula given by Lauwagie *et al*. (2003). After non-destructive measurement, MOE was measured using classical four-point static bending in accordance with the EN 789 (2004) to validate resonalyser results. Once validated, MOE decrease of the specimens was calculated according to resonalyser data with Eq. (6.1):

$$ED = (E_b - E_a) \times 100 / E_b \qquad (6.1)$$

with ED: MOE decrease of the specimen (%); E_a : MOE of the specimen after fungal decay (GPa); E_b: MOE of the specimen before fungal decay (GPa).

6.2.5. Mass loss

In order to obtain the oven dry mass of the conditioned specimens before fungal decay, six control specimens measuring $50 \times 50 \times$ (panel thickness) mm^3 for each type of panel were used. MC of the control specimens was acquired using Eq. (6.2).

$$MC_c = (m_c - m_d) \times 100 / m_d \qquad (6.2)$$

with MC_c: the moisture content of the control specimen after conditioning (%); m_c: mass of the control specimen after conditioning (g); m_d: oven dry mass of the control specimen (g).

MC of the specimens before fungal decay was assumed to be consistent with MC of the control specimens. As such, the oven dry mass of the test specimens before fungal decay can be obtained using Eq. (6.3).

$$m_l = m / (1 + MC_c) \qquad (6.3)$$

with m_l: oven dry mass of the specimen before fungal decay (g); m: mass of the specimen before fungal decay (g).

At the end of fungal decay testing, MOE of the specimens was measured using four-point static bending after which samples were oven dried (Fig. 6.2). The specimens were weighed before and after static bending to correct for potential mass loss during testing. Mass loss of the specimens caused by fungal decay was thus calculated with Eq. (6.4).

$$M = [m_l - m_o \times (m_{be} / m_{af})] \times 100 / m_l \qquad (6.4)$$

with M: mass loss of the specimen (%); m_o: oven dry mass of the specimen after static bending (g); m_{be}: mass of the specimen before static bending (g); m_{af}: mass of the specimen after static bending (g).

6.2.6. Mass loss distribution in plywood

X-ray CT scanning is based on the absorption of X-rays by the object under study. This absorption depends on the energy at which the scan is performed, the chemical composition and the density of the material. The plywood samples scanned here consist of a combination of wood, water and glue, governing the attenuation and thus the reconstructed greyscale values. Due to the glue line can hardly be decayed by fungi, the variation of wood and water was considered only to investigate the grey scale value of plywood veneers (Eq. (6.5), (6.6) and (6.7)).

$$G = G_w + G_h \qquad (6.5)$$

$$G_w = \mu^{w'} \times \rho^w \qquad (6.6)$$

$$G_h = \mu^{h'} \times \rho^h \qquad (6.7)$$

with G: the average grey scale value of the material; G_w: the average grey scale value of oven dry wood; G_h: the average grey scale value of pure water; $\mu^{w'}$: the attenuation coefficient per unit mass of wood (cm^2/g); ρ^w: the density of wood substance (g/cm^3); $\mu^{h'}$: the attenuation coefficient per unit mass of water (cm^2/g); ρ^h: the density of water (g/cm^3).

Although fungal decay can degrade the cell wall of wood and then decrease its density, the basic chemical composition of wood will not change significantly. Normally, white rot fungi could decompose both carbohydrate (cellulose and hemicelluloses) and lignin (George, 1991). Therefore, we assume that fungal decay does not change the attenuation coefficient of the wood, which is surely valid at lower decay levels. The attenuation coefficient of wood can then be obtained by scanning a reference material that has a chemical composition and density similar to that of wood cell walls

using Eq. (6.8) (De Ridder et al., 2011b). In combination with a known MC, the grey scale value of the specimen before and after fungal decay can be obtained according to Eq. (6.9). The attenuation coefficient of water was also obtained by scanning demineralized water of each X-ray CT scan performed.

$$\mu^{w'} = G_r / \rho_r \qquad\qquad (6.8)$$

$$G_i = (G_i^r \times \rho_i^w) / \rho_r + \mu_i^{h'} \times \rho_i^w \times MC_i \qquad\qquad (6.9)$$

with G_r: the average grey scale value of the reference material. ρ_r: the density of the reference material (g/cm^3); G_i: the average grey scale value of the specimen at time i; G_i^r: the average grey scale value of the reference material at time i; $\mu_i^{h'}$: the attenuation coefficient per unit mass of water at time i (cm^2/g); ρ_i^w: the density of wood at time i (g/cm^3); MC_i: the moisture content of the specimen at time i (%);

The average grey scale value of one layer was obtained with X-ray tomography by selecting the central region of this layer. According to Eq. (6.9), the density of this layer can be calculated. No measureable change in dimensions was detected after fungal decay. Hence, mass loss in the different layers of the specimen was thus finally obtained with Eq. (6.10).

$$M_i = (\rho_{bi}^w - \rho_{ai}^w) \times 100 / \rho_{bi}^w \qquad\qquad (6.10)$$

with M_i: mass loss of layer i of the specimen (%); ρ_{bi}^w: the density of wood of layer i before fungal decay (g/cm^3); ρ_{ai}^w: the density of wood of layer i after fungal decay (g/cm^3).

Based on the mass loss of each layer, the mass loss of the entire specimen can be calculated using Eq. (6.11).

$$M_e = \sum M_i \times T_i \times 100 / T \qquad\qquad (6.11)$$

with M_e: average mass loss of the specimen (%); T_i: the thickness of the layer i; T: total thickness of the specimen.

6.3 Results and Discussion

6.3.1 Validation of the MOE determined with resonalyser

Fig. 6.5 illustrates the linear relationship between the MOE measured with static bending and the corresponding resonalyser of the specimens before and after fungal decay, showing that the MOE of the plywood and MDF can be measured accurately with resonalyser. The MOE of standard MDF after fungal decay could not be measured due to severe weakening of mechanical properties and

disintegration of the structure. Fig. 6.6 shows that cracks emerge after 6 weeks of fungal decay testing. Standard MDF is a product aiming at interior use in non-humid conditions. Obviously, water absorption could separate the fibers bonded with UF due to the weak internal bond strength (Dunky, 1998). Large cracks probably causes too much noise in the signal when measuring MOE using resonalyser. Static bending also failed to determine a proper MOE for this product under test.
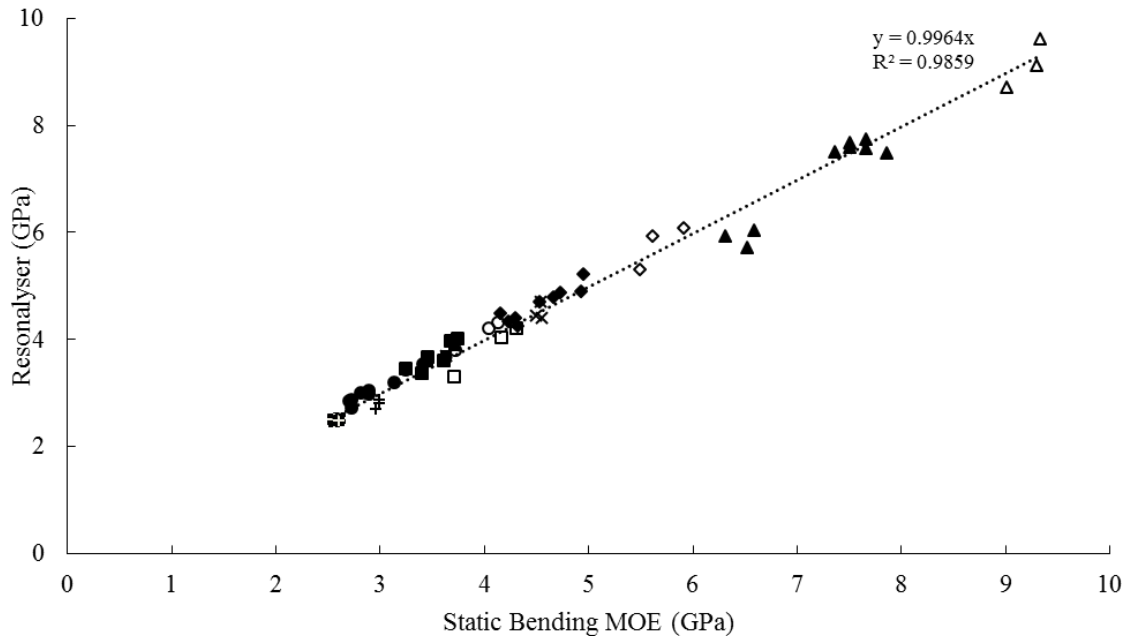
Fig 6.5. Comparison of MOE measured with static bending and resonalyser of the specimens before fungal decay (no fill) and after fungal decay (black fill). ○ = P1, □ = P2, △ = B1, ◊ = O1, × = standard MDF, + = MDF-C.
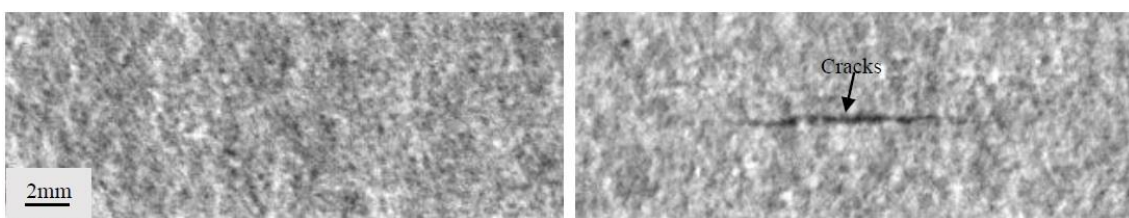
Fig 6.6. Cross section of standard MDF before (left) and after 6 weeks fungal decay (right) obtained with X-ray CT scanning.

6.3.2 Relating MOE decrease and mass loss

There is a linear relationship between the MOE decrease and mass loss increase of plywood (Fig. 6.7). Fungi degrade the wood cell walls and as such decrease strength (Walker, 1993). These linear relationships are different for different panel types. After 14 weeks fungal decay, MOE decrease of okoumé plywood is approximately 23%, while mass loss is only 4%. Contrastly, birch plywood loses nearly 15% mass and shows a merely 25% MOE decrease. Compared to okoumé, birch has high

density, high mechanical strength and low water resistance (Li et al., 2014). Free water can quickly penetrate into birch plywood, probably accelerating fungal growth resulting in a higher mass loss. Despite of this higher mass loss, the MOE decrease is close to the MOE decrease of okoumé plywood, which is due to the high density of birch plywood (Larjavaara and Muller-Landau, 2010). For okoumé plywood, a high water resistance effectively reduces water uptake and thus fungal decay, which, however, still results in mechanical strength decrease. Poplar has not only a relatively low density, and low mechanical strength but also a low water resistance. Poplar plywood shows a 30% MOE decrease and 8% mass loss after 14 weeks fungal decay. For P2, mass loss is less than 3% due to suppressed fungal growth in the culture vessel, yet P1 and P2 have a similar structure apart from the glue types which are UMF and PF respectively. The MOE decreases approximately 15% for a mass loss of 1.5% in both P1 and P2.
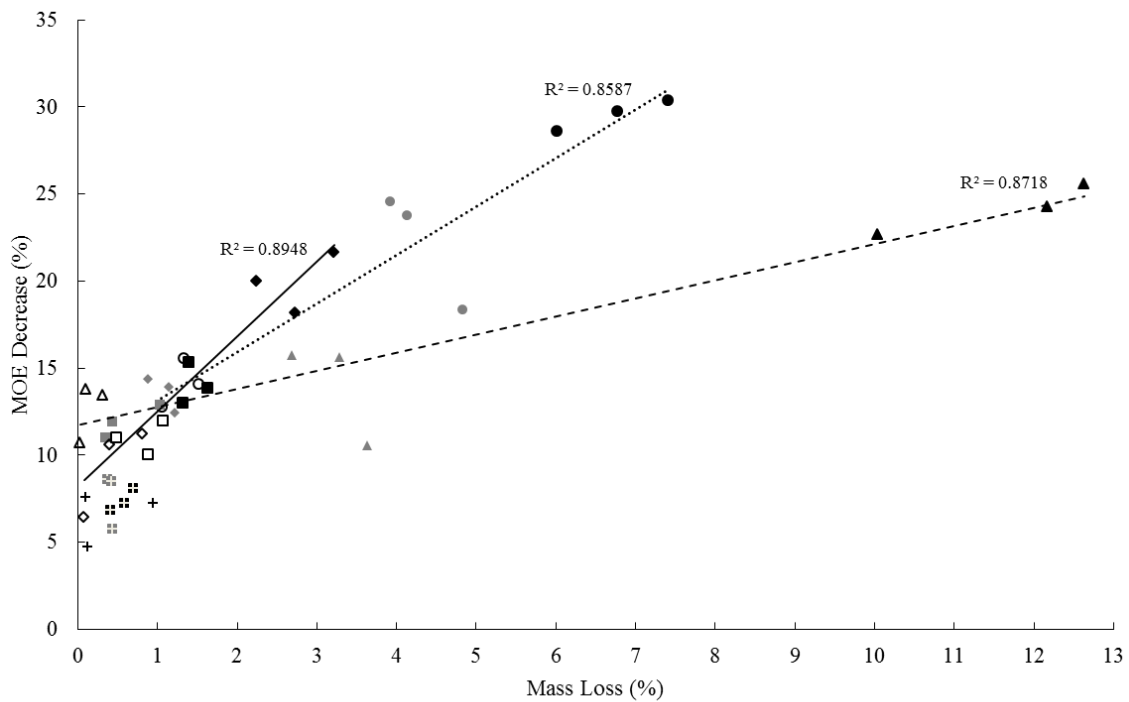
Fig 6.7. Relating MOE decrease and mass loss of the specimens after 6 weeks (no fill), 10 weeks (grey fill) and 14 weeks (black fill) fungal decay. ○ = P1, ··· = P1 trend line, □ = P2, Δ = B1, − − = B1 trend line, ◊ = O1, — = O1 trend line, + = MDF-C.

The MOE decrease is as large as 15% when mass loss is almost zero for B1 (Fig. 6.7). Large MOE decrease in reference samples is also found when mass loss is unmeasurable (Fig. 6.8). Hence, mass loss of the specimens is not the only reason for mechanical strength decrease in fungal decay testing. Due to the hysteresis, 2% and 1% higher MC in respectively plywood and MDF-C specimens was detected after fungal decay. Based on the study of solid wood, 2% MC increase can cause nearly 4%

MOE decrease (George, 1991). In addition to higher MC, MOE decrease of the specimens after fungal decay could be due to the following two reasons. At one hand this could be due to the hemicellulose and lignin decomposition in the incipient fungal decay stage (Winandy and Morrell, 1993). At the other hand structural changes also contribute to strength loss, such as cracks, induced by the water dynamics. This concords with the microstructure of the specimens obtained with X-ray CT scanning (Fig. 6.9 white arrow). Typically in the first layer, significant cracks emerge after 6 weeks fungal exposure. According to the results from reference samples exposed in non-inoculated vermiculite, obvious MOE decrease (larger than 5%) is detected when mass loss is insignificant (Fig. 6.8). It indicates that water dynamics is an important factor for mechanical strength decrease of plywood in service.

It is therefore not sufficient to evaluate the biological durability based on mass loss only when aiming at testing a material used in a load-bearing situation like plywood. It is necessary to consider the influence of water dynamics and wood structural changes on the mechanical strength of the specimens.

Fig 6.8. Relating MOE decrease and mass loss of the reference samples. ○ = P1, □ = P2, Δ = B1, − ◊ = O1, + = MDF-C.

Fig 6.9. The first, second and third layer of B1 before (left) and after 6 weeks (right) fungal decay obtained with X-ray CT scanning. White arrows indicate cracks.

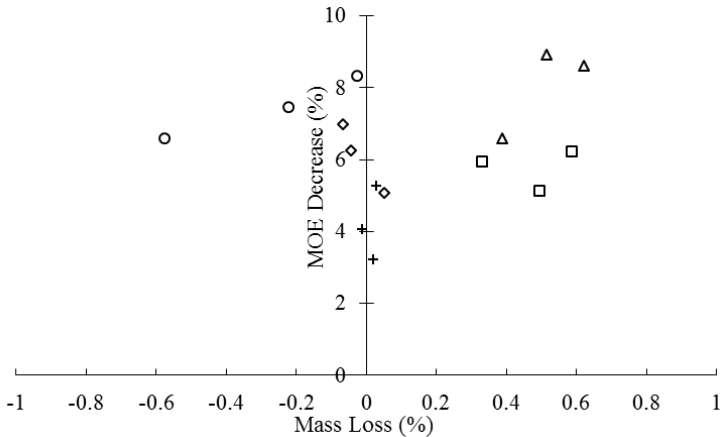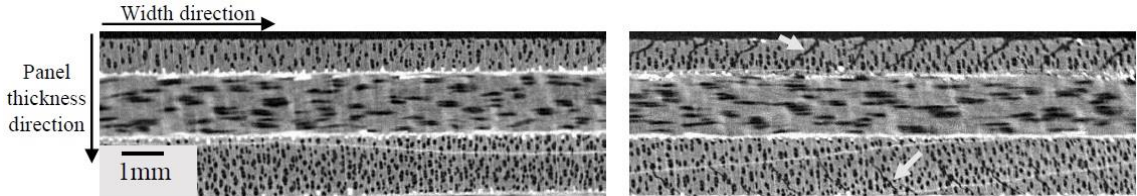Although fungi grow well in the culture vessel with MDF-C, mass loss is less than 1.5% after 14 weeks fungal decay (Fig. 6.7), which is consistent with the product data sheet. Acetylation blocks the free hydroxyls within the wood fibers through formation of acetyl groups and thus the ability of the wood fibers to adsorb water is reduced, rendering the MDF panels very durable. Probably partially non-acetylated fibers could still be degraded and give rise to the small mass loss. Bonding strength decrease caused by water uptake could be another reason for MOE decrease. These factors induce in total an almost 10% MOE decrease. According to the high resolution X-ray images, no obvious structural changes are detected. Considering the rather low initial mechanical strength, a small mass loss and moderate MOE decrease during fungal decay, MDF-C is suitable to be used as facade of buildings or as a surface cladding of other materials.

6.3.3 Mass loss in different layers of plywood

One specimen from each group of the plywood panel types P1 (poplar), B1 (birch) and O1 (okoumé) was selected for mass loss analysis (Fig. 6.10). The results indicate that the average mass loss estimated with X-ray tomography correlates well with the actual average mass loss obtained gravimetrically. For all specimens, higher mass loss values are recorded in the surface layers as expected.

Free water is key for fungal growth, otherwise the enzymes released by the fungus will not be transported (Schmidt, 2006). Water transport is thus a key factor of determining the fungal decay and mass loss in the specimens. Apparently, compared to the even layers, it takes longer for water to penetrate the interior of the odd layers due to the long distance in longitudinal direction. Water movement along the longitudinal direction of veneers in P1 and B1 is rather fast when the grain direction of the veneer is parallel to the glue line according to the moisture distribution mapped using neutron radiography and the internal structure revealed with X-ray tomography (Li et al., 2014). Fig. 6.11 shows that the grain direction in the odd layers of the specimen from B1 is not parallel to the glue line compared with the specimen from P1. The non-parallel grain direction slows water penetration along the odd layers of B1. Due to the long distance and slow water movement, mass loss in the odd layers is lower than in the even layers for birch plywood (Fig. 6.10B1). This phenomenon, however, does not appear in the inner layers of P1, which agrees with the fact that the grain direction of the odd layers is parallel to the glue line (Fig. 6.11).

The low mass loss of 3.2% in the 4th layer of P1 is somewhat deviating. Relatively long distance ($\pm$ 7 mm) to the surface of the panel could be a reason. The existence of veneer checks and gaps between veneers induces the possibility of fungi growth along the thickness direction of the panel (Li et al., 2014). Low mass loss in the central layer, however, is not found in B1 probably because the presence

of soluble toxic materials and sodium hydroxide in PF could inhibit the fungi crossing the glue line (George, 1991; Laks et al., 2002).

Compared to poplar and birch plywood, the mass loss in okoumé plywood is only 2.7% next to higher wood durability, most probably related to the higher water resistance (Li et al., 2014), playing a key role in the mass loss of the plywood panels. Fig. 6.10 shows that approximately 60% mass loss occurs in two top veneers, which indicates fungi can hardly degrade the interior of the specimen although fully accessible. Compared to overall mass loss of only 2.7%, the MOE decrease is 18.2%. This phenomenon is partially due to MOE decrease induced by water dynamics. Based on high resolution X-ray CT scanning, there is no apparent structural change in O1 after 14 weeks fungal decay. The rather large MOE decrease could be a result of the mass loss in the surface layers, which is consistent with the fact that the mechanical strength of plywood is mainly dominated by the outer layers (Simpson and TenWolde, 1999).
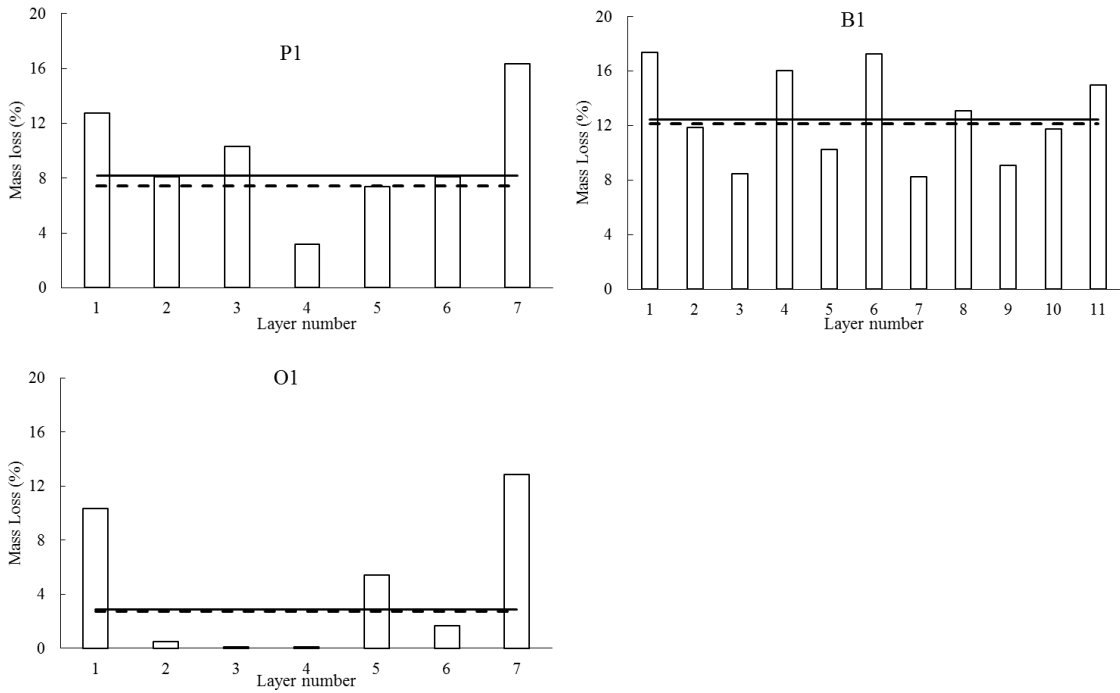

Fig 6.10. Mass loss in different layers of plywood (bars), gravimetrical average mass loss (dash line) and average mass loss estimated with X-ray tomography (solid line) of the plywood specimens after 14 weeks fungal decay.
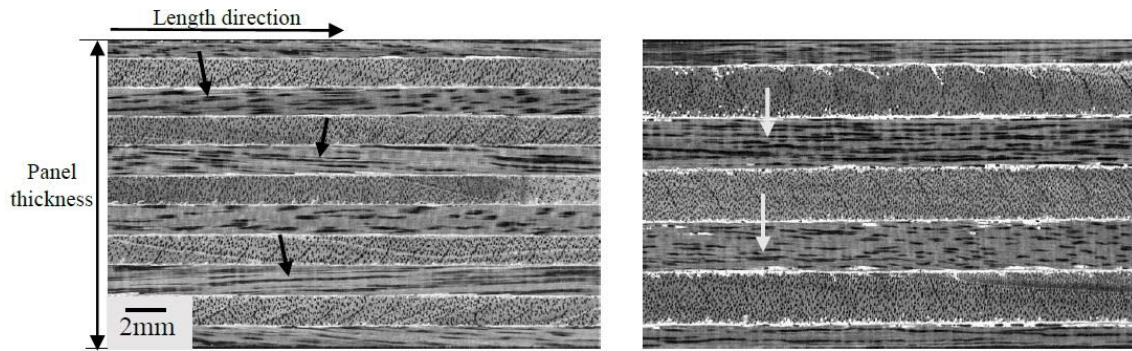
Fig 6.11. Microstructure of B1 (left) and P1 (right) before fungal decay obtained with X-ray CT scanning. Arrows indicate the grain direction of the veneers.

6.4 Conclusion

Resonalyser is a valuable technique to non-destructively monitor modulus of elasticity (MOE) of plywood and MDF, whereas X-ray CT scanning has proven to be an essential tool to visualize the interior structure and assess local mass loss non-destructively. The MOE of standard MDF decreases significantly in dynamic water conditions due to the internal structural changes such as cracks. After 14 weeks fungal attack, mass loss and MOE decrease for MDF-C is approximately 1.5% and 10% respectively. MDF-C is thus suitable for outdoor, non-load-bearing use. For plywood, there is a linear relationship between MOE decrease and mass loss. Approximately 10% MOE decrease occurs at the incipient stage of fungal decay, while mass loss is still less than 1%, which is mainly due to water dynamics and cracks in the surface layers. The influence of mass loss on MOE decrease is different for different types of plywood. For example the MOE decrease and mass loss are 23% and 4% in okoumé plywood, while being 25% and 15% in birch plywood respectively, which is mainly induced by the different wood density. Mass loss in the different layers of plywood is not similar, with rather large mass loss in the top veneers. The mass loss in the core veneers is influenced by the grain direction and structure of veneers. More specifically wood grain direction non-parallel to the glue line slows water transport and decreases mass loss.

Non-destructive methods allow us to understand the details of biological degradation in wood based materials. It is hard to evaluate the influence of biological degradation on the properties of wood by only measuring the average mass loss. The MOE decrease is another important parameter that needs to be taken into account when investigating biological degradation, which is affected by different factors, *i.e.* water dynamics, structural changes and mass loss distribution. Determination of mass loss distribution with X-ray tomography can be proposed as a way to check the distribution of biocidal active. The influence of moisture dynamics on the biological durability of WBP is relevant to the time of wetness in the different parts of the products.

Acknowledgement

6

7 General conclusions

Wood-based panels (WBP) are primarily adhesive bonded pieces of wood in a panel format. They can be produced from timbers from sustainably managed forests, but can also simply use low grade wood and wood residues. Therefore, WBP can be seen as environmental friendly products. Due to the advantages of being ecological sustainable and flexible in usage, WBP are widely used both as base for decorative end use and as construction material. The disadvantages of WBP, however, are also obvious. Generally speaking, they are prone to water uptake and vulnerable to biological degradation. Hence, water resistance and biological durability are commonly regarded as two key factors determining the performance of WBP in service. In practice, the solutions like the use of coating and specific treatment are widely used to improve water resistance of WBP. Complementary to these methods, optimizing the panels' structural characteristics can be considered as an environmentally friendly and cost saving approach to improve moisture behavior.

The rationale of this dissertation is to understand the hygro-mechanical performance of WBP through investigating the internal structure and structural characteristics. Therefore, several representatives, like plywood, OSB and MDF were used in this research. Visualizing the internal structure, mapping the moisture distribution and measuring the mechanical properties were carried out using both standard and new innovative methodology. The dissertation covers three main parts. The first part focuses on understanding the relationship between water transport behavior and structural characteristics of WBP. This was analyzed based on parameters, like the structure of wood components / pieces, the glue types, the glue distribution and type of additives. Suggestions on how to improve water resistance of WBP by optimizing their structural characteristics are given. The second part of this dissertation focuses on the investigation of the performance of plywood during outdoor exposure according to the detailed information of moisture dynamics and structural variations. An adapted electrical MC measurement method was searched to continuously monitor the moisture distribution in different layers of plywood. Combining the moisture distribution with specimens' structural characteristics and internal structural variations based on periodic X-ray CT scanning allowed to study the performance of plywood in outdoor weathering exposure conditions. In the last part, the effort was mainly on the biological durability of plywood and MDF. The biological degradation was assessed by calculating the mass loss, measuring MOE, visualizing the structural variations and mapping the mass loss distribution.

The new methodology allowed to use non-destructive visualization of the internal structure and to measure the moisture distribution and the mechanical strength of WBP. As such the multi-properties of each individual can be followed over time. It is, therefore, a valuable alternative for methods that require destructive assessment of a large amount of samples to come to reliable statistical conclusions.

Hereafter the conclusion is compiled depending on the research questions proposed in Introduction.

The structural characteristics and moisture transport behavior of WBP

How do structural characteristics influence water transport behavior of plywood?

In **chapter 2**, moisture transport behavior in plywood and related solid wood specimens was studied. Moisture distribution in the specimens was quantified using neutron radiography. High resolution X-ray CT scanning was used to visualize the internal structure and moisture distribution. The results reveal that compared with solid wood, veneer checks and gaps between veneers can increase water uptake of plywood. For plywood, water resistance is influenced by the adhesive, veneer wood species and veneer grain direction. Specifically, UMF glue has a better water resistance than PF due to a higher barrier performance. Water resistance of plywood is anyhow closely related to the corresponding wood species used. Veneer with non-parallel grain direction to glue line can increase water uptake from the panel surface or can decrease the water absorption from the side edges of plywood.

What is the impact of structural characteristics on water transport behavior of MDF and OSB?

Moisture transport behavior in MDF and OSB was investigated in **chapter 3** using a gantry-based X-ray CT scanning system. This scanning system is proven to be an effective approach for dynamically monitoring water transport in WBP. Side edges are the main entrance of water penetration in both MDF and OSB during immersion test. Water resistance of the side edges, however, can be improved using a more compact structure. Water can quickly reach the interior of MDF and OSB specimens through the long fibers or strands, which causes internal structural variations. Water transport in MDF glue is significantly influenced by the adhesive, additives and chemical treatment of the fibers. Compared to UF, MUF could increase significantly water resistance and structural stability of MDF. Water repellent additives further improve water resistance of MDF. Fiber acetylation significantly increases the water resistance and the structural stability of MDF. For OSB, the structure of strands influences the water transport behavior. For example, water uptake can be reduced if the grain direction of strands is perpendicular to the water uptake direction. Water uptake can also be reduced when the strands are covered with a water resistant adhesive.

The moisture behavior of plywood during outdoor exposure

How can we measure the moisture distribution in WBP in a continuous setup?

The possibility of using an adapted electrical resistance moisture content (MC) measurement method to monitor moisture distribution in wood based materials was assessed in **chapter 4**. X-ray tomography was proven to be an effective way to obtain the actual regional MC in wood based materials. According to actual MC obtained with X-ray tomography, we found that electrical resistance MC measurement method can effectively monitor the MC between two electrodes if this

7

MC is evenly distributed in this area. Otherwise, it is difficult to obtain an accurate value of the actual MC. In practical applications, this method can be optimized by carefully analyzing and checking the position of electrodes and the wood microstructure between electrodes. As wood species with a uniform density distribution are suitable to use electrical resistance method for monitoring moisture distribution. It is also feasible to apply this method to monitor moisture distribution in different layers of plywood.

What is the moisture behavior of plywood in service according to the moisture distribution and structural variations?

Plywood specimens were exposed in two different outdoor conditions for approximately one year as described in **chapter 5**. During this period, MC in different layers of the specimens was continuously monitored using the above mentioned electrical resistance MC measurement method. The internal and surface structure of the specimens were periodically recorded with X-ray CT and flatbed scanning respectively. The detailed field weather information was also collected. The results showed that moisture distribution in plywood is not homogeneous during outdoor exposure. The second layer of PF glued plywood is prone to water accumulation, while a UMF glue line can effectively prevent water uptake. Top veneers with higher thickness can lag moisture accumulation in the inner layers. Cracks appear in the top and second layer of these specimens with low water resistance. These cracks increase water uptake in the inner layers of plywood. Weathering conditions have a significant impact on the moisture distribution in plywood. Continuous rain causes moisture accumulation in the inner layers. High temperature and intensive solar radiation are the main factors for water evaporation. The MC variation in the second layer correlates with the alternation of day and night.

Biological degradation of plywood and MDF

How does moisture entrapment impact the mechanical strength and biological durability of WBP?

In **chapter 6** both plywood and MDF specimens were exposed to wet vermiculite inoculated with *Pleurotus ostreatus* for 14 weeks. Resonalyser and X-ray CT scanning were used to non-destructively monitor the MOE and internal structure of the specimens. According to the actual MOE measured using static bending test, resonalyser can be seen as a reliable method to measure MOE of plywood and MDF. Standard MDF loses most of the mechanical strength due to the emerging of cracks. MDF produced from acetylated fibers lose 10% of the MOE, while the mass loss less than 1%. The plywood specimens show approximately 10% MOE decrease at incipient biological degradation corresponding to a mass loss less than 1%. This stresses the importance of assessing the biological durability of plywood and MDF based on the MOE decrease rather than merely on mass loss. There is a linear relationship between mass loss and MOE decrease of plywood at significant mass loss levels. This linear relationship, however, is different for the different plywood types. Based

on X-ray tomography, mass loss distribution in different layers of the plywood specimens was quantified. Since higher mass loss was detected in the surface layers, this relates to the significant MOE decrease of the specimens.

Concluding remarks and discussion

This PhD work focused on investigating the hygro-mechanical performance of WBP using non-destructive methods. The methods, *i.e.* X-ray tomography and neutron radiography, make it possible to visualize and map the interior properties of wood based materials. Thanks to these non-destructive approaches, the performance of WBP could be continuously or periodically monitored. Therefore it is feasible to timely evaluate the quality and predict the service life of products, which is valuable for optimizing the application of WBP products based on a fit for purpose approach. In future research, we likely can decide the quality and service life of wood products according to their temporal properties. The safety level of a wood construction can thus be evaluated better. However, these non-destructive methods still need to be further improved. Currently, they are mainly used in laboratory testing due to the size and concept of equipment used and the strict requirements for preparing the specimens. For example, the X-ray CT scanner generally is not portable and not suitable to scan large specimens.

In general, the quality of WBP products is judged based on standards. For instance, MC is determined by comparing the weight of water with wood substance in a piece of wood. In service, moisture distribution in wood, however, is not always homogeneous. If using the average MC obtained with standard methods to evaluate the moisture behavior, this induces errors. Meanwhile, the standards could be improved if more parameters are considered. The mass loss values are commonly used in determining the biological degradation of wood based materials. However, the mechanical properties decrease significantly prior to any measurable mass loss. Considering the importance of mechanical properties in deciding the performance of WBP, it is necessary to combine mass loss with mechanical measurements to evaluate the biological degradation of WBP. Hence, in future research, the data obtained with standard methods need to be further analyzed in more detail focusing on the practical application conditions.

The WBP specimens used are prepared from commercial products, therefore, it is hard to control or specify the wood species of fibers or strands. Wood species will impact the performance of the MDF and OSB products. In future research, it is of interest to study hygro-mechanical performance of MDF and OSB made from fibers or strands with specific wood species.

The specimens used in this work are prepared from several WBP products available on the European market. Different types of plywood and MDF are studied. However, the moisture behavior of OSB is only studied based on one type of product and the mechanical properties of OSB were not

7

investigated. Compared to plywood and MDF, OSB is a non-homogeneous products and hence it is difficult to non-destructively measure its mechanical properties using the resonalyser. It is also hard to track or quantify water transport in the interior of OSB due to the significant swelling in dynamic moisture conditions. Considering the importance of OSB, it is necessary to devote more efforts to investigate its hygro-mechanical performance. In order to reach this aim, methods with a better performance on non-destructively mapping the moisture distribution and measuring the mechanical strength of OSB need to be searched. It is well known that temperature has an impact on the accuracy of MC value converted with electrical resistance. In this research, temperature distribution in plywood specimens during outdoor exposure, however, was not monitored due to lack of suitable devices. Hence, temperature compensation on electrical MC value was not performed. To improve the accuracy of electrical MC, a suitable device that can monitor both MC and temperature distribution need to be searched.

Modelling moisture dynamics in WBP is helpful for guiding its production and service life prediction. In comparison to solid wood, moisture dynamics in WBP are also influenced by structural characteristics and factors linked to glue line, additives and possible treatment. In practical applications, the emerging of cracks in wood pieces and glue lines, apparently also impact moisture dynamics. The ideas and results given in this dissertation show the possibility to study the interrelationship between structural characteristics and moisture behavior as well as structural changes during outdoor exposure. In future, an artificial neural network (ANN) model is possible to be designed to predict moisture dynamics in plywood. In this prediction model, the input layers could consist of several input nodes, such as veneer species, glue type, the amount of veneer checks, veneer thickness, veneer grain direction and exposure conditions. Another possible way of predicting moisture dynamics of plywood is to build a statistical model based on factors like glue type, veneer thickness and veneer wood species. This statistical model could be further optimized by matching with experimental data. Finally, it is also possible to estimate moisture dynamics depending on classical moisture transport theory of penetrating wood, voids and glue line. Yet the latter approach is most probably a very difficult one.

Predicting the service life of WBP is non-trivial. Generally, average MC and wood temperature are regarded as the essential parameters to predict the biological durability and service life of wood based materials. According to the findings of this work, parameters such as moisture distribution, mass loss distribution and structural variations also have an impact on the service life of WBP. Similar with moisture distribution, temperature distribution in WBP could be also inhomogeneous when WBP are exposed outside. It will apparently impact the accuracy of service life predicted using only average temperature. These parameters are mainly determined by the panels' structural characteristics and the exposure climate conditions. Researchers have used wood MC and wood temperature as well as

weather data to predict service life of solid wood (Brischke and Rapp, 2008; Scheffer, 1971). These service life prediction models would be adapted and applied in WBP if the relation between panels' structural characteristics and moisture dynamics could be taken into account. Apparently, more work is still required if this theory is to be implemented. For instance, panels with different structural characteristics need to be tested in different exposure conditions to establish a database of input parameters.

In this dissertation, we give many suggestions on optimizing the structural characteristics of WBP to improve their hygro-mechanical performance. Specifically, the use of veneers made from wood species like okoumé as outer layers, can improve water resistance of plywood panels. Veneers with grain direction fully parallel to the glue line are suitable to be used in the outer of plywood while those deviating can be used for inner veneers. Veneers with less veneer checks have good water resistance and should be used in the outer layers of plywood. Inner side of the veneer, generally, has large checks and then should be the inward sides of surface layers. For MDF and OSB, small wood pieces, water resistant glue and a compact structure can improve water dynamics of panels. These suggestions, however, are not yet implemented in the production of the panels. In future research, producing WBP with optimized structural characteristics can be assessed in laboratory condition first. More considerations and difficulties are expected as applying these suggestions in industry. How to improve the quality of WBP products cost effectively, remains a key question for all WBP producers. Certainly, the option to improve the quality of WBP by optimizing the structural characteristics looks bright.

7

Reference List

Abdolzadeh, H., Doosthoseini, K., Karimi, A.N., Enayati, A.A., 2011. The effect of acetylated particle distribution and type of resin on physical and mechanical properties of poplar particleboard. European Journal of Wood and Wood Products 69, 3-10.

Akgul, D.S., Savas, N.G., Eskalen, A., 2014. First report of wood canker caused by Botryosphaeria dothidea, Diplodia seriata, Neofusicoccum parvum, and Lasiodiplodia theobromae on Grapevine in Turkey. Plant Dis 98, 568-568.

Akgul, M., Ayrilmis, N., Camlibel, O., Korkut, S., 2013a. Potential utilization of burned wood in manufacture of medium density fiberboard. J Mater Cycles Waste 15, 195-201.

Akgul, M., Korkut, S., Camlibel, O., Ayata, U., 2013b. Some chemical properties of luffa and its suitability for medium density fiberboard (MDF) production. Bioresources 8, 1709-1717.

Ali, I., Jayaraman, K., Bhattacharyya, D., 2014. Effects of resin and moisture content on the properties of medium density fibreboards made from kenaf bast fibres. Ind Crop Prod 52, 191-198.

Antikainen, T., Rohumaa, A., Hunt, C.G., Levirinne, M., Hughes, M., 2015. Estimating the spread rate of urea formaldehyde adhesive on birch (Betula pendula Roth) veneer using fluorescence. European Journal of Wood and Wood Products 73, 69-75.

Arta-Obeng, E., Via, B.K., Fasina, O., 2012. Effect of microcrystalline cellulose, species, and particle size on mechanical and physical properties of particleboard. Wood and Fiber Science 44, 227-235.

Aung, M.M., Yaakob, Z., Kamarudin, S., Abdullah, L.C., 2014. Synthesis and characterization of Jatropha (Jatropha curcas L.) oil-based polyurethane wood adhesive. Ind Crop Prod 60, 177-185.

Aydin, I., Colakoglu, G., Colak, S., Demirkir, C., 2006. Effects of moisture content on formaldehyde emission and mechanical properties of plywood. Building and Environment 41, 1311-1316.

Ayrilmis, N., Kaymakci, A., 2012. Reduction of formaldehyde emission from light MDF panels by adding chestnut shell flour. Holzforschung 66, 443-446.

Azizi, K., Tabarsa, T., Ashori, A., 2011. Performance characterizations of particleboards made with wheat straw and waste veneer splinters. Compos Part B-Eng 42, 2085-2089.

Reference list

Barry, A., Corneau, D., 2006. Effectiveness of barriers to minimize VOC emissions including formaldehyde. Forest Prod J 56, 38-42.

Benthien, J.T., Bahnisch, C., Heldner, S., Ohlmeyer, M., 2014. Effect of fiber size distribution on medium-denstiy fiberboard properties caused by varied steaming time and temperature of defibration process. Wood and Fiber Science 46, 175-185.

Bergsten, U., Lindeberg, J., Rindby, A., Evans, R., 2001. Batch measurements of wood density on intact or prepared drill cores using x-ray microdensitometry. Wood Science and Technology 35, 435-452.

Bonigut, J., Krug, D., Stuckenberg, P., 2014. Dimensional stability and irreversible thickness swell of thermally treated oriented strandboards (OSB). European Journal of Wood and Wood Products 72, 593-599.

Boon, J.G., Hashim, R., Sulaiman, O., Hiziroglu, S., Sugimoto, T., Sato, M., 2013. Influence of processing parameters on some properties of oil palm trunk binderless particleboard. European Journal of Wood and Wood Products 71, 583-589.

Boone, M.A., De Kock, T., Bultreys, T., De Schutter, G., Vontobel, P., Van Hoorebeke, L., Cnudde, V., 2014. 3D mapping of water in oolithic limestone at atmospheric and vacuum saturation using X-ray micro-CT differential imaging. Mater Charact 97, 150-160.

Brabant, L., 2013. Latest developments in the improvement and quantification of high resolution X-ray to tomography. PhD Thesis, Ghent University, Belgium.

Brabant, L., Vlassenbroeck, J., De Witte, Y., Cnudde, V., Boone, M.N., Dewanckele, J., Van Hoorebeke, L., 2011. Three-dimensional analysis of high-resolution X-ray computed tomography data with Morpho+. Microscopy and Microanalysis 17, 252-263.

Brischke, C., Lampen, S.C., 2014. Resistance based moisture content measurements on native, modified and preservative treated wood. European Journal of Wood and Wood Products 72, 289-292.

Brischke, C., Rapp, A.O., 2008. Dose–response relationships between wood moisture content, wood temperature and fungal decay determined for 23 European field test sites. Wood Science and Technology 42, 507-518.

Brischke, C., Rapp, A.O., Bayerbach, R., 2008a. Measurement system for long-term recording of wood moisture content with internal conductively glued electrodes. Building and Environment 43, 1566-1574.

Brischke, C., Rapp, A.O., Bayerbach, R., Morsing, N., Fynholm, P., Welzbacher, C.R., 2008b. Monitoring the "material climate" of wood to predict the potential for decay: Results from in situ measurements on buildings. Building and Environment 43, 1575-1582.

Brischke, C., Welzbacher, C., Meyer, L., Bornemann, T., Larsson-Brelid, P., Pilgård, A., Frühwald Hansson, E., Westin, M., Rapp, A.O., Thelandersson, S., Jermer, J., 2011. Service life prediction of wooden components - Part 3: Approaching a comprehensive test methodology, IRG/WP/20464. The 42rd International Research Group on Wood Protection, Stockholm.

Cai, J.C., Perfect, E., Cheng, C.L., Hu, X.Y., 2014. Generalized modeling of spontaneous imbibition based on hagen-poiseuille flow in tortuous capillaries with variably shaped apertures. Langmuir 30, 5142-5151.

Carll, C.G., 2009. Decay hazard (Scheffer) index values calculated from 1971-2000 climate normal data.

Chen, S., Liu, X., Fang, L., Wellwood, R., 2009. Digital X-ray analysis of density distribution characteristics of wood-based panels. Wood Science and Technology 44, 85-93.

Chen, S.G., Liu, X.H., Fang, L.M., Wellwood, R., 2010. Digital X-ray analysis of density distribution characteristics of wood-based panels. Wood Science and Technology 44, 85-93.

Christian, L., Sanabria, S.J., Mannes, D., Niemz, P., 2013. Combination of neutron imaging (NI) and digital image correlation (DIC) to determine intra-ring moisture variation in Norway spruce. Holzforschung.

Comstock, G.L., 1970. Directional permeability of softwoods. Wood and Fiber Science 1, 283-289.

Curling, S.F., Clausen, C.A., Winandy, J.R., 2002. Experimental method to quantify progressive stages of decay of wood by basidiomycete fungi. International Biodeterioration & Biodegradation 49, 13-19.

de Freitas, R.R., Molina, J.C., Calil, C., 2010. Mathematical model for timber decay in contact with the ground adjusted for the state of Sao Paulo, Brazil. Mater Res-Ibero-Am J 13, 151-158.

De Ridder, M., Van den Bulcke, J., Vansteenkiste, D., Van Loo, D., Dierick, M., Masschaele, B., De Witte, Y., Mannes, D., Lehmann, E., Beeckman, H., Van Hoorebeke, L., Van Acker, J., 2011a. High-resolution proxies for wood density variations in Terminalia superba. Annuals of Botany 107, 293-302.

De Ridder, M., Van den Bulcke, J., Vansteenkiste, D., Van Loo, D., Dierick, M., Masschaele, B., De Witte, Y., Mannes, D., Lehmann, E., Beeckman, H., Van Hoorebeke, L., Van Acker, J., 2011b.

High-resolution proxies for wood density variations in Terminalia superba. Annals of botany 107, 293-302.

De Smet, J., Van Acker, J., 2006. Testing methodology and CE-marking for biological performance of plywood for exterior construction purposes, COST Action E44 conference on Wood resources and panel properties, Valencia, Spanje, pp. 189-200.

Del Menezzi, C.H.S., Tomaselli, I., 2006. Contact thermal post-treatment of oriented strandboard to improve dimensional stability: A preliminary study. Holz Roh Werkst 64, 212-217.

Demirkir, C., Ozsahin, S., Aydin, I., Colakoglu, G., 2013. Optimization of some panel manufacturing parameters for the best bonding strength of plywood. Int J Adhes Adhes 46, 14-20.

Dierick, M., Denis, V., Masschaele, B., Van den Bulcke, J., Van Acker, J., Cnudde, V., Van Hoorebeke, L., 2014. Recent micro-CT scanner developments at UGCT. Nucl Instrum Meth B 324, 35-40.

Dierick, M., Van Loo, D., Masschaele, B., Boone, M., Van Hoorebeke, L., 2010. A LabVIEW (R) based generic CT scanner control software platform. J X-Ray Sci Technol 18, 451-461.

Domec, J.C., Lachenbruch, B., Meinzer, F.C., 2006. Bordered pit structure and function determine spatial patterns of air-seeding thresholds in xylem of Douglas-fir (Pseudotsuga menziesii; Pinaceae) trees. Am J Bot 93, 1588-1600.

Drow, J.T., 1957. Effect of moisture on the compressive, bending, and shear strengths, and on the toughness of plywood, Forest Products Laboratory, Forest Service U. S. Department of Agriculture.

Dunky, M., 1998. Urea-formaldehyde (UF) adhesive resins for wood. Int J Adhes Adhes 18, 95-107.

El-Kassas, A.M., Mourad, A.H.I., 2013. Novel fibers preparation technique for manufacturing of rice straw based fiberboards and their characterization. Mater Design 50, 757-765.

European Committee for standardisation EN 317, 1994. Particleboards and fibreboards - Determination of swelling in thickness after immersion in water. Brussels Belgium

European Committee for standardisation CEN/TS 12038, 2002. Durability of wood and wood-based products — Wood-based panels — Method of test for determining the resistance against wood-destroying basidiomycetes. Brussels Belgium.

European Committee for standardisation EN 789, 2004. Timber structures – Test methods – Determination of mechanical properties of wood-based panels. Brussels Belgium.

Evans, P.D., Morrison, O., Senden, T.J., Vollmer, S., Roberts, R.J., Limaye, A., Arns, C.H., Averdunk, H., Lowe, A., Knackstedt, M.A., 2010. Visualization and numerical analysis of adhesive distribution in particleboard using X-ray micro-computed tomography. Int J Adhes Adhes 30, 754-762.

Evans, P.D., Thay, P.D., Schmalzl, K.J., 1996. Degradation of wood surfaces during natural weathering. Effects on lignin and cellulose and on the adhesion of acrylic latex primers. Wood Science and Technology 30, 411-422.

Fang, L., Chang, L., Guo, W.J., Ren, Y.P., Wang, Z., 2013. Preparation and characterization of wood-plastic plywood bonded with high density polyethylene film. European Journal of Wood and Wood Products 71, 739-746.

Fang, Q., Cui, H.W., Du, G.B., 2014. Montmorillonite reinforced phenol formaldehyde resin: Preparation, characterization, and application in wood bonding. Int J Adhes Adhes 49, 33-37.

FAO, 2013. Forest products statistics.

Follrich, J., Muller, U., Gindl, W., 2006. Effects of thermal modification on the adhesion between spruce wood (Picea abies Karst.) and a thermoplastic polymer. Holz Roh Werkst 64, 373-376.

Ford, B.M., Pollock, M.W., Wetula, J.J., 1995. Fire retardant oriented strand board structure element, in: Washington, D.U.S.P.a.T.O. (Ed.), U.S.

Freyburger, C., Longuetaud, F., Mothe, F., Constant, T., Leban, J.M., 2009. Measuring wood density by means of X-ray computer tomography. Ann Forest Sci 66.

Fromm, J.H., Sautter, I., Matthies, D., Kremer, J., Schumacher, P., Ganter, C., 2001. Xylem water content and wood density in spruce and oak trees detected by high-resolution computed tomography. Plant Physiol 127, 416-425.

Ganev, S., Cloutier, A., Gendron, G., Beauregard, R., 2005a. Finite element modeling of the hygroscopic warping of medium density fiberboard. Wood and Fiber Science 37, 337-354.

Ganev, S., Gendron, G., Cloutier, A., Beauregard, R., 2005b. Mechanical properties of MDF as a function of density and moisture content. Wood and Fiber Science 37, 314-326.

Gao, Q., Shi, S., Zhang, S.F., Li, J.Z., Liang, K.W., 2011. Improved plywood strength and lowered emissions from soybean meal/melamine urea-formaldehyde adhesives. Forest Prod J 61, 688-693.

Gao, W., Du, G.B., 2013. Curing kinetics of nano cupric oxide (CuO)-modified PF resin as wood adhesive: effect of surfactant. J Adhes Sci Technol 27, 2421-2432.

George, T., 1991. Science and technology of wood: structure, properties, utilization. Van Nostrand Reinhold, New York.

Gerhards, C.C., 1982. Effect of moisture-content and temperature on the mechanical-properties of wood - an analysis of immediate effects. Wood Fiber Sci 14, 4-36.

Gilani, M.S., Abbasion, S., Lehmann, E., Carmeliet, J., Derome, D., 2014. Neutron imaging of moisture displacement due to steep temperature gradients in hardwood. Int J Therm Sci 81, 1-12.

Gillespie, R.H., River, B.H., 1976. Durability of adhesives in plywood. Forest Prod J 26, 21-25.

Haines, D.W., Leban, J.M., Herbe, C., 1996. Determination of Young's modulus for spruce, fir and isotropic materials by the resonance flexure method with comparisons to static flexure and other dynamic methods. Wood Science and Technology 30, 253-263.

Han, J., Zou, Y., 2012. Study on the bending mechanical properties of bamboo plywood used middle temperature PF resine. Sustainable Development of Urban Environment and Building Material, Pts 1-4 374-377, 1239-1243.

Hassanein, R., de Beer, F., Kardjilov, N., Lehmann, E., 2006. Scattering correction algorithm for neutron radiography and tomography tested at facilities with different beam characteristics. Physica B-Condensed Matter 385-86, 1194-1196.

Haygreen, J.G., 1996. Forest products and wood science an introduction, 3rd ed. Iowa State University Press, Ames.

Herve, V., Mothe, F., Freyburger, C., Gelhaye, E., Frey-Klett, P., 2014. Density mapping of decaying wood using X-ray computed tomography. International Biodeterioration & Biodegradation 86, 358-363.

Himmel, S., Irle, M., Legrand, G., Perez, R., Mai, C., 2014. Effects of recovered wood on the formaldehyde release of particleboards. Holzforschung 68, 669-678.

Hoglmeier, K., Weber-Blaschke, G., Richter, K., 2014. Utilization of recovered wood in cascades versus utilization of primary wood-a comparison with life cycle assessment using system expansion. Int J Life Cycle Ass 19, 1755-1766.

Hon, D.N.S., Feist, W.C., 1986. Weathering characteristics of hardwood surfaces. Wood Science and Technology 20, 169-183.

Hoong, Y.B., Paridah, M.T., 2013. Development a new method for pilot scale production of high grade oil palm plywood: Effect of hot-pressing time. Mater Design 45, 142-147.

Imam, S.H., Gordon, S.H., Mao, L.J., Chen, L., 2001. Environmentally friendly wood adhesive from a renewable plant polymer: characteristics and optimization. Polym Degrad Stabil 73, 529-533.

Imam, S.H., Mao, L.J., Chen, L., Greene, R.V., 1999. Wood adhesive from crosslinked poly (vinyl alcohol) and partially gelatinized starch: Preparation and properties. Starch-Starke 51, 225-229.

Issa, C.A., Kmeid, Z., 2005. Advanced wood engineering: glulam beams. Constr Build Mater 19, 99-106.

James, W.L., 1988. Electric moisture meters for wood, Dept. of Agriculture, Forest Service, Forest Products Laboratory. pp. 12.

Jeong, S.G., Cha, J., Kim, S., Seo, J., Lee, J.H., Kim, S., 2014. Preparation of thermal-enhanced epoxy resin adhesive with organic PCM for applying wood flooring. J Therm Anal Calorim 117, 1027-1034.

Jocham, C., Schmidt, T., Wuzella, G., Teischinger, A., Kandelbauer, A., 2011. Adhesion Improvement of powder coating on medium density fibreboard (MDF) by thermal pre-treatment. J Adhes Sci Technol 25, 1937-1946.

Joffre, T., Wernersson, E.L.G., Miettinen, A., Hendriks, C.L.L., Gamstedt, E.K., 2013. Swelling of cellulose fibres in composite materials: Constraint effects of the surrounding matrix. Compos Sci Technol 74, 52-59.

Johansson, J., Kifetew, G., 2010. CT-scanning and modelling of the capillary water uptake in aspen, oak and pine. European Journal of Wood and Wood Products 68, 77-85.

Jumhuri, N., Hashim, R., Sulaiman, O., Nadhari, W.N.A.W., Salleh, K.M., Khalid, I., Saharudin, N.I., Razali, M.Z., 2014. Effect of treated particles on the properties of particleboard made from oil palm trunk. Mater Design 64, 769-774.

Khan, M.A., Ashraf, S.M., Malhotra, V.P., 2004. Development and characterization of a wood adhesive using bagasse lignin. Int J Adhes Adhes 24, 485-493.

Knudson, R.M., Wang, B.J., Zhang, S.Y., 2006. Properties of veneer and veneer-based products from genetically improved white spruce plantations. Wood and Fiber Science 38, 17-27.

Kojima, Y., Nakata, S., Suzuki, S., 2009. Effects of manufacturing parameters on hinoki particleboard bonded with MDI resin. Forest Prod J 59, 29-34.

Kojima, Y., Shimoda, T., Suzuki, S., 2011. Evaluation of the weathering intensity of wood-based panels under outdoor exposure. Journal of Wood Science 57, 408-414.

Kojima, Y., Suzuki, S., 2011a. Evaluating the durability of wood-based panels using internal bond strength results from accelerated aging treatments. Journal of Wood Science 57, 7-13.

Kojima, Y., Suzuki, S., 2011b. Evaluation of wood-based panel durability using bending properties after accelerated aging treatments. Journal of Wood Science 57, 126-133.

Korai, H., Hattori, K., 2013. Effects of surface coating on durability improvement of particleboard subjected to outdoor exposure. Mokuzai Gakkaishi 59, 361-366.

Korai, H., Osada, T., Sumida, A., 2014a. Effects of air injection on properties of particleboard manufactured using a radio-frequency hot press. Journal of Wood Science 60, 66-73.

Korai, H., Osada, T., Sumida, A., 2014b. Properties of particleboard manufactured using an air-injection radio-frequency hot press. Journal of Wood Science 60, 59-65.

Kropf, F.W., Sell, J., Feist, W.C., 1994. Comparative weathering tests of north-American and European exterior wood finishes. Forest Prod J 44, 33-41.

Kuroda, K., Kagawa, A., Tonosaki, M., 2013. Radiocesium concentrations in the bark, sapwood and heartwood of three tree species collected at Fukushima forests half a year after the Fukushima Dai-ichi nuclear accident. J Environ Radioactiv 122, 37-42.

Laks, P.E., Richter, D.L., Larkin, G.M., 2002. Fungal susceptibility of interior commercial building panels. Forest Prod J 52, 41-44.

Larjavaara, M., Muller-Landau, H.C., 2010. Rethinking the value of high wood density. Funct Ecol 24, 701-705.

Lauwagie, T., Sol, H., Roebben, G., Heylen, W., Shi, Y.M., Van der Biest, O., 2003. Mixed numerical-experimental identification of elastic properties of orthotropic metal plates. Ndt & E International 36, 487-495.

Lee, W.C., Biblis, E.J., 1976. Hygroscopic properties and shrinkage of southern yellow pine plywood. Wood Fiber Sci 8, 152-158.

Lehmann, E., Hartmann, S., Wyer, P., 2005. Neutron radiography as visualization and quantification method for conservation measures of wood firmness enhancement. Nucl Instrum Meth A 542, 87-94.

Lehmann, E.H., Frei, G., Kuhne, G., Boillat, P., 2007. The micro-setup for neutron imaging: A major step forward to improve the spatial resolution. Nucl Instrum Meth A 576, 389-396.

Li, W.Z., Van den Bulcke, J., De Windt, I., Van Loo, D., Dierick, M., Brabant, L., Van Acker, J., 2013. Combining electrical resistance and 3-D X-ray computed tomography for moisture

distribution measurements in wood products exposed in dynamic moisture conditions. Building and Environment 67, 250-259.

Li, W.Z., Van den Bulcke, J., Mannes, D., Lehmann, E., De Windt, I., Dierick, M., Van Acker, J., 2014. Impact of internal structure on water-resistance of plywood studied using neutron radiography and X-ray tomography. Constr Build Mater 73, 171-179.

Li, X., Li, Y.H., Zhong, Z.K., Wang, D.H., Ratto, J.A., Sheng, K.C., Sun, X.S., 2009. Mechanical and water soaking properties of medium density fiberboard with wood fiber and soybean protein adhesive. Bioresource Technol 100, 3556-3562.

Lindgren, L.O., 1991. Medical cat-scanning - X-ray absorption-coefficients, CT-numbers and their relation to wood density. Wood Science and Technology 25, 341-349.

Liu, Y., Li, K.C., 2002. Chemical modification of soy protein for wood adhesives. Macromol Rapid Comm 23, 739-742.

Liu, Y., Li, K.C., 2007. Development and characterization of adhesives from soy protein for bonding wood. Int J Adhes Adhes 27, 59-67.

Macindoe, L., Leonard, J., 2012. Moisture content in timber decking exposed to bushfire weather conditions. Fire and Materials 36, 49-61.

Mannes, D., Lehmann, E., Cherubini, P., Niemz, P., 2007. Neutron imaging versus standard X-ray densitometry as method to measure tree-ring wood density. Trees 21, 605-612.

Mannes, D., Sonderegger, W., Hering, S., Lehmann, E., Niemz, P., 2009. Non-destructive determination and quantification of diffusion processes in wood by means of neutron imaging. Holzforschung 63, 589-596.

Marinho, N.P., do Nascimento, E.M., Nisgoski, S., Valarelli, I.D., 2013. Some physical and mechanical properties of medium-density fiberboard made from giant bamboo. Mater Res-Ibero-Am J 16, 1387-1392.

Masschaele, B., Dierick, M., Van Loo, D., Boone, M.N., Brabant, L., Pauwels, E., Cnudde, V., Van Hoorebeke, L., 2013. Hector: A 240kv micro-ct setup optimized for research. 11th International Conference on X-Ray Microscopy, Shanghai, China, pp. 463.

Masschaele, B.C., Cnudde, V., Dierick, M., Jacobs, P., Van Hoorebeke, L., Vlassenbroeck, J., 2007. UGCT: New x-ray radiography and tomography facility. Nucl Instrum Meth A 580, 266-269.

Meder, R., Codd, S.L., Franich, R.A., Callaghan, P.T., Pope, J.M., 2003. Observation of anisotropic water movement in Pinus radiata D. Don sapwood above fiber saturation using magnetic resonance micro-imaging. Holz Roh Werkst 61, 251-256.

Mendes, R.F., Bortoletto, G., Garlet, A., Vidal, J.M., de Almeida, N.F., Jankowsky, I.P., 2014. Resistance of pinus taeda plywood treated with preservativesto attack by decay fungi. Cerne 20, 105-111.

Mendes, R.F., Bortoletto, G., Vidal, J.M., de Almeida, N.F., Jankowsky, I.P., 2013. Effect of preservative treatment on the physical and mechanical properties of plywood. Sci For 41, 507-513.

Meyer, L., Brischke, C., 2015. Interpretation of moisture monitoring data - Relevance of moisture content thresholds for fungal decay, IRG/WP/10839. The 46th Annual meeting of the International Research Group on Wood Protection. Viña del Mar, Chile.

Migneault, S., Koubaa, A., Erchiqui, F., Chaala, A., Englund, K., Krause, C., Wolcott, M., 2008. Effect of fiber length on processing and properties of extruded wood-fiber/HDPE composites. J Appl Polym Sci 110, 1085-1092.

Mo, X.Q., Cheng, E.Z., Wang, D.H., Sun, X.S., 2003. Physical properties of medium-density wheat straw particleboard using different adhesives. Ind Crop Prod 18, 47-53.

Moslemi, A.A., 1967. Dynamic viscoelasticity in hardboard. Forest Prod J 17, 25-33.

Moubarik, A., Charrier, B., Allal, A., Charrier, F., Pizzi, A., 2010. Development and optimization of a new formaldehyde-free cornstarch and tannin wood adhesive. European Journal of Wood and Wood Products 68, 167-177.

Mounji, H., Bouzon, J., Vergnaud, J.M., 1991. Modeling the process of absorption and desorption of water in 2 dimensions (transverse) in a square wood beam. Wood Science and Technology 26, 23-37.

Nakanishi, T.M., Matsubayashi, M., 1997. Nondestructive water imaging by neutron beam analysis in living plants. J Plant Physiol 151, 442-445.

Nasser, R.A., Al-Mefarrej, H.A., Abdel-Aal, M.A., Alshahrani, T.S., 2014. Effects of tree species and wood particle size on the properties of cement-bonded particleboard manufacturing from tree prunings. J Environ Biol 35, 961-971.

Nayeri, M.D., Tahir, P.M., Jawaid, M., Ashaari, Z., Abdullah, L.C., Bakar, E.S., Namvar, F., 2014. Medium density fibreboard made from Kenaf (Hibiscus cannabinus L.) stem: effect of thermo-mechanical refining and resin content. Bioresources 9, 2372-2381.

Nazerian, M., Sadeghiipanah, V., 2013. Cement-bonded particleboard with a mixture of wheat straw and poplar wood. J Forestry Res 24, 381-390.

Ozsahin, S., 2012. The use of an artificial neural network for modeling the moisture absorption and thickness swelling of oriented strand board. Bioresources 7, 1053-1067.

Ozsahin, S., Aydin, I., 2014. Prediction of the optimum veneer drying temperature for good bonding in plywood manufacturing by means of artificial neural network. Wood Science and Technology 48, 59-70.

Pan, Z.L., Cathcart, A., Wang, D.H., 2006. Properties of particleboard bond with rice bran and polymeric methylene diphenyl diisocyanate adhesives. Ind Crop Prod 23, 40-45.

Pang, S.S., Herritsch, A., 2005. Physical properties of earlywood and latewood of Pinus radiata D. Don: Anisotropic shrinkage, equilibrium moisture content and fibre saturation point. Holzforschung 59, 654-661.

Paul, W., Ohlmeyer, M., Leithoff, H., Boonstra, M.J., Pizzi, A., 2006. Optimising the properties of OSB by a one-step heat pre-treatment process. Holz Roh Werkst 64, 227-234.

Pelaez-Samaniego, M.R., Yadama, V., Garcia-Perez, T., Lowell, E., Amidon, T., 2014. Effect of hot water extracted hardwood and softwood chips on particleboard properties. Holzforschung 68, 807-815.

Pizzi, A., 2001. High performance MUF resins of low melamine content by a number of novel techniques. Wood Adhesives 2000, 219-239.

Pleinert, H., Lehmann, E., 1997. Determination of hydrogenous distributions by neutron transmission analysis. Physica B 234, 1030-1032.

Pommier, R., Breysse, D., Dumail, J.F., 2013. Non-destructive grading of green Maritime pine using the vibration method. European Journal of Wood and Wood Products 71, 663-673.

Pries, M., Wagner, R., Kaesler, K.H., Militz, H., Mai, C., 2013. Acetylation of wood in combination with polysiloxanes to improve water-related and mechanical properties of wood. Wood Science and Technology 47, 685-699.

Qin, G.H., Jiang, Y.Z., Qiao, Y.L., 2013. Selection of poplar hybrid clones (Populus ssp.) from backcrossed progenies of the aigeiros section for industrial purpose. Silvae Genet 62, 52-61.

Reinprecht, L., Kmet'ova, L., 2014. Fungal resistance and physical-mechanical properties of beech plywood having durable veneers or fungicides in surfaces. European Journal of Wood and Wood Products 72, 433-443.

River, B.H., 1994. Outdoor aging of wood-based panels and correlation with laboratory aging. Forest Prod J 44, 55-65.

Rosner, S., Riegler, M., Vontobel, P., Mannes, D., Lehmann, E.H., Karlsson, B., Hansmann, C., 2012. Within-ring movement of free water in dehydrating Norway spruce sapwood visualized by neutron radiography. Holzforschung 66, 751-756.

Roy, J.J., Sun, L.H., Ji, L.H., 2014. Microalgal proteins: a new source of raw material for production of plywood adhesive. J Appl Phycol 26, 1415-1422.

Sabo, R., Basta, A.H., Winandy, J.E., 2013. Integrated study of the potential application of remediated CCA treated spruce wood in MDF production. Ind Eng Chem Res 52, 8962-8968.

Sandberg, K., Salin, J.-G., 2010. Liquid water absorption in dried Norway spruce timber measured with CT scanning and viewed as a percolation process. Wood Science and Technology 46, 207-219.

Santos, W.L.F., da Silva, A.J.P., Cabral, A.A., Mercury, J.M.R., 2014. Particleboard manufactured from tauari (Couratari oblongifolia) wood waste using castor oil based polyurethane resin. Mater Res-Ibero-Am J 17, 657-663.

Sari, B., Nemli, G., Ayrilmis, N., Baharoglu, M., Bardak, S., 2013. The influences of drying temperature of wood particles on the quality properties of particleboard composite. Drying Technology 31, 17-23.

Scheffer, T.C., 1971. A climate index for estimating potential for decay in wood structures above ground. Forest Prod J 21, 25-31.

Schirp, A., Wolcott, M.P., 2005. Influence of fungal decay and moisture absorption on mechanical properties of extruded wood-plastic composites. Wood and Fiber Science 37, 643-652.

Schmidt, O., 2006. Wood and tree fungi. Biology, damage, protection, and use. Springer, Berlin.

Schulte, P.J., Castle, A.J., 1993. Water flow through perforation plates: a fluid mechanical approach. Journal of Experimental Botany 44, 1135-1142.

Sedighi-Gilani, M., Griffa, M., Mannes, D., Lehmann, E., Carmeliet, J., Derome, D., 2012. Visualization and quantification of liquid water transport in softwood by means of neutron radiography. International Journal of Heat and Mass Transfer 55, 6211-6221.

Sedighi-Gilani, M., Vontobel, P., Lehmann, E., Carmeliet, J., Derome, D., 2014. Liquid uptake in Scots pine sapwood and hardwood visualized and quantified by neutron radiography. Materials and Structures 47, 13.

Sekino, N., Inoue, M., Irle, M., Adcock, T., 1999. The mechanisms behind the improved dimensional stability of particleboards made from steam-pretreated particles. Holzforschung 53, 435-440.

Setliff, E.C., 1986. Wood decay hazard in Canada based on scheffer climate index formula. Forest Chron 62, 456-459.

Shupe, T.F., Wu, Q.L., Hartley, I.D., 2002. Calibration of moisture meters for southern hardwoods. Forest Prod J 52, 59-62.

Simpson, W., 1980. Sorption theories applied to wood. Wood Fiber Sci 12, 183-195.

Simpson, W., TenWolde, A., 1999. Wood handbook: Wood as an engineering material. Gen. Tech. Rep. FLP-GTR-113. USDA–Forest Service, Forest Products Laboratory.

S. Sperry, J., 2003. Evolution of water transport and xylem structure. International Journal of Plant Sciences 164, 115-127.

Suchsland, O., Woodson, G.E., 1987. Fiberboard manufacturing practices in the United States. Agriculture handbook/United States. Dept. of Agriculture (USA).

Sun, X.Z., Bian, K., 1999. Shear strength and water resistance of modified soy protein adhesives. J Am Oil Chem Soc 76, 977-980.

Suttie, E., Alexander, J., Maes, M., 2015. Durable fibre for durable MDF – testing Tricoya, IRG/WP/40704. The 46th international research group on wood protection, Viña del Mar, Chile.

Suzuki, S., Takeda, K., 2000. Production and properties of Japanese oriented strand board I: effect of strand length and orientation on strength properties of sugi oriented strand board. Journal of Wood Science 46, 289-295.

Taghiyari, H.R., 2013. Nano-zycosil in MDF: gas and liquid permeability. European Journal of Wood and Wood Products 71, 353-360.

Taghiyari, H.R., Bari, E., Schmidt, O., 2014a. Effects of nanowollastonite on biological resistance of medium-density fiberboard against Antrodia vaillantii. European Journal of Wood and Wood Products 72, 399-406.

Taghiyari, H.R., Moradi-Malek, B., Kookandeh, M.G., Bibalan, O.F., 2014b. Effects of silver and copper nanoparticles in particleboard to control Trametes versicolor fungus. International Biodeterioration & Biodegradation 94, 69-72.

Taghiyari, H.R., Rangavar, H., Nouri, P., 2013. Fire-retarding properties of nanowollastonite in MDF. European Journal of Wood and Wood Products 71, 573-581.

Thoemen, H., Irle, M., Sernek, M., 2010. Wood-based panels: An introduction specialists. Brunel University Press.

Trinh, H.M., Militz, H., Mai, C., 2012a. Modification of beech veneers with N-methylol-melamine compounds for the production of plywood. European Journal of Wood and Wood Products 70, 421-432.

Trinh, H.M., Militz, H., Mai, C., 2012b. Modification of beech veneers with N-methylol melamine compounds for the production of plywood: natural weathering. European Journal of Wood and Wood Products 70, 279-286.

Van Acker, J., De Smet, J., 2007. Moisture dynamics of plywood in exterior applications as a basis for service life prediction., In proceedings of the international panel products symposium IPPS, Cardiff, South Wales, UK, pp. 47-60.

Van den Bulcke, J., Boone, M., Van Acker, J., Stevens, M., Van Hoorebeke, L., 2009a. X-ray tomography as a tool for detailed anatomical analysis. Ann Forest Sci 66.

Van den Bulcke, J., Boone, M., Van Acker, J., Van Hoorebeke, L., 2009b. Three-dimensional X-ray imaging and analysis of fungi on and in wood. Microscopy and Microanalysis 15, 395-402.

Van den Bulcke, J., Cookson, L.J., De Windt, I., Li, W.Z., Van Acker, J., 2014. Statistical analysis of 40 years of preservative in-ground stake testing in Australia, IRG/WP/20552. The 45th International Research Group on Wood Protection, St George, Utah, USA.

Van den Bulcke, J., De Windt, I., Defoirdt, N., De Smet, J., Van Acker, J., 2011. Moisture dynamics and fungal susceptibility of plywood. International Biodeterioration & Biodegradation 65, 708-716.

Van den Bulcke, J., Van Acker, J., De Smet, J., 2009c. An experimental set-up for real-time continuous moisture measurements of plywood exposed to outdoor climate. Building and Environment 44, 2368-2377.

van Houts, J.H., Wang, S.Q., Shi, H.P., Pan, H.J., Kabalka, G.W., 2004. Moisture movement and thickness swelling in oriented strandboard, part 1. Analysis using nuclear magnetic resonance microimaging. Wood Science and Technology 38, 617-628.

Viitanen, H., Toratti, T., Makkonen, L., Peuhkuri, R., Ojanen, T., Ruokolainen, L., Raisanen, J., 2010. Towards modelling of decay risk of wooden materials. European Journal of Wood and Wood Products 68, 303-313.

Viitanen, H.A., 1997. Modelling the time factor in the development of brown rot decay in pine and spruce sapwood - The effect of critical humidity and temperature conditions. Holzforschung 51, 99-106.

Vlassenbroeck, J., Dierick, M., Masschaele, B., Cnudde, V., Hoorebeke, L., Jacobs, P., 2007a. Software tools for quantification of X-ray microtomography. Nucl Instrum Meth A 580, 442-445.

Vlassenbroeck, J., Dierick, M., Masschaele, B., Cnudde, V., Van Hoorebeke, L., Jacobs, P., 2007b. Software tools for quantification of X-ray microtomography at the UGCT. Nuclear Instruments and Methods in Physics Research Section A: Accelerators, Spectrometers, Detectors and Associated Equipment 580, 442-445.

Walker, J.C.F., 1993. Primary wood processing: principles and practice, 1st ed. Chapman & Hall, London; New York.

Wang, J., Wu, X., Jiang, M., Morris, P., 2007. Decay hazard classification in china for exterior above-ground wood, IRG/WP/20357. The 38th International Research Group on Wood Protection, Stockholm.

Wang, S., Winistorfer, P.M., Young, T.M., Helton, C., 2001. Step-closing pressing of medium density fiberboard; Part 1. Influences on the vertical density profile. Holz Roh Werkst 59, 19-26.

Wang, S.Q., Winistorfer, P.M., 2000. The effect of species and species distribution on the layer characteristics of OSB. Forest Prod J 50, 37-44.

Wang, S.X., Jamsa, S., Mahlberg, R., Ihalainen, P., Nikkola, J., Mannila, J., Ritschkoff, A.C., Peltonen, J., 2014. Treatments of paper surfaces with sol-gel coatings for laminated plywood. Appl Surf Sci 288, 295-303.

Wang, Z., Li, L., Gong, M., 2012. Measurement of dynamic modulus of elasticity and damping ratio of wood-based composites using the cantilever beam vibration technique. Constr Build Mater 28, 831-834.

Wang, Z.J., Gu, Z.B., Hong, Y., Cheng, L., Li, Z.F., 2011. Bonding strength and water resistance of starch-based wood adhesive improved by silica nanoparticles. Carbohyd Polym 86, 72-76.

Reference list

Watanabe, K., Lazarescu, C., Shida, S., Avramidis, S., 2012. A novel method of measuring moisture content distribution in timber during drying using CT scanning and image processing techniques. Drying Technology 30, 256-262.

Watanabe, K., Saito, Y., Avramidis, S., Shida, S., 2008. Non-destructive measurement of moisture distribution in wood during drying using digital X-ray microscopy. Drying Technology 26, 590-595.

Williams, R.S., 2005. Handbook of wood chemistry and wood composites. Chapter 7: weathering of wood. CRC Press LLC.

Winandy, J.E., Morrell, J.J., 1993. Relationship between incipient decay, strength, and chemical-composition of Douglas-Fir heartwood. Wood and Fiber Science 25, 278-288.

Winistorfer, P.M., Xu, W., 1996. Layer water absorption of medium density fiberboard and oriented strandboard. Forest Prod J 46, 69-72.

Yang, X.Y., Amano, T., Ishimaru, Y., Iida, I., 2003. Application of modal analysis by transfer function to nondestructive testing of wood II: modulus of elasticity evaluation of sections of differing quality in a wooden beam by the curvature of the flexural vibration wave. Journal of Wood Science 49, 140-144.

Ye, X.P., Julson, J., Kuo, M.L., Womac, A., Myers, D., 2007. Properties of medium density fiberboards made from renewable biomass. Bioresource Technol 98, 1077-1084.

Yildiz, S., Gumuskaya, E., 2007. The effects of thermal modification on crystalline structure of cellulose in soft and hardwood. Building and Environment 42, 62-67.

Younesi-Kordkheili, H., Kazemi-Najafi, S., Eshkiki, R.B., Pizzi, A., 2015. Improving urea formaldehyde resin properties by glyoxalated soda bagasse lignin. European Journal of Wood and Wood Products 73, 77-85.

Youngquist, J.A., Rowell, R.M., Krzysik, A., 1986. Mechanical-properties and dimensional stability of acetylated aspen flakeboard. Holz Roh Werkst 44, 453-457.

Zdravkovic, V., Lovric, A., Stankovic, B., 2013. Dimensional stability of plywood panels made from thermally modified poplar veneers in the conditions of variable air humidity. Drvna Ind 64, 175-181.

Zhang, H.Y., Liu, J., Lu, X.N., 2013. Reducing the formaldehyde emission of composite wood products by cold plasma treatment. Wood Res-Slovakia 58, 607-616.

Zhang, J.Z., Kang, H.J., Gao, Q., Li, J.Z., Pizzi, A., Delmotte, L., 2014. Performances of Larch (larix gmelini) tannin modified urea-formaldehyde (TUF) resin and plywood bonded by TUF resin. J Appl Polym Sci 131.

Zhang, M., Wong, E.D., Kawai, S., Kwon, J.H., 1998. Manufacture and properties of high-performance oriented strand board composite using thin strands. Journal of Wood Science 44, 191-197.

Zhu, D., Damodaran, S., 2014. Chemical phosphorylation improves the moisture resistance of soy flour- based wood adhesive. J Appl Polym Sci 131.

Curriculum Vitae

Personal details

Full name: Wanzhao Li

Gender: Male

Date and place of birth: April 23rd 1986, Gansu, China

Phone: 0032 (0)9 264 61 47

Address: Wondelgemstraat 75, 9000 Ghent, Belgium

Email: Wanzhao.Li@UGent.be

Education

2011 - 2016: PhD in wood science and technology, Ghent University, Ghent, Belgium.

2008 - 2011: Master in wood science and technology, Beijing Forestry University, Beijing, China.

2004 - 2008: Bachelor in packaging engineering, Beijing Forestry University, Beijing, China.

Publications (A1 peer reviewed publications)

Wanzhao Li, Jan Van den Bulcke, David Mannes, Eberhard Lehmann, Imke De Windt, Manuel Dierick, Joris Van Acker. (2014). Impact of internal structure on water-resistance of plywood studied using neutron radiography and X-ray tomography. Construction and Building Materials 73: 171–179.

Wanzhao Li, Jan Van den Bulcke, Imke De Windt, Denis Van Loo, Manuel Dierick, Loes Brabant, Joris Van Acker. (2013). Combining electrical resistance and 3-D X-ray computed tomography for moisture distribution measurements in wood products exposed in dynamic moisture conditions. Building and Environment 67: 250 – 259.

Wanzhao Li, Jan Van den Bulcke, Imke De Windt, Jelle Dhaene, Joris Van Acker. Moisture behavior and structural changes of plywood during outdoor exposure. European Journal of Wood and Wood Products. (Accepted)

Wanzhao Li, Jan Van den Bulcke, Thomas De Schryver, Joris Van Acker. Investigating water transport in MDF and OSB using a gantry-based X-ray CT scanning system. (Under review)

Wanzhao Li, Jan Van den Bulcke, Imke De Windt, Nele Defoirdt, Jelle Dhaene, Manuel Dierick, Hugo Sol, Joris Van Acker. Relating MOE decrease and mass loss due to fungal decay in plywood and MDF using resonalyser and X-ray CT scanning. International Biodeterioration & Biodegradation (Under review)

International conference papers

Wanzhao Li, Jan Van den Bulcke, Imke De Windt, Manuel Dierick, Joris Van Acker. Investigating plywood behavior in outdoor conditions. Proceedings of the International Panel Products Symposium (IPPS), Venue Cymru, Llandudno, North Wales, UK, 7-8 October, 2015. pp. 185-192. (*Oral presentation*)

Wanzhao Li, Jan Van den Bulcke, Imke De Windt, Manuel Dierick, Joris Van Acker. Non-destructive monitoring of structure and moisture dynamics of plywood exposed outdoors to improve service life prediction and fit-for-purpose design. IRG/WP/15-20570. The 46th international research group on wood protection (IRG-WP) annual meeting, Viña del Mar, Chile, 10-14 May, 2015. (*Oral presentation*)

Wanzhao Li, Jan Van den Bulcke, Imke De Windt, Denis Van Loo, Manuel Dierick, Loes Brabant, Joris Van Acker. Non-destructive measurement of moisture distribution in wood using 3D X-ray scanning and electrical resistance**.** 1st International Conference on Tomography of Materials and Structures, Gent, Belgium, 1–5 July, 2013. pp. 171-173. *(Poster presentation)*

Joris Van Acker, Imke De Windt, **Wanzhao Li**, Jan Van den Bulcke. Time of Wetness (ToW) simulation based on testing moisture dynamics of wood. COST FP1303: Performance and maintenance of bio-based building materials influencing the life cycle and LCA. Kranjska Gora, Slovenia, 23-24 October, 2014. pp. 59-60.

Jan Van den Bulcke, Imke De Windt, **Wanzhao Li**, David Mannes, Eberhard Lehmann, Joris Van Acker. Moisture dynamics of modified wood. 7th European conference on wood modification, Lisbon, Portugal, 10-12 March, 2014. *Proceedings*.

Jan Van den Bulcke, Laurie J Cookson, Imke De Windt, **Wanzhao Li**, Joris Van Acker. Statistical analysis of 40 years of preservative in-ground stake testing in Australia. IRG/WP/14-20552. The 45th international research group on wood protection (IRG-WP) annual meeting, ST George, UT, USA, 11-15 May, 2014.

Others:

Cost Action FP 1006, 1st training school. Material preparation (boards and solid wood) for material surface modification using chemical and thermal treatments. Ljubljana, Slovenia, 8-9 March 2012.

Cost Action FP 1006, 4th training school. X-ray tomography and service life prediction. Gent, Belgium, 15-16 April 2013.

Cost Action FP 1006, 3rd workshop. Process and service life modelling. Gent, Belgium, 17-19 April 2013.